STUDY OF STRUCTURAL, ELECTRICAL TRANSPORT AND MAGNETIC PROPERTIES OF Ni-Cu-Zn FERRITES

Khulna University Of Engineering & Technology
KUET
Bangladesh
Central Library

By

Suvendu Kumar Bahadur
Roll No: 0755504
Session: January-2007

A THESIS SUBMITED TO THE DEPARTMENT OF PHYSICS, KHULNA UNIVERSITY OF ENGINEERING & TECHNOLOGY, KHULNA- 9203 IN PARTIAL FULFILMENT OF THE REQUIRMENT FOR THE DEGREE OF MASTER OF PHILOSOPHY

DEPARTMENT OF PHYSICS
KHULNA UNIVERSITY OF ENGINEERING & TECHNOLOGY
KHULNA - 9203, BANGLADESH
JULY- 2013

DECLARATION

This is to certify that the thesis work entitled as **"Study of Structural, Electrical Transport and Magnetic Properties of Ni-Cu-Zn Ferrites"** has been carried out in partial fulfillment of the requirement for M. Phil. degree in the department of physics, Khulna University of Engineering & Technology, Khulna-9203, Bangladesh. The above research work or any part of this work has not been submitted to anywhere for the award of any degree or diploma. No other person's work has been used without due acknowledgement.

1. Supervisor

.....

Prof. Dr. Shibendra Shekher Sikder

2. Co-supervisor

.....

Mrs. Shireen Akhter

Candidate

Suvendu Kumar Bahadur.

Suvendu Kumar Bahadur

To

MY PARENTS

KHULNA UNIVERSITY OF ENGINEERING & TECHNOLOGY
DEPARTMENT OF PHYSICS

Approval

This is to certify that the thesis work submitted by *Suvendu Kumer Bahadur* entitled "*Structural, Electrical Transport and Magnetic Properties of Ni-Cu-Zn Ferrites*" has been accepted by the board of examiners for the partial fulfillment of the requirements for the degree of *Master of Philosophy* in the Department of *Physics*, Khulna University of Engineering & Technology, Khulna, Bangladesh in 26 July 2013.

Board of Examiners

Sl. No. **Name, Designation & Address**

1. Prof. Dr. Shibendra Shekher Sikder
   Department of Physics
   Khulna University of Engineering & Technology
   ..... 26/07/13 .....
   Chairman & Supervisor

2. Head
   Department of Physics
   Khulna University of Engineering & Technology
   .....
   Member

3. Mrs. Shireen Akhter
   Chief Scientific Officer and Head
   Materials Science Division
   Atomic Energy Centre, Ramna
   .....
   Co- Supervisor & Member

4. Prof. Dr. Md. Abdullah Elias Akhter
   Department of Physics
   Khulna University of Engineering & Technology
   .....
   Member

5. Prof. Dr. Faruque-Uz-Zaman Chowdury
   Department of Physics
   Chittagong University of Engineering & Technology
   .....
   Member (External)

ATOMIC ENERGY CENTRE

4 KAZI NAZRUL ISLAM AVENUE
P.O. BOX - 164, RAMNA, DHAKA - 1000
BANGLADESH

Cable : ATOMCENT
Telex : 632203 BATOM BJ
Fax : 880-2-8617946
Tel. : 880-2-8625488
E-mail : aecd@citechco.net

3 June, 2013
Md. Toyebur Rahman
Controller of Examinations
Office of the Controller of Examination
Khulna University of Engineering & Technology
Khulna-9203, Bangladesh

Report on the thesis entitled **"Study of Structural, Electrical transport and Magnetic properties of Ni-Cu-Zn ferrites"** submitted by Suvendu Kumar Bahadur, M. Phil. student of the Department of Physics, Khulna University of Engineering & Technology, Khulna-9203, Bangladesh.

The thesis is good piece of experimental research work with scientific thoughts and innovation. The research is focused on the influence of several compositions of Ni-Cu-Zn soft ferrites are synthesize, characterized and investigated to optimize Fe deficient. General formula of the sample is $(Ni_{0.28}Cu_{0.10}Zn_{0.62}O)(Fe_2O_3)_{1-x}$ [where x = 0.00, 0.02, 0.04, 0.06 & 0.08]. The properties of Ni-Cu-Zn ferrites are influenced considerably by sintering temperature. In the thesis attempts have been made to present a systematic review of different experimental research works related to this study.

Samples were prepared by solid state reaction and characterized by X-ray Diffraction (XRD) studies. All the samples were of single phase. Throughout the experimental study of ferrite samples modern equipments have been employed such as X-ray diffractometer, Impedance Analyzer, B-H loop tracer, DC and AC resistivity, Dielectric constant and Vibrating Sample Magnetometer (VSM). It is observed from the analysis of the experimental results that this study may play an important role to do more research for the development of efficient miniaturized devices for which soft magnetic materials are needed.

Detail Reports:

In chapter I, the candidate has elaborated the aims and objective of the present work. Contain a brief introduction of ferrites, brief review works and an outline of the thesis. In this chapter an idea of the experimental methods have been given.

In chapter II, describes about theoretical background of the research work and has been written in a well manner.

In chapter III, contains the detailed description of the experimental works and has been written logically. It describes the methodology of ferrite sample preparation, composition of the studied ferrite system and gives description of the apparatus used for the characterization of the prepared ferrite samples.

ATOMIC ENERGY CENTRE

4 KAZI NAZRUL ISLAM AVENUE
P.O. BOX - 164, RAMNA, DHAKA - 1000
BANGLADESH

Cable : ATOMCENT
Telex : 632203 BATOM BJ
Fax : 880-2-8617946
Tel. : 880-2-8625488
E-mail : aecd@citechco.net

In chapter IV, deals with the results and discussion on $(Ni_{0.28}Cu_{0.10}Zn_{0.62}O)(Fe_2O_3)_{1-x}$ [where x = 0.00, 0.02, 0.04, 0.06 & 0.08]. The motivation was to see the effects of small deficiency of iron on the structural, magnetic and transport properties. This chapter gives an idea about the structure of the samples, bulk density, Curie temperature, permeability, hysteresis behavior and the dielectric properties of the samples. The results are explained scientifically and in a logical manner.

In chapter V, presents the overall conclusion from the whole experimental investigations on Fe deficient Ni-Cu-Zn ferrites.

Details of the references have also been listed.

Recommendation:

Considering the overall presentation and the volume of work, results and analysis of the data, I recommend that the candidate Suvendu Kumar Bahadur, Roll No. 0755504, Session 2007, be awarded M. Phil degree of the **Khulna University of Engineering & Technology, Khulna-9203, Bangladesh.**

Shkhter 3.6.2013

Mrs. Shireen Akhter
Head & Chief Scientific Officer
Materials Science Division
Atomic Energy Centre
4, Kazi Nazrul Islam Avenue, Dhaka-1000
Bangladesh

Acknowledgements

University never approves higher degrees such as M. Phil / Ph. D. without deep knowledge on the certain matter of interested student. To achieve those qualities and to perform my M. Phil research I have had a lot of help from many individuals in various ways. To maintain code of action research I take opportunity here to express cordial and formal respect. I express, with due respect, my deep sense of sincere gratitude and indebtedness to my supervisor professor Dr. Shibendra Shekher Sikder, Department of Physics, Khulna University of Engineering & Technology (KUET) for his indispensable guidance, keen interest, constructive suggestions, fruitful discussion and constant inspiration throughout the research work.

I am very much indebted to my Co-Supervisor Mrs. Shireen Akhter, Head and Chief Scientific Officer, Materials Science Division, Atomic Energy Centre, Dhaka, for introducing the present research topic and inspiring guidance and valuable suggestion throughout the research work. It would have not been possible for me to bring out this thesis without her help and constant encouragement.

I am indebted to Professor Dr. Md. Abdullah Elias Akhtar, Head, Department of Physics, Khulna University of Engineering & technology, for his direction and instruction.

I am also grateful to Dr. Dilip Kumar Saha, Chief Scientific Officer, Materials Science Division, Atomic Energy centre, Dhaka of his generous help in doing measurements and analysis XRD results and whose vast knowledge in the field of science has enlightened me of this research work.

I am very much indebted to Engineer Dr. A. K. M. Abdul Hakim, Consultant, Department of Glass and Ceramic Engineering, Bangladesh University of Engineering and Technology (BUET) Dhaka for introducing the present research topic and inspiring guidance and valuable suggestion throughout the research work.

I am mostly indebted for ever to Dr. Md. Zakir Hossain Khan, Physics Department, Fultala College, Khulna. I become able to feel and realize it was not

possible to complete my thesis work except his cordial help with generous thinking, expert skillful suggestion and perfect instruction.

I am grateful to Mr. Nazrul Islam Khan, Mr. H. N. Das and Mr. M.A. Mamun, Scientific Officer, Materials Science Division, Atomic Energy centre, Dhaka, for providing me with technical assistance during my research work.

I gratefully acknowledge Prof. Dr. Jolly Sultana, Department of Physics, KUET, for Co-operation and inspiration during this work. My thanks are also for Md. Kamrul Hasan Reza, Md. Asaduzzaman, Assistant Professor, Mr. Md. Torikul Islam, Mrs. Nipa Debnath, Mr. Sujit Kumer Shil, Lecturer, Department of Physics, KUET, for their tireless co-operation in my thesis work. I want to mention Prof. Dr. Mihir Ranjan Halder, Department of Mechanical Engineering, Dr. Md. Robiul Islam, Department of Humanities and Md. Jahirul, EEE, for their moral support.

My thanks are also for Prof. Dr. Md. Sultan Mahmud, Dr. Saroat Noor, Mr. Pritish Kumar Roy, Mr. Siba Pada Mondol, Mr. Ratan Kumar Howlader, Md. Gofur, Mr. Zased, Mr. Asad, Mr. Samir and Mr. Abu Hani Answary for their useful suggestion and help to carry out my research work.

I would like to extend my special thanks to Mr. Kuishik Das, Mr. Proney Mollik and Mr. Aurjun Roy, who inspired and helped me highly to reach to my goal.

I show great honor and realize gratefulness to my School Head Master, Mr. Somor Kanti Choudhury, his late wife and also his whole family. I express my gratefulness to all of my teachers.

My thanks are due to Director, Atomic Energy Centre, Dhaka for his kind permission to use the Laboratory of Magnetic Material Division, Atomic Energy Centre, Dhaka.

I am thankful to Ms. Alhamra, Parveen, Ms. Anjuman Ara Begum, Ms. Nazmunnahar Begum, Ms Mohsin, Mr. Mostafizur Rahman, Mr. Anawar Hossain and Ms. Halima Sadia of Materials Science Division, AECD, for their constant help during my research work.

My special thanks for Nandita Boudi, who inspired me a lot during the period of my research works. I am greatly indebted to my parents, brother and sisters for there constant encouragement and inspiration.

I also wise to thank the authority of Khulna University of Engineering & Technology (KUET), for providing me with the necessary permission and financial assistance for conducting this thesis work.

Suvendu Kumar Bahadur

ABSTRACT

Ni–Cu-Zn ferrites are well known technological magnetic material finding applications in various electrical devices. The present work is focused on the influence on electromagnetic and transport properties of Fe-deficient Ni-Cu–Zn ferrites. These ferrite samples of composition $(Ni_{0.28}Cu_{0.10}Zn_{0.62}O)(Fe_2O_3)_{1-x}$, where x = 0.00, 0.02, 0.04, 0.06 and 0.08 were prepared using the solid state reaction technique. The phase identification was carried out by X-ray diffraction. The X–ray diffraction analysis revealed that the samples crystallize in single phase cubic spinel structure. A slight increase of Curie temperature (T_c), saturation magnetization (M_s) and initial permeability (μ') with increase of Fe-deficient were observed. The permeability spectrum with frequency follows the Snoek's limit. Sample with x = 0.00 sintered at 1100^0C possess the maximum value of relative quality factor (RQF). From the B–H loops, the remanance (B_r) and coercive force (H_c) were determined. Saturation induction (B_s) and $\frac{B_r}{B_s}$ are measured from low field B–H loops is found to increase with increasing Fe-deficient up to x = 0.04 thereafter decrease. DC resistivity increases with increasing Fe-deficient up to x = 0.06 and thereafter decrease. The dielectric constant is found to decrease continuously with increasing frequency and remains almost constant at higher frequency range. From hysteresis parameter it was revealed that optimum soft magnetic properties corresponds to the composition with x = 0.06 sintered at 1100^0C having highest permeability, maximum induction, minimum coercivity and hysteresis losses.

List of Symbols

AC current	I
Angular frequency	ω
Anisotropy field	H_k
Anisotropy constant	K_1
Average anisotropy	<K>
Bohr magneton	μ_B
Bragg's angle	θ
Bulk density	d_B
Charge of electron	e
Capacitance	C
Coercivity	H_c
Cross-sectional area of toroids	S
Curie temperature	T_c
DC resistivity	ρ_{dc}
Dielectric constant	ε'
Diffraction angle	θ
Energy per unit area of a 180° Bloch wall	γ
Exchange integral	J
Exchange coupling constant	J_{ij}
Exchange correlation length	L_o
Face centered cubic	fcc
Frequency	f
Full width at half maxima	FWHM
Ferromagnetism	FM
Grain size	D
Heating rate	β
Imaginary part of initial permeability	μ''
Impedance	Z

Inductance	L
Initial permeability	μ_i
Inter planner spacing	d
Loss factor	tan δ
Magnetization	M
Magnetic field	H
Magnetic induction	B
Magnetocrystalline anisotropy constant	K_1
Neel temperature	T_N
Nelson-Riley function	$F(\theta)$
Number of turns	N
Peak temperature	T_p
Permeability of free space	μ_o
Quality factor	QF
Reactance	X
Real part of initial permeability	μ'
Retentivity	B_r
Remanent ratio	M_r
Resistance	R
Resistivity	ρ
Saturation magnetization	M_s
Saturation induction	B_s
Saturation polarization	J_s
Susceptance	B
Susceptibility	χ
X-density	d_x
X-ray diffraction	XRD
Yafet-Kittel	Y-K
Wavelength	λ

Contents

CHAPTER- III Experimental Procedure

List of Figures

CHAPTER- IV

List of Tables

CHAPTER - I

Introduction

Chapter –I Introduction

1.1 Introduction

The history of ferrite began centuries before the birth of Christ with discovery of stones that attract iron. The most abundant deposits of these stones were found in Asia Minor, and hence the name of the materials becomes magnetite (Fe_3O_4). The term ferrite has been misused but is commonly used as a class of magnetic oxide compounds that contain iron oxide as a major component [1.1]. Ferrites constitute a special branch of ferrimagnetism. By ferrites are certain double oxide iron and another metal. The term ferrite denotes a group of iron oxides, which have the general formula $MO.Fe_2O_3$, where M is a divalent metal ion such as Mn^{2+}, Fe^{2+}, Co^{2+}, Ni^{2+}, Cu^{2+}, Zn^{2+}, Mg^{2+} or Cd^{2+}. Ferrite exhibits a spontaneous magnetization at room temperature, like ferromagnetic materials. They consists of spontaneously magnetized domains, show the phenomenon of magnetic saturation and hysteresis loop, and have a critical temperature T_C, called Curie temperature. These are of very high resistivity such as $10^2 - 10^{10}\ \Omega - Cm$ which is very high than that of iron. This outstanding property of ferrites makes them highly demandable for high frequency applications. This fact way first mentioned by S. Hilpert [1.2]. Now a days ferrites are employed truly in a wide range of applications, and have contributed to the advances in electronics like as transformer cores, inductors, high quality filters, radio frequency circuits, rod antennas, read/write heads for high speed digital tape and operating devices [1.3-1.5].

Polycrystalline soft ferrites prepared from the metal oxides are magnetic semiconductors and have made important contributions, both technological and conceptual to the development and electronics. Soft ferrites still remain the best magnetic materials and can not be replaced by any other magnetic materials with respect to their very high frequency application because they are inexpensive, more stable, easily manufactured [1.6]. The requisites for a modern ferrite are so many in numbers that only extensive research in this field can meet the huge demand of the rapid growing technology. The demanded characteristics are as follows:

Khulna University of Engineering & Technology
Khulna Bangladesh
Central Library

- Excellent magnetic and electrical performance
- Exact mechanical dimensions
- High quality
- Low price
- Large number of controllable parameters over a wide range of synthesis temperature.

The ferrites were developed into commercially important materials chiefly during the year 1933-1945 by Sonek [1.7] and his associates at the Philips Research Laboratories in Holland. In a classical paper published in 1948 Neel [1.8] provided the theoretical key to an understanding of the ferrites. The magnetic ferrites mainly fall in to two groups with different crystals structures:

(i) **Cubic:** These have the general formula $MO.Fe_2O_3$, when M is a divalent metal ion like Mn, Ni, Fe, Co, Mg and Cu etc. Cobalt ferrites are magnetically hard but all other cubic ferrite in magnetically soft.

(ii) Hexagonal: The most important in this group is barium ferrite $BaO.Fe_2O_3$ which is magnetically hard.

The most popular combination is Ni-Zn and Mn-Zn ferrite. Ferrite crystallizes with two magnetic sub-lattice i.e. tetrahedral (A) site and octahedral (B) site based on Neel's model. Magnetic and electrical properties of ferrites are strongly dependent on distribution of cation in A and B-sites and their valence state [1.9-1.10]. The properties of Ni-Zn ferrites can be tailored by substituting them with different metal ions such as Co^{2+}, Mg^{2+}, Mn^{2+}, Cu^{2+} etc. The Ni-Zn ferrites are one of the most versatile responsible cost magnetic materials for general use in both low and high frequency devices because of their high resistivity, low dielectric losses, mechanical hardness, high Curie temperature and chemical stability. High sintering temperature can be reduced by using CuO with Ni-Zn ferrites as well as with the addition of some oxides heaving low melting point. Spinel ferrites of different composition have been studied and used for a long time to get useful products. Many researchers have worked on different types ferrites in order to improve

there electrical and magnetic properties. Researchers have not yet been able to formulate a rigid set of rules for ferrites about a single property. Scientists still continue their efforts to achieve the optimum parameters of ferrites, like high saturation magnetization, high permeability, high resistivity etc. Since the research on ferrites is so rest, it is difficult to collect all of the experimental results and information about all types of ferrites in every aspect. The systematic research is still necessary for a more comprehensive understanding and properties of such material.

Ni-Cu-Zn ferrites contains inverse $NiFe_2O_4$, $CuFe_2O_4$ and normal $ZnFe_2O_4$ ferrites in which according to the favorable fit the charge distribution, Ni^{2+} and Cu^{2+} ions shows strong performance to B-sites. Zn^{2+} ions show a strong preference for 'A' sites due to its electronic configuration. The structural formula can be presented by

$$[Zn_{0.62}Fe_{1-x}]_A[Ni_{0.28}Cu_{0.10}Fe_{1+x}]_BO_4,$$

where the third bracket with suffixed A indicates tetrahedral site 'A' and B indicates octahedral site 'B'. Sometimes Cu^{2+} distributed into both sites.

According to the modern theories, the magnetism in solids arises due to orbital and spins motions of electrons as well as spins of the nuclei. The motion of electrons is equivalent to an electric current which produces the magnetic effects. The major contribution comes from the spin of unpaired valence electrons which produces permanent electronic magnetic moments. A number of such magnetic moments may align themselves in different direction to generate a net non-zero magnetic moment. Thus the nature of magnetization produced depends on the number of unpaired valence electron present in the atoms of the solid and on the relative orientations of the neighboring magnetic properties [1.11] O^{2-} anion has no magnetic moment. Since it has been completely filled shells with P-type outer most orbital. On the other hand $Ni^{2+}(d^8)$, $Cu^{2+}(d^9)$, $Zn^{2+}(d^{10})$ and $Fe^{3+}(d^5)$ cations of the ferrite have 2, 1, 0 and 5 unpaired electrons respectively. Therefore Ni, Cu and trivalent Fe have magnetic moments due to unfilled

3d sub-shell. Zn^{2+} by contrast is diamagnetic because the outer sub shell of it is completely filled.

Ni-Cu-Zn ferrites have potential application in the fabrication of multilayer chip inductors (MLCI) and various electronic applications such as telecommunication because of their good electro-magnetic properties at high density covering a wide range of compositions. In the present research work efforts has been under taken Ni-Cu-Zn ferrites of composition $Ni_{1-x}Cu_yZn_xFe_{2-z}O_4$, where the composition of Cu, Zn, Ni and Fe were made to present a systematic review of various experimental and theoretical observed facts related to this study.

1.2 The Aim and Objectives of the Present Work

The main objectives of the present research work were to synthesis Ni-Cu-Zn ferrites of composition $Ni_{1-x-y}\ Cu_y\ Zn_x\ Fe_{2-z}\ O_4$, where the composition of Ni, Cu, Zn and Fe was made $(Ni_{0.28}\ Cu_{0.10}\ .Zn_{0.62}\ O)\ (Fe_2O_3)_{1-x}$, where X=0.00, 0.02, 0.04, 0.06, 0.08. The raw materials that would be used in the synthesis of ferrites samples will be commercially available nano particles of 20-70 nanometer. The value of x, y and z would be maintained in such way a low sintering temperature is as ascertained. The Fe deficiency in the chosen composition is proposed to have high resistivity and low sintering temperature. The amount to Fe deficiency should be maintained in such way so that prepared materials ensure high permeability as a prime requisite for a good inductor material. The Cu addition would ensure good sinter ability. The low melting point additive as sintering aid would be optimized to a minimum value so that the magnetic properties are not jeopardized but an effective low temperature sintering is achieved. Finally structural, electrical transport and magnetic properties of all the prepared samples such as magnetization, Curie temperature, magnetic permeability, magnetic loss components, coercivity, resistivity, dielectric constant etc. would be studied in detail to find out an optimum composition.

1.3 Experimental reason for Choosing this Research Work

Ferrite samples have been prepared by conventional double sintering ceramic technique using high purity oxide nano materials. The experimental methods that would be used in this research work were as follows.

- Sintering of the samples has been carried out in a microprocessor controlled high temperature furnace.
- The prepared samples have been characterized in terms of their Crystal structure, unit cell parameters and phases present in the prepared samples with the help of X-ray diffraction (XRD) technique. The porosity of the prepared samples has been calculated from the theoretical density (using XRD data) and the bulk density.
- Permeability, magnetic loss factor and relative quality factor as a function of frequency temperature has been determined using an impedance analyzer,
- Hysteresis parameters have been determined by B-H loop tracer.
- Curie temperature has been determined by permeability versus temperature measurement with the help of a oven using a LCR meter.
- Magnetization of the samples has been measured as a function of field and temperature using vibrating sample magnetometer (VSM).
- DC/AC electrical resistivity and dielectric properties as a function of frequency and temperature has been studied with the help of electrometer/Inductance meter.

1.4 Review Works

Ferrites, i.e. ferromagnetic cubic spinals are technically important materials. They have been extensively investigated in order to improve good soft magnetic properties. A ferromagnetic material is defined as one which below a transition temperature, possesses a spontaneous magnetization that arises from non parallel arrangement of the strongly coupled magnetic moments. The most important advances were made in ferrimagnetism in the field of magnetic oxides. The advancement of high frequency ferrites was initiated

by the work done by J. L. Snoek [1.7] who found that associated with excellent properties in the high frequency range, Mn-Zn and Ni-Zn ferrites provide a family of magnetic materials useful for radio and TV sets as well as carrier telephony as cores of inductors transformers and so forth. Technological advances in a variety of areas have generated a growing demand for the soft magnetic materials in advances. Among the soft magnetic materials, polycrystalline ferrites have received special attention due to their good magnetic properties and high electrical resistivity over a wide range of frequencies; starting from a few hundred Hz to several GHz. Spinel type ferrites are commonly used in many electronic and magnetic devices due to their high magnetic permeability and low magnetic losses [1.12-1.13] and also used in electrode materials for high temperatures applications because of their high thermodynamic stability electrical resistivity, electrolytic activity and resistance to corrosion [1.14-1.15]. Many investigators have focused their attention on the improvement of electromagnetic properties of the ferrite by divalent ions substitution. Generally the divalent metal ions (M^{2+}); Ni, Zn, Cu, Mg, Mn, Co or mixtures of these are substituted in different spinel ferrites.

The studies on microstructure and composition related magnetic properties have been reported for Ni-Cu-Zn ferrites by several researchers, which are also given below:

A. M. Abdeen [1.16] studied electric conduction in Ni-Zn ferrite. The real AC and DC electrical conductivities increases as the temperature increases indicating the studied samples are semiconductors in nature. The AC electrical conductivity increases with increasing angular frequency below Curie temperature (T_C) and above T_C it is independent of nature. The values of T_C decreases with increasing of Zn content ant activation energy below and above T_C decreases with increasing Zn-content.

Ahmed et al. [1.17] investigated the influence of zinc ion substitution on densification in Ni-Zn ferrite. They found rapid densification with increase Zn^{2+} concentration. Sun et al. [1.18] reported the initial permeability and relative loss factor increased while the cut off frequency decreased with increasing Zn content in $(Ni_{1-x}Zn_x)Fe_2O_4$ ferrite. Zn substituted $(Cu_{1-x}Zn_x)Fe_2O_4$ ferrite had been prepared by Ajmal et

al. [1.19]. They found that sintered density increased with increasing Zn concentration. Both saturation magnetization and magnetic moment increased with increasing Zn concentration up to x = 0.02 and then decreased with further addition of Zn.

Nakamura [1.20] reported on frequency dispersion of permeability in ferrite composite materials. The permeability increases with increasing density of composite materials. As the ferrite content decreases, both the shoulder frequency of real part of permeability dispersion; both the real and imaginary parts of the low frequency permeability is significantly reduced, and the peak frequency of imaginary part of permeability shifts toward higher frequency. Nakamura et al [1.21] reported on low temperature sintering Ni-Cu-Zn ferrite and its permeability spectra. The post sintering density and the complex permeability Ni-Cu-Zn ferrite ceramic can be controlled by altering the particle size of the sintering oxide materials and calcinations temperature.

Hoque et al. [1.22] reported that the magnetization of initial permeability and saturation magnetization at 0.2 in $(Ni_{1-x}Cu_x)Fe_2O_4$ ferrite, which could be attributed to the maximum sintering density obtained for this composition. Hoque et al. [1.23] reported the effect of Cu substitution Mg-Zn ferrites. The found a remarkable increase in the bulk density with increasing Cu-substitution for Mg. By incorporating CuO, the initial permeability of the samples increased. Saturation magnetization increased slightly with increasing Cu content up to $x \leq 0.30$ and then it decreased for x = 0.35. Cu substitution is also used in hard ferrites for improving properties [1.24]. Rezlescu et al. [1.25] reported the effect of Cu substitution on the physical properties of $(Mg_{0.5-x}Cu_xZn_{0.5})Fe_2O_4$ + 0.5MgO ferrites. They found that the density increased up to x = 0.30 whereas, resistivity increased up to x = 0.10 and permeability increased with Cu-content as well. E. Rezlescu et. al. [1.26] also reported that the sintered density and resistivity of $(Mg_{0.5-x}Cu_xZn_{0.5})Fe_2O_3$ ferrite increased up to x = 0.3, whereas permeability increased up to x = 0.4.

Ni-Cu-Zn ferrites are widely used multilayer chip devices. These devices were studied by K. O. Low and F. R. Sale [1.27], such as multilayer chip inductors, are

produced by Co-firing ferrite layers with an internal silver conductor. The low sintering temperature is attributed to its Cu-content because the Cu-containing ferrites were claimed to suffer thermal dissociation at temperature around 990^0C. Kin O. Low et al. [1.28] has design of Ni-Cu-Zn ferrites to suit a particular application where consideration was given on thermal dissociation temperature so that electromagnetic properties are not affected. Average crystalline size increase linearly with calcinations temperature, the lattice parameter and the ionic radius of octahedral sites increases with copper concentrations. The saturation magnetization decreases with increasing non magnetic Cu-content.

Caltun et al. [1.29] studied the microstructure and of the permeability spectra of Ni-Cu-Zn ferrites. The particle size increases when the sintering temperature is raised. For the same chemical composition and different sintering temperature it was found that the real permeability in the low frequency region decreases by addition of CuO. As sintering temperature increases, the natural resonance frequency, where the imaginary permeability had a maximum value, shifted towards low frequency from to 0.5MHz.

Dimeri et al. [1.30] studied the effect of compositional variation on structural, dielectric and magnetic properties of the Cu substituted $(Ni_{0.6-x}Cu_xZn_{0.4})Fe_2O_4$ ferrite. The results showed that addition of copper promoted grain growth, resulting increase in grain size. However, T_C was understandably lowered with the increase in Cu-content. A Saturation magnetization value of 92 emu/gm was obtained for the composition $x = 0.2$. Ferrite with Cu concentration of $x = 0.4$ showed the highest initial permeability.

The extensive literature survey reveals that the synthesis of crystalline Ni-Cu-Zn ferrite powder through solid state method has been attempted by a number of researchers. The electromagnetic properties have been reported with various Fe concentrations in Ni-Cu-Zn ferrites [1.31-1.32]. Optimization of Fe concentration with respect to Ni, Cu and Zn is essential to achieve desirable electromagnetic properties in the ferrites.

1.5 Organization of the Thesis

The Thesis has been divided into five chapter:

Chapter-I presents a brief introduction of Ni-Cu-Zn ferrite and organization of the thesis.

Chapter-II briefly describes the theories necessary to understand the present work.

Chapter-III enunciates with the detail experimental process related to this research work.

Chapter-IV describes the results and discussion about the optimization of Fe deficiency in $(Ni_{0.8}\ Cu_{0.10}Zn_{0.62}O)(Fe_2O_3)_{1-x}$ ferrites.

Chapter-V contains the concluding remarks.

Finally a complete list of references has been given towards the end of the chapters.

Chapter - II

Theoretical Background

Chapter-II Theoretical Background

2.1 Origin of Magnetism

The origin of magnetism lies in the orbital and spin motions of electrons and how the electrons interact with one another. The best way to introduce the different types of magnetism is to describe how materials respond to magnetic fields. The motion of electrons is equivalent to an electric current which produces the magnetic effects. The major contribution comes from the spin of unpaired valence electrons which produces permanent electronic magnetic moments. The circulating electron produces its own orbital magnetic moment, measured in Bohr magnetons (μ_B), and there is also a spin magnetic moment associated with it due to the electron itself spinning, like the earth, on its own axis.

In most materials there is resultant magnetic moment, due to the electrons being grouped in pairs causing the magnetic moment to be cancelled by its neighbor. A number of such magnetic moments may align themselves in different directions to generate a net non-zero magnetic moment. Thus the nature of magnetization produced depends on the number of unpaired valence electrons present in the atoms of the solid and on the relative orientation of the neighboring magnetic moments. The main distinction is that in some materials there is no collective interaction of atomic magnetic moments, whereas in other materials there is a very strong interaction between atomic moments.

The magnetism in solids can be classified into the following five major groups:

(i) Diamagnetism
(ii) Paramagnetism
(iii) Ferromagnetism
(iv) Antiferromagnetism
(v) Ferrimagnetism

Materials in the first two groups are those that exhibit no collective magnetic interactions and arte not magnetically ordered. Materials in last three groups exhibit long-range magnetic order below a certain critical temperature. Ferromagnetic and ferromagnetic materials are usually what we consider as being magnetic (i.e. behaving like iron). The remaining three are so weakly magnetic that they are usually thought of as "nonmagnetc". The varieties of magnetic ordering are schematically presented in Fig.-2.1.

A brief description of the above mentioned classes of magnetic materials are described below

2.1.1 Diamagnetism

Diamagnetism is a fundamental property of all matter, although it is usually very weak. It is due to the non-cooperative behavior of orbiting electrons when exposed to an applied magnetic field. Diamagnetic substance are composed of atoms which have no net magnetic moments (i.e., all the orbital shells are filled and there are no unpaired electrons). However, when exposed to a field, a negative magnetization is produced and thus the susceptibility is negative. It obeys Lenz's law. The other characteristic behavior of diamagnetic materials is that the suspectibility is temperature independent. The typical values of suspectibity on the order of 10^{-5} to 10^{-6}. Most of the materials are diamagnetic, including Cu, B, S, N_2 and most organic compounds.

2.1.2 Paramagnetism

Paramagnetic materials possess a permanent dipole moment due to incomplete cancellation of electron spin and /or orbital magnetic moments (unpaired electrons). In the absence of an applied magnetic field the dipole moments are randomly oriented; therefore the material has no net macroscopic magnetization. When a field is applied these moments tend to align by rotation towards the direction of the applied field and the

material acquires a net magnetization [2.1-2.4]. The magnetic moment can be oriented along an applied field to give rise to positive suspectibility, and the values of suspectibility are very small the order of 10^{-5} to 10^{-3}. O_2, NO, Mn and Cr are just a few examples of the paramagnetic materials. The susceptibility of paramagnetic materials is inversely dependent on temperature, which is known as Curie law (Fig.-2.1a).

$$\chi = \frac{C}{T} \quad , \tag{2.1}$$

where C is the Curie constant.

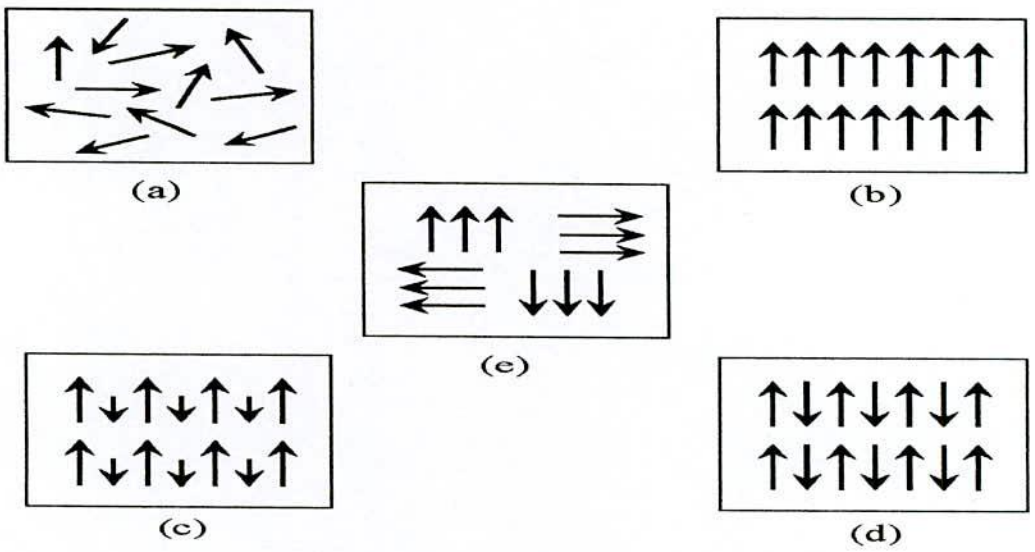

Fig. 2.1 Varieties of magnetic orderings (a) paramagnetic, (b) ferromagnetic, (c) ferrimagnetic, (d) antiferromagnetic and (e) super paramagnetic.

2.1.3 Ferromagnetism

A ferromagnet, like a paramagnetic substance, has unpaired electrons. However, in addition to the electrons intrinsic magnetic moments wanting to be parallel to an applied field, there is also in these materials a tendency for these magnetic moments to want to be parallel to each other. Thus even when the applied field is removed, the

electrons in the material can keep each other continually pointed in the same direction. Every ferromagnetic substance has its own individual temperature, called the Curie temperature, above which it loses its ferromagnetic properties [2.5]. This is because the thermal tendency to disorder overwhelms the energy lowering due to ferromagnetic order. The susceptibility of a ferromagnetic material does not follow the Curie law, but displayed a modified behavior defined by Curie-Weiss law Fig. 2.2 (b)

$$X = \frac{C}{T - \theta} \tag{2.2}$$

where C is a constant and θ is called Weiss constant. For ferromagnetic materials, the Weiss constant is almost identical to the Curie temperature (T_c). The elements Fe, Ni and Co and many of their alloys are typical ferromagnetic materials.

Two distinct characteristics of ferromagnetic materials are:

- Spontaneous magnetization and
- The existence of magnetic ordering temperature (Curie temperature)

The spontaneous magnetization is the net magnetization that exists inside a uniformly magnetized microscopic volume in the absence of a field. The magnitude of this magnetization, at 0K is dependent on the spin magnetic moments of electrons. Spontaneous magnetization is the term used to describe the appearance of an ordered spin state (magnetization) at zero applied magnetic field in a ferromagnetic or ferrimagnetic material below a critical point called the Curie temperature or T_c. This fact led Weiss to make the bold brilliant assumption that a molecular field acted in a ferromagnetic substance below its Curie temperature as well as above and that this field was so strong that it could magnetize the substance to saturation even in the absence of an applied field. The substance is then self-saturating or spontaneously magnetized. Saturation magnetization is an intrinsic property independent of particle size by dependent on temperature. Even through electronic exchange forces in ferromagnets are very large thermal energy eventually overcomes the exchange energy and produces a randomizing effect. This occurs at a particular temperature called the Curie temperature (T_c). Below

the Curie temperature the ferromagnetic is ordered and above it, disordered. The saturation magnetization goes to zero at the Curie temperature.

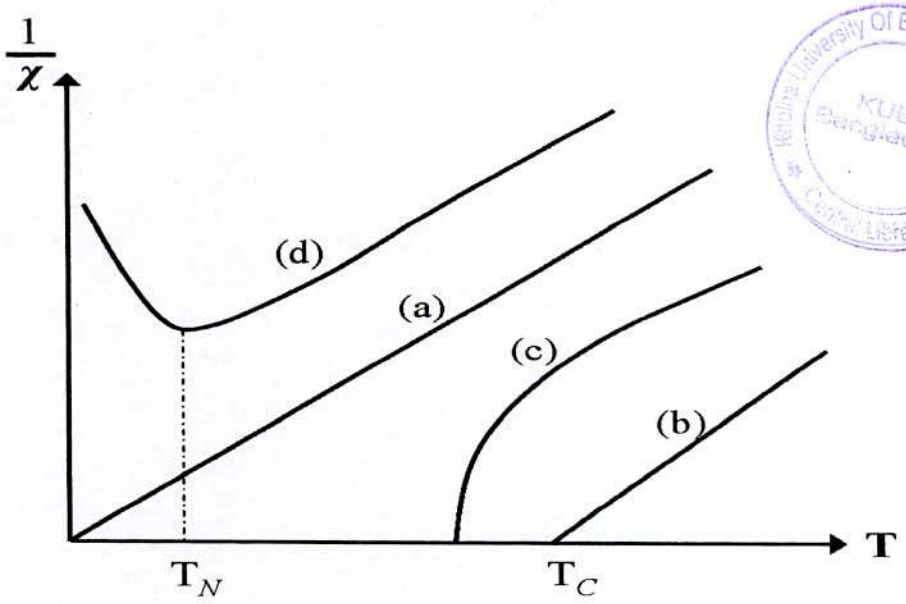

Khulna University Of Engineering & Technology
KUET
Bangladesh
Central Library

Fig.-2.2 The inverse susceptibility varies with temperature T for (a) Paramagnetic (b) Ferromagnetic (c) Ferrimagnetic and (d) Antiferromagnetic materials, T_N and T_C are Neel temperature and Curie temperature, respectively.

2.1.4 Antiferromagnetism

Antiferromagnitism material adjacent magnetic moment parallel to each other without an applied field. In the simplest case adjacent magnetic moments are equal in magnitude and opposite therefore these is no over all magnetization. The natural state makes it different for the material to become magnetized in the direction of the applied field but still demonstrates a relative permeability slightly greater than above a critical temperature known as the Neel temperature the material becomes paramagnetic [2.4]. The antiferromagnetic susceptibility is followed by the Curie-Weiss law with a negative θ

as in the inverse susceptibility as a function of temperature is shown in Fig. 2.1 (d). Common examples of materials with antiferromagnetic ordering include MnO, FeO, CoO and NiO.

2.1.5 **Ferrimagnitism**

Ferrimagnetic material has the aligned magnetic moments are not of the same size; that is to say there is more than one type of magnetic ion. An overall magnetization is produced but not all the magnetic moment may give a positive contribution to the overall magnetization. The magnitude of magnetic moment in one direction defers from that of the opposite directions. As a result a net magnetic moment remains in the absence of external magnetic field the behavior of susceptibility of a ferrimagnrtic material also obeys Curie-Weiss law and has a negative Q as well as in Fig. 2.2(c) while these materials may also demonstrate a relative permeability greater than1, their temperature dependence are not as consistent as with ferromagnetic materials and can result is some very unusual results. Ferrimagnetism is therefore similar to ferromagnetism. It exhibits all the hallmarks to ferromagnetic behavior like spontaneous magnetization, Curie temperature hysteresis, and remanence. However ferro and ferrimagnets have very different magnetic ordering. In ionic compounds, such as oxides, more complex forms of magnetic ordering can occur as a result of the crystal structure. The magnetic structure is composed of two magnetic sub lattices (called A and B) separated by oxygen's. The exchange interactions are mediated by the oxygen anions. When this happens, the interactions are called indirect or super exchange interactions.

2.2 **Theory of Ferrimagnetism**

Ferrimagnetic substances exhibit a substantial spontaneous magnetization at room temperature, just like ferrimagnetics, and this fact alone makes them industrially important. Again like ferrimagnetics, they consist of self-saturated domains, and they exhibit the phenomena of magnetic saturation and hysteresis. Their spontaneous magnetization disappears above a certain critical temperature T also called the Curie

temperature, and then they become paramagnetic. Ferromagnetic were not recognized as forming a distinct magnetic class until 1948. In a classic paper published in 1948, Neel[2.6] provided the theoretical key to an understanding of the ferrites.

The word ferrimagnetisms was coined by Neel to describe the properties of those substances which below a certain temperature exhibit spontaneous magnetization arising from a non-parallel alignment of atomic magnetic moments. In his original paper Neel envisaged a partitioning of the moments into two sub-lattices, which because of their mutual interaction are aligned anti parallel to each other, thus producing a total magnetic moment equal to the difference between their individual magnitudes.

Almost all known ferrimagnetic compounds have rather complex structures, with at least two crystallographically in equivalent sites for the magnetic ions to provide basis for the sub-lattices, but there appears to be no fundamental reason for this, since ordering of the type shown in Fig.-3(b). The temperature at long-range order sets in, now generally known as the Neel point T_N, is determined largely by the strength of the interaction between nearest neighbors, though under special conditions of symmetry other factors may also be important.

This difference can arise in several ways, and some of these are shown diagrammatically in Fig.-2.3. Fig.-2.3(a) shows the case in which there are different numbers of similar magnetic moments in the sub-lattices. In some respects this arrangement superficially resembles that of a normal antiferromagnetic substance with unequal partitioning of the sub-lattices, but many of the properties of such a substance are similar to those of a ferromagnet with a reduced number of magnetic moments. Fig.-2.3(b) shows the case of equal numbers of dissimilar moments. The dissimilarity can arise either because the magnetic ions are chemically different, or because a different local environment leads to different effective magnetic moments in ions having the same spin. So far only the first of these possibilities has been observed. A third type of arrangement is shown in Fig.-2.3(c). This is the case originally considered by Neel and it represents a very large number of substances, including most of the ferrites. In this arrangement one sub-lattice contains two different types of magnetic moment, one of

which also occurs in equal numbers on the second sub-lattice, so that the net effect is that of just the one type of moment. An extension of this case arises when the second sub-lattice also contains two types of moments, as shown in Fig.-2.3(d).

An extension of the Neel theory has been given by Yafet and Kittel (1952) [2.7], who pointed out that if there are strong interactions between the ions within a given sub-lattice, in addition to the interaction between the sub-lattices, then a triangular arrangement such as shown in Fig.-2.3(e)will have a lower energy than the uniaxial Neel type arrangements may then occur (see also Yoshimori 1959, Villain 1959, Bertaut 1960). Obviously such situations can be extended to a large number of variants, involving various three-dimensional multi-spin-axis arrangements.

An alternative type of multi-spin-axis arrangement, which does not seem to have been considered before, arises when there are strong local anisotropy forces tending to hold each spin in a particular direction relative to the crystal sub-lattice. Consider, for example, the simple case of a cubic crystal in which one sub-lattice consists of three types of moment, each of which is bound by some anisotropy forces to one of the three cube axes. Interaction with a second sub-lattice, which we may for simplicity assume to be fee, then produces a compromise arrangement such as shown in Fig.-2.3(f). So far there is no direct experimental evidence for such an arrangement, but it seems very likely that some ferrimagnetic rare earth compounds have this type of arrangement.

In general there is nothing to limit the number of sub-lattices and their direction of alignment, and it is important to realize that the simple arrangements we have discussed are only a first approximation in most real crystals. However, for the explanation of many phenomena the simple Neel theory is often quite adequate.

Several facts led Neel to envisage a distinct form of magnetic structure for the ferrites. Crystallographic studies have provided the clue that the cations in a ferrite crystal occupy two crystallographically different kinds of position called a sites and B sites. Neel

made the basic assumption that the exchange interaction between these two sits is negative, meaning that the spin orientation is opposite to each other. This thing also happens in antiferromagnetism. The difference is that, in case of ferrimagnetism magnitudes of the A and B sublattice magnetizations are not equal and a net spontaneous magnetization results.

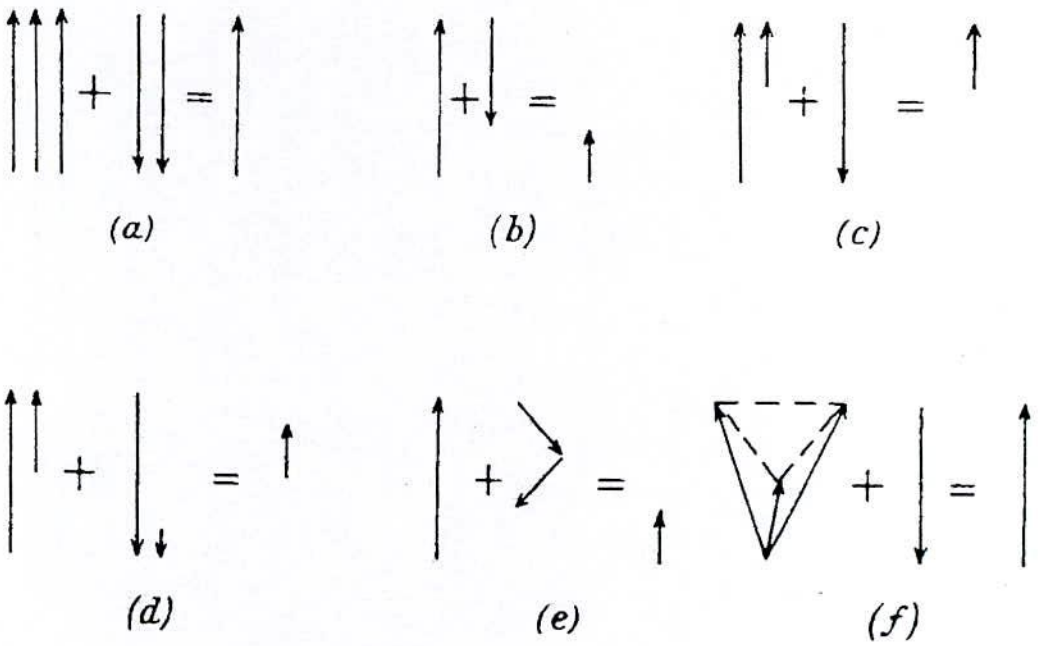

Fig.2.3 Illustration of six simple sub-lattice arrangements which can give rise to a spontaneous ferromagnetic moment.

The exchange interaction acting in ferrites is of a different kind. As pointed out by Neel, the cations are mutually separated by bigger anions (oxygen ions) which practically excludes a direct contact between the cation orbitals, making any direct exchange at least very weak. Instead, we encounter Supper Exchange i.e. indirect exchange via oxygen p orbital that may be strong enough to order the magnetic moments. The strength of this

interaction depends on the degree of orbital overlap of oxygen p orbital and transition metal d orbital. The interaction decreases as the metal ions move apart and the angle between them decreases from 180^0 to 90^0. In Neel's theory, the interaction are taken as effective inter and intra-sublattice interactions A-A , B-B and A-B. The type of magnetic order depends on their relative strength. The theory of super exchange as given by Anderson (1959, 1963) and the semi empirical rules provided by Good Enough (1958) and Kanamori (1959) yield some predictions concerning the sign and strength of this interaction. It is found that A-A interaction is weak compared to B-B interaction. But angle between B-B interaction is 90^0 thus making it weak compared to A-B interaction where angle is 125^0. Thus anti parallel spin alignment takes in two sub lattices. The interaction energy density may be written as

$$U = -2JS_i - S_j \tag{2.3}$$

In the exchange integral, J in equation (2.3) is positive, we achieve ferromagnetism. A negative J may give rise to anti-ferromagnetism or ferrimagnetism. The mean exchange fields acting on A and B sites may be written as

$$\begin{aligned} B_A &= \lambda M_A - \mu M_B \\ B_B &= \mu M_A - \nu M_B \end{aligned} \tag{2.4}$$

All constants λ, μ, v are taken to be positive. The minus sign than corresponds to an antiparallel interaction. The interaction energy density is

$$\begin{aligned} U &= -\frac{1}{2}\left(B_A . M_A + B_B . M_B\right) \\ &= \frac{1}{2}\lambda M_A^2 + \mu M_A M_B + \frac{1}{2}\nu M_B^2 \end{aligned} \tag{2.5}$$

This is lower when M_A is anti-parallel to M_B than when M_A is parallel to M_B. The energy of antiparallel alignment should be compared with zero, because a possible solution is $M_A = M_B = 0$. Thus when

$$\mu M_A M_B \geq \frac{1}{2}\left(\lambda M_A^2 + \nu M_B^2\right) \qquad (2.6)$$

\the ground state will have MA directed opposite to MB. Under certain conditions there may be non-collinear spin arrays of still lower energy.

The susceptibility of ferrimagnets is readily formulated if we assign separate Curie constants CA and CB to the two sublattices. Neglecting intra sublattice interaction we have ferrimagnets:

Sub lattice A	Sub lattice B	
$B_A = -\mu M$	$B_B = -\mu M_A$	
$M_A T = C_A (B_a - \mu M_B)$	$M_B T = C_B (B_a - \mu M_A)$	(2.7)

Here B_a is applied field. These equations have a non zero solution for M_A and M_B in zero applied field if

$$\begin{vmatrix} T & \mu C_A \\ \mu C_B & T \end{vmatrix} = 0 \qquad (2.8)$$

from which the ferrimagnetic Curie temperature $T = \theta_F$ is given by

$$\theta_F = \mu\left(C_A C_B\right)^{1/2} \qquad (2.9)$$

we solve eq^{n}. (2.9) for M_A and M_B to obtain the susceptibility at $T > \theta_F$:

$$x = \frac{M_A + M_B}{B_a} = \frac{(C_A + C_B)T - 2\mu C_A C_B}{T^2 - \theta_F^{\,2}} \tag{2.10}$$

This is more complicated than the Curie – Weiss law for Ferro magnets at $T > \theta_F$.

2.3 Classification of Ferrites and its Relevance

Ferrites are essentially ceramic materials, compound of iron, boron, barium, strontium, lead, zinc, magnesium or manganese. The ingredients are mixed, preferred, milled/crushed, dried, shaped and finally pressed and fired into their final hard and brittle state. Now a days newer family of ferrite materials have been discovered, which are rare-earth types. Additives of rare-earth metals like lanthanum oxide (La_2O_3) are used to study the effect of enhancing the magnetic properties. They are primarily used as permanent magnets. These ferrites are very stable with the excellent characteristic of high resistively.

Ferrites are classified two categories based on their coercive field strength. They are

(i) Soft ferrite with coercive field strength < 10 Oe

(ii) Hard ferrite with coercive field strength > 125 Oe

The unique feature of high coercivity and high-energy product of the hexagonal ferrites is their high uniaxial magnetocrystalline anisotropy about 100 times higher than the soft ferrite with cubic structured. Therefore, hard ferrites constitute the major fraction since they are used where energy per unit eight and cost are important considerations [2.8].

According to the crystallographic structures ferrites fall into three categories

(i) Cubic ferrites of spinel type

(ii) Cubic ferrites of the garnet type and

(iii) Hexagonal ferrites

Ferrites fallen into two groups with different crystal structures are shown in the following block diagram shown in Fig. 2.4

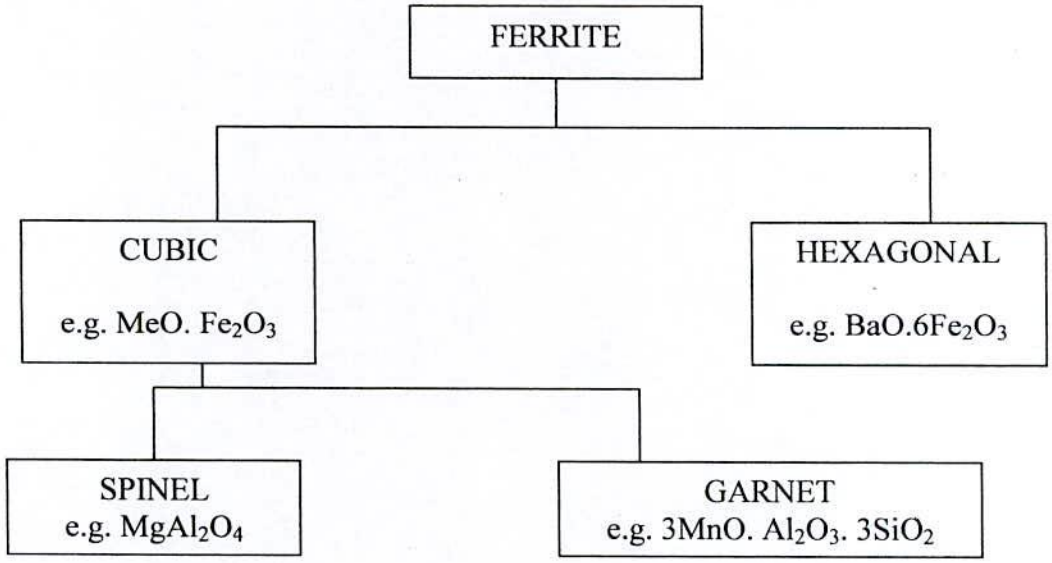

Fig. 2.4 Classification of Ferrites

2.3.1 Soft Magnetic Materials

The wide variety of magnetic materials can be divided into two groups, the magnetically soft and the magnetically hard. Soft magnetic materials are those materials that are easily magnetized and demagnetized. They have low magnetocrystalline anisotropy resulting in reduced coercivity and high permeability. They typically have intrinsic coercivity less than 1000 Am^{-1}. They are used primarily to enhance and/or channel the flux produced by an electric current. The important parameter, often used as a figure of merit for soft magnetic materials, is the high relative permeability (μ_r, where $\mu_r = \frac{B}{\mu_o H}$), which is a measure of how readily the material responds to the applied magnetic field. The other main parameters of interest are the coercivity, the saturation magnetization and the electrical conductivity.

The types of applications for soft magnetic materials fall into two main categories: AC and DC. In DC applications the material is magnetized in order to perform an operation and then demagnetized at the conclusion of the operation, e.g. an electromagnet on a crane at a scrap yard will be switched on to attract the scrap steel and then switched off to drop the steel. In AC applications the material will be continuously cycled from being magnetized in one direction to the other, throughout the period of operation, e.g. a power supply transformer. A high permeability will be desirable for each type of application but the significance of the other properties varies.

For DC applications the main consideration for material selection is most likely to be the permeability. This would be the case, for example, in shielding applications where the flux must be channeled through the material. Where the material is used to generate a magnetic field or to create a force then the saturation magnetization may also be significant. For AC applications the important consideration is how much energy is lost in the system as the material is cycled around its hysteresis loop. The energy loss can originate from three different sources: (1) hysteresis loss, which is related to the area contained within the hysteresis loop; (2) eddy current loss, which is related to the generation of electric currents in the magnetic material and the associated resistive losses and (3) anomalous loss, which is related to the movement of domain walls within the material. Hysteresis losses can be reduced by the reduction of the intrinsic coercivity, with a consequent reduction in the area contained within the hysteresis loop. Eddy current losses can be reduced by decreasing the electrical conductivity of the material and by laminating the material, which has an influence on overall conductivity and is important because of skin effects at higher frequency. Finally, the anomalous losses can be reduced by having a completely homogeneous material, within which there will be no hindrance to the motion of domain walls.

2.3.2 Soft Ferrites

At high frequency metallic soft magnetic materials simply cannot be used due to the eddy current losses. Therefore, soft ferrites, which are ceramic insulators, become the

most desirable material. These materials are ferrimagnetic with a cubic crystal structure and the general composition $MO.Fe_2O_3$, where M is a transition metal such as nickel, manganese, magnesium or zinc. The magnetically soft ferrites first came into commercial production in 1948.

Mn Zn ferrite, sold commercially as ferroxcube, can be used at frequencies up to 10MHz, for example in telephone signal transmitters and receivers and in switch mode power supplies (also referred to as DC-DC converters). For these type of application the driving force to increase frequency is to allow miniaturization.

Additionally, part of the family of soft ferrites, are the microwave ferrites, e.g. yttrium iron garnet. These ferrites are used in the frequency range from 100MHz to 500GHz, for waveguides for electromagnetic radiation and in microwave devices such as phase shifters.

2.3.3 Hard Ferrites

Hard magnets are characterized by high remanent inductions and high coercivities. They generally exhibit large hysteresis losses. Hard ferrite referred to as permanent magnets retain their magnetism after being magnetized. Hard ferrite likes Ba-ferrite, Sr-ferrite, Pb-ferrite are used in communication device operating with high frequency currents because of their high resistivity, negligible eddy currents and lower loss of energy due to Joule heating and hysteresis. These are found useful in many applications including fractional horse-power motors, automobiles, audio- and video-recorders, earphones, computer peripherals, and clocks.

2.3.4 Cubic Ferrites with Spinel Structure

The cubic ferrite has the general formula $MO.Fe_2O_3$ where M is one of the divalent cations of the transition elements such as Mn, Ni, Mg, Zn, Cd, Cu, Co etc. A combination of these ions is also possible and it can be named as solid solution of two

ferrites or mixed spinel ferrites. Generally, M represents a combination of ions which has an average valency of two. The trivalent iron ion in $MO.Fe_2O_3$ can partially be replaced by another trivalent ion such as Al^{3+} or Cr^{3+}, giving rise to mixed crystals. The structure of ferrite is derived from the mineral $MgAl_2O_4$ determined by Bragg [2.9]. These ferrites crystallize in the FCC spinel structure. The spinel lattice is composed of a close-packed oxygen arrangement in which 32 oxygen ions form the unit cell (the smallest repeating unit in the crystal network). These anions are packed in a face centered cubic (FCC) arrangement leaving two kinds of spaces between anions: tetrahedral coordinated sites (A), surrounded by four nearest oxygen atoms, and octahedral coordinated sites (B), surrounded by six nearest neighbor oxygen atoms. These are illustrated in Fig. 2.4. In total, there are 64 tetrahedral sites and 32 octahedral sites in the unit cell, of which only 8 tetrahedral sites and 16 octahedral sites are occupied, resulting in a structure that is electrically neutral [2.10- 2.11].

The localization of ions either in the A or B sites depends fundamentally on the ion and lattice sizes. Also it has been observed to depend on the temperature and the orbital preference for specific coordination. In general, divalent ions are larger than trivalent ions. This is because trivalent ion nuclei produce greater electrostatic attraction, hence their electron orbits contract. The octahedral sites are larger than the tetrahedral sites, thus, the divalent ions are localized in the octahedral sites whereas trivalent ions are in the tetrahedral sites [2.10].

According to the site occupancy of the metal ions, the spinel ferrites are classified as (a) normal spinel; where the tetrahedral (A-sites) are occupied by divalent metal ions and trivalent ions occupy B sites. A majority of these ferrites present paramagnetic behavior, (b) inverse spinel; where all the divalent ions are present in the octahedral site while trivalent ions are located on both A and B sites. The spin moments of the trivalent ions in an inverse spinel are canceled (direction of moment on A sites is opposed to B sites) whereas the spin moments of the divalent ions are aligned, resulting in a net magnetic moment [2.11] and (c) mixed spinel; where divalent ions are present both in tetrahedral and octahedral sites.

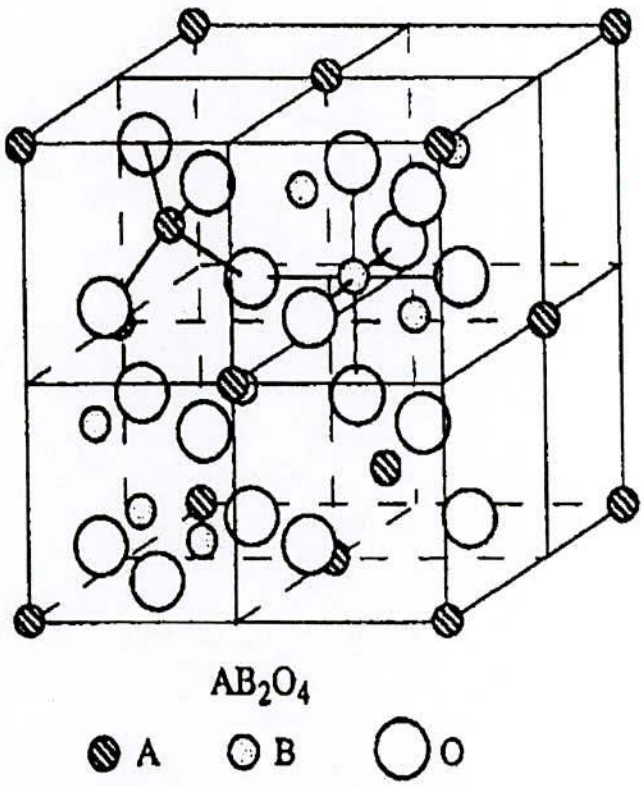

Fig. 2.5 Schematic of two subcells of a unit cell of the spinel structure, showing octahedral and tetrahedral sites

The cubic ferrite is easily magnetized and demagnetized; it has high permeability and saturation magnetization, low electrical conductivity, and the anisotropy energy is dominated by the anisotropy constant K_1. If K_1 is greater than zero, the easy direction is the cube edge direction (100) whereas if K_1 is less than zero, the body direction is preferred (111). For most ferrites the value of K_1 is negative, with the exception of cobalt ferrite [2.10].

2.3.5 Cation Distribution in Spinels

The cation distribution in the spinel $Me^{2+}Me^{3+}O_4$ can be as follows [2.12, 213];

- **Normal**

The Me^{2+} cations are in tetrahedral positions, while the two Me^{3+} cations are in octahedral sites. The square brackets are generally used to represent the octahedral sites, i.e. $Me^{2+}[Me^{3+}]O_4$

- **Inverse**

In this case the Me^{2+} cation and one of the Me^{3+} cations are in octahedral positions while the second Me^{3+} cation occupies a tetrahedral site. The arrangement is as $Me^{3+}[Me^{2+}Me^{3+}]O_4$.

- **Intermediate**

The arrangement of the form like $Me^{3+}_{1-\delta}Me^{2+}_{\delta}\left[Me^{3+}_{1-\delta}Me^{2+}_{1+\delta}\right]O_4$ is often referred as intermediate, where δ is called the inversion parameter. δ = 0.0 for completely normal and δ = 1.0 for completely inverse spinels and 0 <δ <1 for intermediate spinels.

The factors affecting the cation distribution over A and B-sites are as follows [2.12, 2.14];

- the size of the cations
- the electronic configurations of the cations
- the electronic energy
- the saturation magnetization of the lattice

Smaller cations (trivalent ions) prefer to occupy the A-sites. The cations have special preference for A and B-sites and the preference depends on the following factors.

- ionic radius
- size of interstices
- temperature
- Orbital preference for the specific coordination

The preference of cations is according to Verway-Heilman scheme [2.15, 2.16];

- ions with preference for A-sites Zn^{2+}, Cd^{2+}, Ga^{2+}, In^{3+}, Ge^{4+}
- ions with preference for B-sites Ni^{2+}, Cr^{3+}, Ti^{4+}, Sn^{4+}
- Indifferent ions Mg^{2+}, Al^{3+}, Fe^{2+}, Co^{2+}, Mn^{2+}, Fe^{3+}, Cu^{2+}

Moreover the electrostatic energy also affects the cation distribution in the spinel lattice. The cations of the smallest positive charge reside on the B-sites having six anions in surrounding i.e. the most favorable electrostatic conduction.

2.4 Magnetic Properties of Ferrites

Ferromagnetic materials are characterized by a high magnetization (magnetic moments per unit volume) which can be achieved even in polycrystalline materials by the application of relatively small magnetic field. In a ferromagnetic material; the individual atomic (atom with partly filled 3d or 4f shells) or ionic moments arising from unpaired spins are permanent, and interact strongly with one another in a manner which tends to cause parallel alignment of the nearby moments. The moments of a large number of neighboring ions are thus parallel, even in the absence of an applied field. These regions or domains, of spontaneous magnetization exist in both single and polycrystalline materials, and within a domain the value of the saturation magnetization M is the maximum that can be achieved in the material at the given temperature.

The origin of the interaction lies in the so-called quantum mechanical exchange [2.17-2.18], but, in a phenomenological description of magnetism, it is possible to regard that the obliging forces are arising from an internal magnetic field called the Weiss molecular field [2.19]. Weiss assumed that spontaneous magnetization properties disappear at the curie point when the thermal energy is equal to the energy of the individual ionic moment in Weiss induction field then,

$$B_W = kT_c + \mu B_m, \tag{2.11}$$

Where k is Boltzmann constant, T_c is Curie temperature, μ's permeability and B_m is the Weiss molecular field. It is convenient to write $B_m = \mu_0 H$; below the Weiss molecular field H is used. Weiss assumed that the molecular field H_m was proportional to the magnetization M i.e.,

$$H_m = \gamma M, \tag{2.12}$$

where M is the magnetization in the material and γ is the constant of proportionality called molecular field coefficient.

A ferrite may be defined as the one, which below a certain temperature bears a spontaneous magnetization that, arises from non-parallel arrangement of the strongly coupled atomic dipoles. Ferrite is the substance consists of two sublattices with magnetic moments of one sublattice tending to antiparallel to those of other. When the sublattice magnetizations are not equal there will be a net magnetic moment. The term

ferrimagnetism has been used in broad sense in order to include the materials with more then two sublattice and with other spin configurations, such as triangular or spiral configurations. It is usually assumed that a ferrimagnetic material has an appreciable net magnetization, although no precise definition of the term appreciable has been given. The two sublattices are denoted by A and B. If the magnetic moments of the ions at A and B-sites are unequal, this inequality may be due to;

- Presence of elements in different ionic states, e.g. Fe^{3+} and Fe^{2+}
- Different elements in the same or different ionic states, e.g. Fe^{3+} and Co^{2+}
- Different crystalline field acting at two sites.

The competition between the forces on the B spins may lead to the triangular configurations.

2.4.1 Electron Spin

With the concept of electron spin introduce by Goldsmith in 1925 and Uhlenbeck in 1926, the origin of magnetism was explained. Spin corresponds to movement of electric charge in the electron, hence an electric current which produces a magnetic moment in the atom. The net magnetic moment is the vector sum of the individual spin and orbital moments of the electrons in the outer shells [2.20]. Next figure illustrate these two phenomenons:

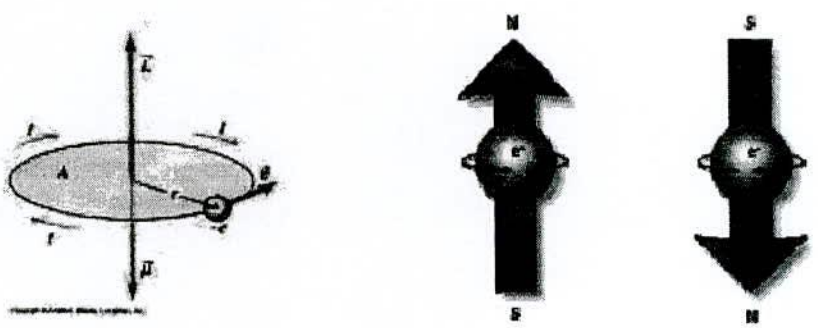

(a) (b)

Fig.2.6 (a) Electron orbit around the nucleus (b) Electron spin

The electron spin can be represented in two modes pointed up or down. In an atom, with opposed paired spins cancel and do not result in magnetic moment, while the unpaired spins will give rise to a net magnetic moment.

2.4.2 Magnetic Dipole

The Earth's magnetic field, which is approximately a magnetic dipole. However, the N- pole and S-pole are labeled here geographically, which is the opposite of the convention for labeling the poles of a magnetic dipole moment

In physics, there are two kinds of dipoles:

• An electric dipole is a separation of positive and negative charges. The simplest example of this is a pair of electric charges of equal magnitude but opposite sign, separated by some (usually small) distance. A permanent electric dipole is called an electrets.

• A magnetic dipole is a closed circulation of electric current. A simple example of this is a single loop of wire with some constant current flowing through it [2.20, 2.21].

2.4.3 Magnetic Field

The magnetic field (B) is a vector field. The magnetic field vector at a given point in space is specified by two properties:

(i) Its direction, which is along the orientation of a compass needle.

(ii) Its magnitude (also called strength), which is proportional to how strongly the compass needle orients along that direction.

The units for magnetic field strength H are ampere/meter. A magnetic field strength of 1 ampere/meter is produced at the center of a single circular conductor with a one meter diameter carrying a steady current of 1 ampere.

2.4.4 Magnetic Moment

A magnet's magnetic moment (μ) is a vector that characterizes the magnet's overall magnetic properties. For a bar magnet, the direction of the magnetic moment points from the magnet's south pole to its north pole, and the magnitude relates to how strong and how far apart these poles are. In SI units, the magnetic moment is specified in terms of A-m^2. A magnet both produces its own magnetic field and it responds to magnetic fields. The strength of the magnetic field it produces is at any given point proportional to the magnitude of its magnetic moment. In addition, when the magnet is put into an external magnetic field, produced by a different source, it is subject to a torque tending to orient the magnetic moment parallel to the field. The amount of this torque is proportional both to the magnetic moment and the external field. A magnet may also be subject to a force driving it in one direction or another, according to the positions and orientations of the magnet and source. If the field is uniform in space, the magnet is subject to no net force, although it is subject to a torque.

2.4.5 Magnetic Moments of Ferrites

The determination of saturation moments of simple ferrites having the formula $Me^{2+}Fe_2^{3+}O_4$ where Me^{2+} is the divalent cation, such as Cu, Co, Ni, Fe, Mn etc. agrees with the Neel's collinear model. The A-B interactions are much larger than the A-A and B-B interactions respectively. The two kinds of magnetic ion forms two sublattices each saturated and magnetized in opposite direction at absolute zero.

Saturation magnetic moments of some selected spinels [2.13] are listed in the Table. (2.1), the first six ferrites are the inverse type i.e $Fe^{3+}[Me^{2+}Fe^{3+}]O_4$. The magnetic moments of the two Fe^{3+} cations compensate each other and the ferrite magnetization becomes equal to M_{Me}^{2+}. Since the theoretical magnetic moment is due to spin only value, the predicted theoretical moment is $M_{Me}^{2+}=2S_{Me}^{2+}$. These values are listed in the Table (2.1) and the experimental and calculated shows good agreement, except cobalt and copper series. The Li ferrite is also completely inverse and its moment is calculated based on the cation distribution $Fe[Li_{0.5}Fe_{2.25}]O_4$ is equal to $2.5\mu_B$, per molecule, is in good agreement with the measured value.

Table- 2.1 Experimental and calculated saturation moments of some spinels

Ferrite	M(μ_B)	2SMe^{2+}(cal.)
$MnFe_2O_4$	5 - 4.4	5
$FeFe_2O_4$	4.2 – 4.08	4
$CoFe_2O_4$	3.3 – 3.9	3
$NiFe_2O_4$	2.3 – 2.40	2
$CuFe_2O_4$	1.3 – 1.37	1
$MgFe_2O_4$	1.1 – 0.86	1.1
$Li_{0.5}Fe_{2.5}O_4$	2.6	2.5

There are two possible reasons for the discrepancies observed between calculated and observed magnetic moments as mentioned in the Table (2.1).

(i) the orbital moments of the divalent ions may not be neglected, the crystal field effects therefore become important.

(ii) the cation distribution must be taken into account.

2.5 Magnetization Process

A review of the magnetization process, namely the response of ferro-(ferri) magnetic material (bulk) to an applied field with a semi-microscopic approach is presented. In ferro-or ferri-magnetic material, the magnetization curves, especially in low magnetic fields differ widely from sample to sample and as a function of the magnetic history of the sample i.e., of the previous fields which have been successively applied.

2.5.1 Magnetization Curve

For unmagnetized bulk material, there is a zero net magnetic moment. It can be predicted that there will be an infinite number of degree of magnetization between the unmagnetized and saturation condition, when the material is subjected to an external magnetic field. These extreme situation correspond respectively, to random orientation of domains complete alignment is one direction with elimination of domain walls. If we

start with the a demagnetized specimen and increase the applied magnetic field, the bulk material will be progressively magnetized by the domain dynamics. The magnetization of the sample will follow the course as shown in Fig 2.7 (2.13). The slope from the origin to a point on the curve or the ratio $\frac{M}{H}$ is defined as magnetic susceptibility. This curve is called Magnetization Curve. This curve is generally perceived as being made of three major portions.

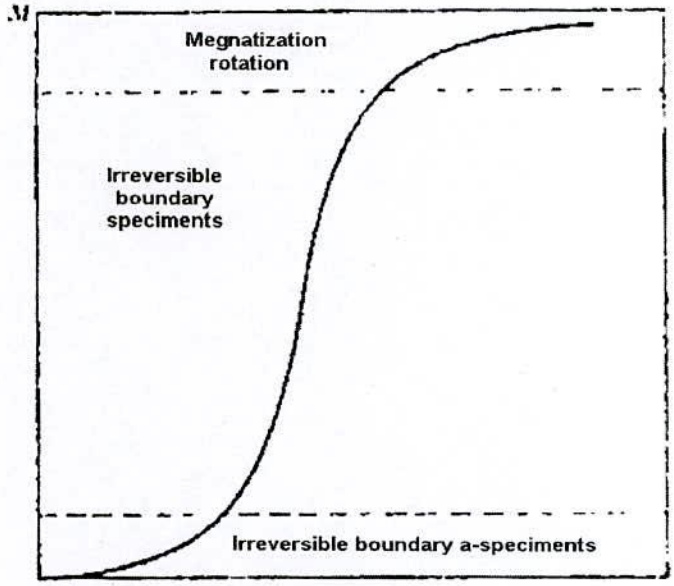

Fig. 2.7 Domain dynamics during various parts of the magnetization curve

The first, the lower section, is the initial susceptibility region and is characterized by reversible domain wall movements and rotations. By reversible means that after the magnetization slightly with an increase in field the original magnetization conditions can be reversed if the field is reduced to initial value. The contribution of the displacement walls to an initial permeability is entirely dependent on the sort of material studied.

In the second stage magnetization curve, if the field is increased, the intensity of the magnetization increases more drastically, is called the irreversible magnetization

range. This range is obtained mainly by the irreversible domain wall motion from one stable state to another.

If the field is increased further, the magnetization curve become less steep and its process become reversible once more. In the third section of magnetization curve, the displacement of domain walls have already been completed and the magnetization take place by rotation magnetization. This range is called rotation magnetization range. Beyond this range the magnetization gradually approaches to saturation magnetization shown in Fig. 2.8.

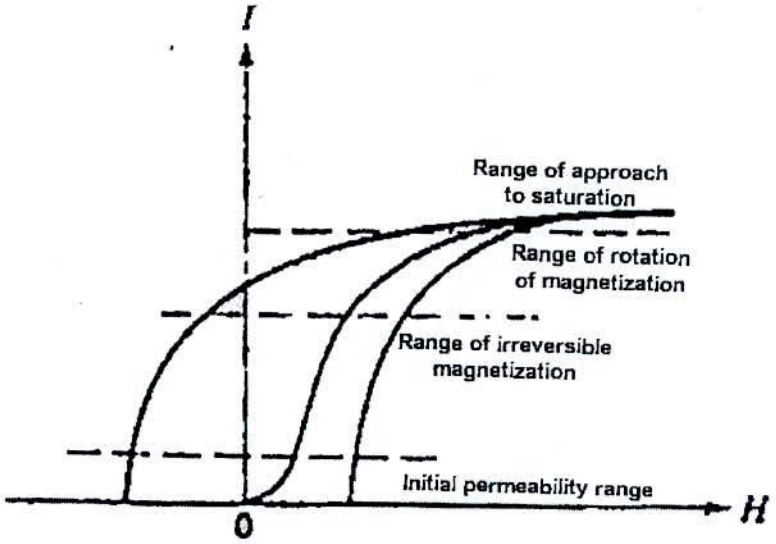

Fig. 2.8 Magnetization curve and the classification of magnetization mechanism

2.5.2 Hysteresis

Magnetic hysteresis is an important phenomenon and refers to the irreversibility of the magnetization and demagnetization process, when a material shows a degree of irreversibility it is known as hysteretic. When a demagnetized ferromagnetic material is placed in as applied magnetic field grows at the expanse of the other domain wall. Such growth occurs by motion of the domain walls. Initially domain wall motion is reversible, and if the applied field is removes the magnetization will return to the initial demagnetized state. In this region the magnetization curve is reversible and therefore

point "b". At this point, it can be seen that some magnetic flux remains in the material even though the magnetizing force is zero. This is referred to as the point of retentivity on the graph and indicates the remanence (B_r) or level of residual magnetism in the material. (Some of the magnetic domains remain aligned but some have lost their alignment). As the magnetizing force is reversed, the curve moves to point "c", where the flux has been reduced to zero. This is called the point of coercivity on the curve (The reversed magnetizing force has flipped enough of the domains so that the net flux within the material is zero).

The force required to remove the residual magnetism from the material is called the coercive force (H_c) or coercivity of the material. As the magnetizing force is increased in the negative direction, the material will again become magnetically saturated but in the opposite direction (point "d"). Reducing **H** to zero brings the curve to point "e." It will have a level of residual magnetism equal to that achieved in the other direction. Increasing **H** back in the positive direction will return **B** to zero. Notice that the curve did not return to the origin of the graph because some force is required to remove the residual magnetism. The curve will take a different path from point "f" back to the saturation point where it with complete the loop.

From the hysteresis loop, a number of primary magnetic properties of a material can be determined.

(i) **Retentivity:** A measure of the residual flux density corresponding to the saturation induction of a magnetic material. In other words, it is a material's ability to retain a certain amount of residual magnetic field when the magnetizing force is removed after achieving saturation. The value of **B** at point "b" on the hysteresis curve.

(ii) **Residual Magnetism** or **Residual Flux:** the magnetic flux density that remains in a material when the magnetizing force is zero. Residual magnetism and retentivity are the same when the material has been magnetized to the saturation point. However, the level of residual magnetism may be lower than the retentivity value when the magnetizing force did not reach the saturation level.

(iii) **Coercive Force:** The amount of reverse magnetic field which must be applied to a magnetic material to make the magnetic flux return to zero. The value of **H** at point "c" on the hysteresis curve.

2.6 Theories of Permeability

Permeability is namely defines as the proportional constant between the magnetic field induction B and applied intensity H:

$$B = \mu H \tag{2.13}$$

If a magnetic material is subjected to an AC magnetic field as given below:

$$H = H_0 e^{i\omega t} \tag{2.14}$$

Then it is observed that the magnetic flux density B experiences a delay. The delay is caused due to presence of various losses and is thus expressed as

$$B = B_0 e^{i(\omega t - \delta)} \tag{2.15}$$

where δ is the phase angle and marks the delay of B with respect to H. The permeability is then given by

$$\mu = \frac{B}{H} = \frac{B_0 e^{i(\omega t - \delta)}}{H_0 e^{i\omega t}} \tag{2.16}$$

$$= \frac{B_0 e^{-i\delta}}{H_0} = \mu' - i\mu'' \tag{2.17}$$

Where $$\mu' = \frac{B_0}{H_0}\cos\delta \tag{2.18}$$

$$\mu'' = \frac{B_0}{H_0}\sin\delta \tag{2.19}$$

The real Part μ' of complex permeability μ as expressed in eq^n. (2.17) represent the component of B which is in phase with H, so it corresponds to the normal permeability. If there is no losses , we should have $\mu = \mu'$, The imaging part μ'' corresponds to the part of B which is delayed by phase angle arranging up to 90° from H . The presence of such a component requires a supply of energy to maintain the alternating magnetization regardless of the origin of delay.

The ratio of μ" to μ' gives

$$\frac{\mu'}{\mu''} = \frac{\frac{B_0}{H_0}\sin\delta}{\frac{B_0}{H_0}\cos\delta} = \tan\delta \qquad (2.20)$$

This tan δ is called the loss Factor or loss tangent. The Q-Factor or quality factor is defined as the reciprocal of this loss factor, i.e

$$Q = \frac{1}{\tan\delta} \qquad (2.21)$$

2.7 Transport Properties

Ferrites are ferromagnetic semiconductors that could be used in electronic devices. The increasing demand for low loss ferrites resulted in detailed investigations on conductivity and on the influence of various substitutions on the electrical conductivity, thermoelectric power, etc. The conduction mechanism in ferrites is quite different from that in semiconductors. In ferrites, the temperature dependence of mobility affects the conductivity and the carrier concentration is almost unaffected by temperature variation. In semiconductors, the band type conduction occurs, where in ferrites, the cations are surrounded by closed pack oxygen anions and as a first approximation can well be treated as isolated from each other. There will be a little direct overlap of the anion charge clouds or orbital. In other words, the electrons associated with particular ion will largely remain isolated and hence a localized electron model is more appropriate than a collective electron (band) model. This accounts for the insulating nature of ferrites. These factors led to the hopping electron model [2.22]. An appreciable conductivity in these ferrites is found to be due to the presence of iron ion ions with different valence states at crystallographically different equivalent lattice sites [2.23]. Conduction is due to exchange of 3d electron, localized at the metal ions, from Fe^{3+} to Fe^{2+}. Various models have been suggested to account for the electrical properties. These are as follows

- Hopping model of electrons
- Small polaron model of electrons

2.7.1 DC Resistivity of Ferrites

Extensive investigation into the origin of the electrical conductivity of the spinels has been carried out by Verwey [2.24] and later on by Van Uitert [2.25] and Jonker [2.45]. The resistivity of ferrites at room temperature can vary , depending on chemical composition between about 10^{-2} to higher than 10^{+11} ohm-cm [2.26]. The low value of resistivity is due to the simultaneous presence of ferrous and ferric ions on equivalent lattice sites (octahedral) as proposed by Verwey [2.24]. For example Fe_3O_4 at room temperature has resistivity of approximately 7×10^{-3} Ohm-cm and Fe_2O_4 with some deficiency in iron and sintered in a sufficiently oxidizing atmosphere so that the product contains no ferrous ions can have a resistivity higher than 7×10^{6} ohm-cm. To make high resistivity ferrites one must sure that there are no ferrous ions in the stoichiometric ferrites.

Temperature dependent resistivity of ferrites follows Arrhenius relation [2.26]:

$$\rho = \rho_0 e^{\frac{E_a}{kT}}, \tag{2.22}$$

Where ρ is the resistively and E_a is the activation energy required for hopping of an electron from one lattice site to another.

2.7.2 AC Resistivity Ferrites

AC resistivity is an important property of ferrites material. Ferrites material has high intrinsic resistivity. It can be changed with change of frequency and temperature.

2.7.3 Conduction Mechanisms

Ferrites are ferrimagnetic semiconductors and exhibit interesting properties that could be used in electronic devices. That is why ferrites attracted the attention of the physicist. The increasing demand for low loss ferrites resulted in detailed investigations on conductivity and on the influence of various substitutions on the electrical conductivity, thermoelectric power, etc.

The conduction mechanism in ferrites is quite different from that in semiconductors. In ferrites the temperature dependence of mobility affects the conductivity and the carrier concentration is almost unaffected by temperature variation. In semiconductors the band type conduction occurs, where in ferrites, the cations are surrounded by closed pack oxygen anions and as a first approximation can well be treated as isolated from each other. There will be a little direct overlap of the anion charge clouds or orbital. In other words the electrons associated with particular ion will largely remain isolated and hence a localized electron model is more appropriate than a collective electron (band) model. This accounts for the insulating nature of ferrites.

These factors led to the hopping electron model [2.27]. An appreciable conductivity in these ferrites is found to be due to the presence of iron with different valence states at crystallographically different equivalent lattice points [2.28]. Conduction is due to exchange of 3d electrons, localized at the metal ions, from Fe^{3+} to Fe^{2+} [2.29]. Assuming that all the Fe^{2+} ions in the B-site to participate in the in hopping transport, the number of charge carriers (n) worked out to be ~ $10^{22}/cm^3$. Since mobility is low, even though n is large.

Many models have been suggested to account for the electrical properties. These are as follows;

(i) Hopping Model of Electrons

(ii) Small Polaron Model

(iii) Phonon Induced Tunneling

2.7.3.1 Hopping Model of Electrons

Jonker [2.30] suggested that in materials like ferrites there is a possibility of exchanging the valency of a considerable fraction of metal ions and especially that of iron ions.

In the presence of lattice vibrations however the ions occasionally come close enough together for transfer to occur with a high degree of probability. Thus only the lattice vibrations induce the conduction and the consequence the carrier mobility shows temperature dependence characterized by activation energy. For such a process of jumping of electrons and holes the motilities are given by;

$$\mu_1 = el_1 f_1 \left[\frac{e^{-\frac{E_1}{k_B T}}}{kT} \right] \text{ and} \tag{2.23}$$

$$\mu_2 = el_2 f_2 \left[\frac{e^{-\frac{E_2}{k_B T}}}{kT} \right], \tag{2.24}$$

where subscripts represent the parameters for electrons and holes, I represent jumping length, f_t and f_2 lattice frequencies active in the jumping process, E_1 and E_2 are activation energies involved in the required lattice deformation.

The general expression for the total conductivity in this case where we have two types of charge carriers can be given as;

$$\sigma = n_1 e \mu_1 + n_2 e \mu_2 \tag{2.25}$$

The temperature dependence of conductivity arises only due to mobility and not due to the number of charge carriers in the sample. It was concluded that for hopping conduction;

- The mobility has a minimum value much lower than the limiting value (0.1 cm^2/Vs) taken as minimum for band conduction [2.31].
- The independence of Seebeck coefficient on temperature is due to fact that in hopping model the number of charge carriers is fixed.
- Thermally activated process with activation energy E_a called hopping activation energy.
- Occurrence of n-p transitions with charge carriers in the Fe^{2+} or oxygen concentration in the system.

2.7.3.2 Small Polaron Model

A small polaron is a defect created when an electronic carrier becomes trapped at a given site as a consequence of the displacement of adjacent atoms or ions. The entire defect (carrier plus distortion) then migrates by an activated hopping mechanism. Small polaron formation can take place in materials whose conduction electrons belong to incomplete inner (d or f) shells which due to small electron overlap, tend to form extremely narrow bands [2.32-2.34]. The migration of small polaron requires the hopping of both the electron and the polarized atomic configurations from one site to an adjacent site. For a fcc lattice the drift mobility takes the form;

$$\mu = (1-c)ea^{\frac{2\Gamma}{kT}} \tag{2.26}$$

where e is the electronic charge, a is the lattice constant, c is the fraction of sited which contain an electron $C = \frac{n}{N}$, n is the number of electrons and N is the jump rate of the polaron from one site to the particular neighboring site given by;

$$\Gamma = P\mu_0 e^{-\frac{E_H}{kT}} \tag{2.27}$$

Here μ_o is the appropriate optical phonon frequency; E_H is the activation energy; p is the probability of the electron transfer after the polarized configuration has moved to the adjacent site. The small polaron model also explains the low mobility, temperature independence of the Seebeck coefficient and thermally activated hopping.

Khulna University Of Engineering & Technology
Central Library

Chapter - III

Experimental Procedure

Chapter-III Experimental Procedure

3.1 Methodology of Ferrite Preparation

The preparation of polycrystalline ferrites with optimum desired properties is still a complex and difficult task. Knowledge and control of the chemical composition, homogeneity and microstructure are very crucial. The ferrite is not completely defined by its chemistry and crystal structure but also requires knowledge and control of parameters of its microstructure such as density, grain size, porosity and their intra and intergranular distribution. It is well known that almost all ferrites decompose at the elevated temperature of we want to melt them under normal conditions. This happens because the oxygen splits off at higher temperature reducing Fe^{3+} and Fe^{2+}. This necessarily implies that ferrite preparation by melting as in case of metals is not possible. The normal methods of preparation of ferrites comprise of the conventional ceramic method or powder metallurgy chemical co-precipitation method and sol-gel method.

In this work conventional ceramic method has been employed for the preparation of Ni-Cu-Zn ferrite samples for its relative simplicity and availability. The excellent powder preparation process and sintering facility available at the magnetic materials division, Atomic Energy Centre, Dhaka has been utilized for the preparation of samples.

3.1.1 Compositions of the Studied Ferrite Systems

In the present research, several compositions of Ni-Cu-Zn soft ferrites are synthesized, characterized and investigated to optimize Fe deficient. General formula of the sample is $(Ni_{0.28}Cu_{0.10}Zn_{0.62}O)\ (Fe_2O_3)_{1-x}$, [where x = 0.00, 0.02, 0.04, 0.06, 0.08]. The properties of Ni-Cu-Zn ferrites are influenced considerably by sintering temperature.

3.1.2 Method of Sample Preparation

The ferrites of different compositions were prepared using ceramic technique involving solid state reaction from metal oxides (NiO, CuO, ZnO and Fe_2O_4) in the from of grained powder having 99.99% purity supplied by GmMH (E-merk, Germany). A series of polycrystalline, samples of mixed ferrites, were prepared by pressing and

subsequent sintering. Different oxides were weighted precisely according to there molecular weight. The weight percentage of the oxide to be mixed for various samples was calculated by using formula

The appropriate weight percentage of each oxide to be mixed for different composition by the following formula:

$$\text{Weight \% of oxide} = \frac{\textit{Molecular weight of oxide} \times \textit{required. weight of the sample}}{\textit{Sum of molecular weight of each oxide in a sample}}$$

The calculated weight of oxide materials, molecular weight of oxides and wt.% calculated for each sample prepared are used for experiments.

3.1.3 Synthesis of Ni-Cu-Zn Ferrites

Ferrites with optimized properties are always demanded delicate handling and caution approach in materials synthesis and appropriate knowledge of thermodynamics control of the chemical composition and homogeneity. There are many processing methods such as solid state reaction method [3.1], high energy ball milling [3.2], sol gel method [3.3], chemical co-precipitation method [3.4], microwave sintering method [3.5], auto combustion method [3.6] etc for the preparation of polycrystalline ferrite materials.

They are mainly divided into two groups.

(i) Conventional Ceramic Method, i.e. Solid State reaction method, involves milling of reactants followed by sintering at elevated temperature.

(ii) Non-conventional method also called wet-method. Among these processes: Sol-Gel synthesis, chemical co-precipitation method, organic precursor method, reverse micelles method, co-spray roasting, activated sintering, etc.

3.1.4 Solid State Reaction Method

This method was used the synthesis of Ni-Cu-Zn ferrites by many researchers [3.6-3.13]. In this method, different metal oxides are mixed and calcined to get ferrite powders.

In the present investigation solid state reaction has been employed for the preparation of Ni-Cu-Zn ferrite samples for its simplicity and availability.

The overall preparation process generally comprised of the following four major steps:

(i) Preparing a mixture of desired composition

(ii) Pre sintering the mixture to form ferrite

(iii) Converting the Raw ferrite into powder and pressing the powder

(iv) Sintering.

The sintering process is irreversible in terms of microstructure, so that constant care could be maintained to keep conditions constant prior to and during sintering. A brief discussion given below will give us the idea about the above mentioned four major steps.

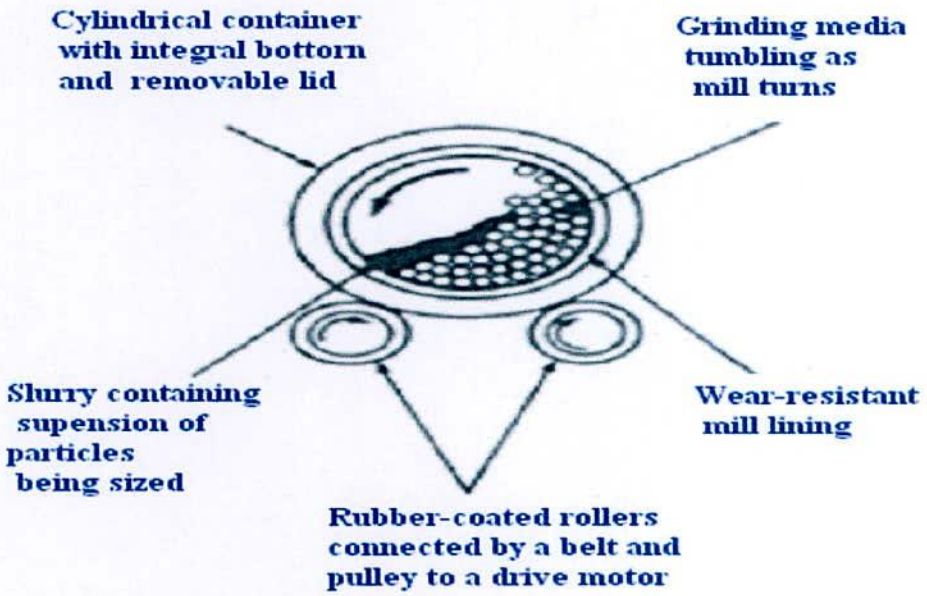

Fig. 3.1 Rubber-lined mill with stainless-steel balls

The constituent in required stoichiometric proportions of materials were thoroughly mixed using ceramic mortar and pestle for 4 hrs and then ball milled in a planetary ball mill in ethyl alcohol media for 2hrs with stainless steel balls of different sizes in diameter Fig. 3.1. The slurry was dried and the powder was pressed into disc shape. The disc shaped sample was pre-sintered at 850°C for 6hrs. The sample was then cooled down to room temperature at the same rate as that of heating. After that samples

shape. The disc shaped sample was pre-sintered at 850°C for 6hrs. The sample was then cooled down to room temperature at the same rate as that of heating. After that samples were crushed again and subsequently wet ball milled for 6hrs hours in distilled water to reduce it to small crystallites of uniform size. In order to produce chemically homogeneous and magnetically better material this prefired lump material was crushed.

Fig. 3.2 Hydraulic press used to make different shaped samples

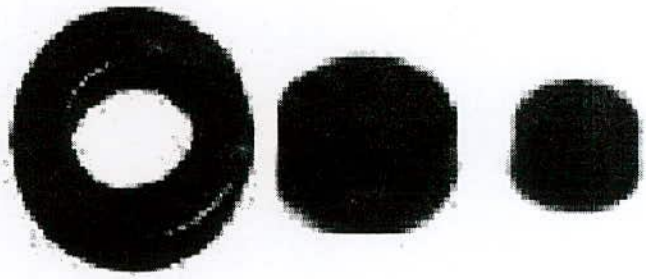

Fig. 3.3 Toroid and disk shape sample

These oxide mixtures were milled thoroughly for 4-6 hours to obtain homogeneous mixture. The mixture was dried and a small amount of saturated solution of polyvinyl alcohol (PVA) were added as a binder and pressed into pellet and toroid shape respectively under pressure 1.75 ton-cm^{-2} and 1.2 ton-cm^{-2} using hydraulic press Fig. 3.2. The prepared samples shown in Fig 3.3 were sintered at 1100°C for 2 hrs with a microprocessor controlled muffle furnace. The samples were polished in order to remove any oxide layer formed during the process of sintering.

3.1.4.1 Preparing a Mixture of Materials

The extend of this work in these step greatly, depending on the starting materials, when component oxide are used, the corresponding step involves a mere mixing of the oxides by wet milling. To avoid iron contamination, mixing is done with stainless steel balls in a steel ball milling machine and a fluid such as distilled water is used to prepare the mixture into slurry. Ferric oxide, Fe_2O_3 and whatever oxides, MO are required are taken in powder form with the captions in the ratio corresponding to that in the final product. Metal carbonate may also be used; during the later firing, CO_2 will be given off and they will be converted to oxides.

3.1.4.2 Pre-sintering the Mixture to Form Ferrite

The slurry prepared in step-1 is dried, palletized and then transferred to a porcelain crucible for pre sintering in a constant temperature of 850°C for $4\frac{1}{2}$ hours. Presintering of the materials was preformed in a furnace named Gallen Kamp at AECD (Atomic Energy Centre, Dhaka). The cooling and heating rates were 4°C/min. The pre-

sintering is very crucial because in this step of sample preparation of ferrite is formed form its component oxides. The solid-state reactions, leading to the formation of ferrites, actually achieved by counter diffusion. This means that the diffusion involves two or more species of ions, which more in opposite direction initially across the interface of two contacting particles of different component oxides.

The following block diagram in Fig. 3.4 represents the method employed for the Ni-Cu-Zn-ferrites

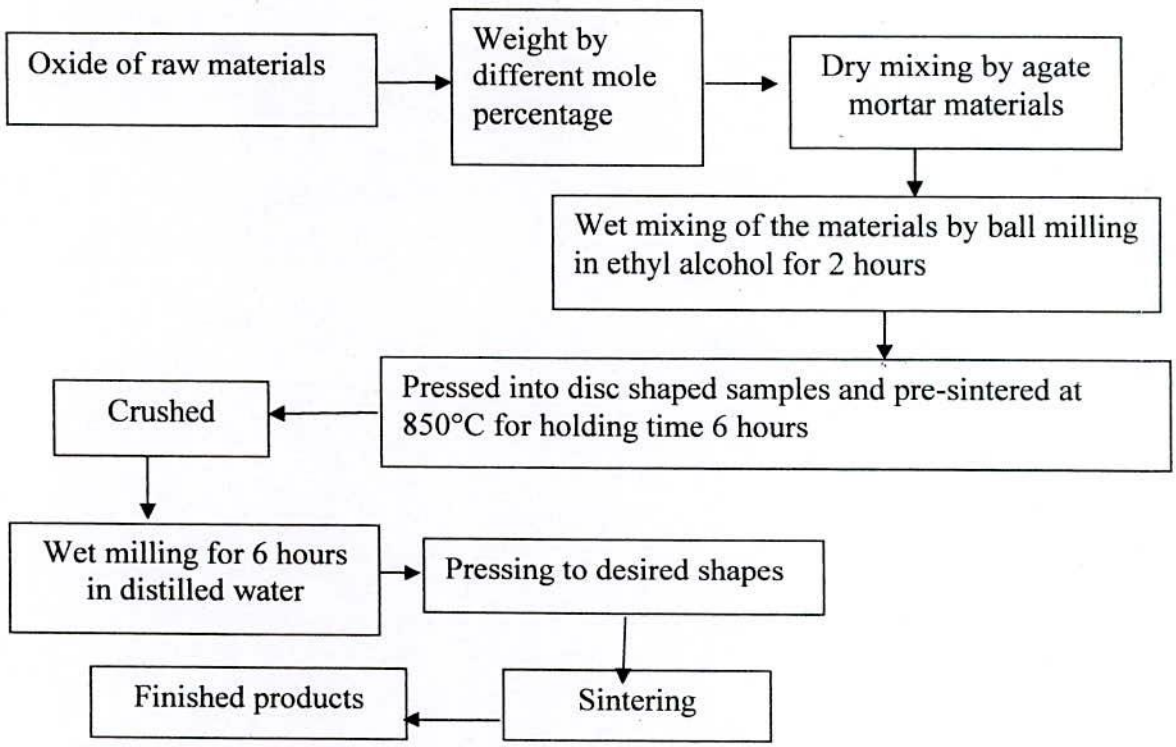

Fig.3.4 Flowchart of ferrite sample preparation

The ferrite is formed essentially in the pre-sintering step but the 'raw' ferrite formed has poor quality. In order to produce chemically homogeneous, dense and magnetically better material of desired shape and size, sintering at an elevated temperature is needed.

3.1.4.3 Converting the Raw Ferrite into Powder and Pressing the Powder

To promote successful sintering in the next step, the powder must be well characterized after grinding with respect to such factors as particle size and distribution particle shape, homogeneity, absorbed gases, impurities and intra particle porosity. Iron contamination due to continuous wear of the mill wall and still ball need to be closely watched and minimized. Now to ground homogeneous powder polyvinyl alcohol is added as a binder. Pressing the powder into compacts of desired shapes is done either by conventional method in a die-punch assembly or by hydrostatic or isocratic compaction. By conventional method in a die-punch assembly a uniformly dense body is difficult owing to the friction gradient of the powder at the walls of the die and between the particles themselves. This problem is some what overcome by the addition of external and internal lubricant to the powder such as a satiric acid.

Mainly, we made three types of samples cylindrical, Tablet and toroidal. Specimen was prepared by a hydraulic press with a pressure at 1 – 10 ton/cm^2 (14 – 140 MPa). The die was designed and made in the workshop of AECD. This is made of nonmagnetic stainless steel.

3.1.4.4 Sintering

Sintering commonly refers to processes involved in the heat treatment of powder compacts at elevated temperatures where diffusion mass transport is appreciable. Sintering is traditionally used for manufacturing ceramic objects, and has also found uses in such fields as powder metallurgy. Successful sintering usually results in a dense polycrystalline solid. However, sintering can proceed only locally (i.e. at contact point of grains), without any appreciable change in the average overall density of a powder compact.

Ceramic processing is based on the sintering of powder compacts rather than melting / solidification / Cold working (Characteristics for metals), because:

(i) Ceramics melt at high temperature

(ii) As solidified microstructures cannot be modified through additional plastic deformation and re-crystallization due to brittleness of ceramics

(iii) The resulting coarse grains would act as facture initiation sites

(iv) Low thermal inductivities of ceramics (< 30 - 50 W/mK), in contract to thermal conductivity not metals (in the range 50 – 300 W/mK) cause large temperature gradients, and thus thermal stress and shock in melting-solidification of ceramics.

This is a heat treatment by which a mass of compacted powder is transformed into a dense object. This is the final and critical step of sample preparation. Sintering is the bonding together of a porous aggregate of particles at high temperature. The thermodynamic driving force is the reduction in the specific surface area of the particles. The sintering mechanism usually involves atomic transport over particle surfaces, along grain boundaries and through the particle interiors. Sintering may result in densification, depending on the predominant diffusion pathway. It is used in the fabrication of metal and ceramic components, the agglomeration of ore fines for further metallurgical processing and occurs during the formation of sandstones and glaciers. Sintering must fulfill three requirements

- to bond the particles together so as to impart sufficient strength to the product
- to density the grain compacts by eliminating the pores and
- To complete the reactions left unfinished in the pre-sintering step.

The theory of heat treatment is based on the principle that when a material has been heated above a certain temperature, it undergoes a structural adjustment or stabilization when cooled at room temperature. The cooling rate plays an important role on which the structural modification is mainly based.

Sintering can be enhanced by the presence of a liquid phase. If the constitution point of an alloy during sintering falls in a solid plus liquid region of the phase diagram, then the liquid persists throughout sintering. Transient liquid phase sintering occurs when the liquid phase is absorbed by the solid phase during sintering. Because the amount of liquid which forms, and the time for which it exists, is dependent on the sintering conditions, transient liquid phase sintering systems are process sensitive. The liquid phase can form directly from the elements when the sintering temperature is between the

melting point of the matrix and the additive, by the melting of eutectic phase mixtures, which form by diffusion or by incipient melting. The liquid flows between the particles filling pores and causing densification by capillary action and through the provision of a fast diffusion pathway. Shrinkage occurs by particle rearrangement if the liquid volume is high enough and the green density is low enough, by the particles changing shape to allow better packing, by pore filling and by solid state sintering if a solid skeleton forms.

Why do we need Sintering?

The principal goal of sintering is the reduction of compact porosity. Sometimes the initial spaces between compacted grains of ceramics are called "voids", to differentiate them from the isolated spaces pores, which occur in the final stages of sintering. Hangs occur in:

i) To bind the particles together so as to impart sufficient strength to the products
ii) To densify the green compacts by eliminating the pores and
iii) To homogenize the materials by completing the reactions left unfinished in the pre-sintering step [3.7]
iv) To make strength of elastic modulus
v) To make hardness and fracture toughness
vi) To make homogenous distribution of grain number, grain size and shape
vii) To improve the average pore size and shape
viii) To get a stable chemical composition and crystal structure

Sintering is a widely used but very complex phenomenon. The fundamental mechanisms of sintering are still a matter of controversy. Experimental quantification of changes in pore fraction and geometry during sintering can be attempted by several techniques, such as: dilatometer, buoyancy, gas absorption, porosimetry, indirect methods (e.g. hardness) and quantitative microscopy etc.

The description of the sintering process has been derived from model experiments (e.g., sintering of a few spheres) and by observing powdered compact behavior at elevated temperatures. The following phenomena were observed:

i) Increase of inter-particle contact area with time

ii) Rounding-off of sharp angles and points of contact

iii) In most cases, the approach of particle centers and overall densification

iv) Decrease in volume of interconnected pores

v) Continuing isolation of pores

vi) Grain growth and decrease in volume of isolated pores

3.2 X-ray Diffraction (XRD)

X-rays are the electromagnetic waves whose wavelength is in the neighborhood of 1Å. The wavelength of an X-ray is that the same order of magnitude as the lattice constant of crystals and it is this which makes X-ray so useful in structural analysis of crystals. X-ray diffraction (XRD) provides precise knowledge of the lattice parameter as well as the substantial information on the crystal structure of the material under study. X-ray diffraction is a versatile nondestructive analytical technique for identification and quantitative determination of various crystalline phases of powder or solid sample of any compound. When X-ray beam is incident on a material, the photons primarily interact with the electrons in atoms and get scattered. Diffracted waves from different atoms can interfere with each other and the resultant intensity distribution is strongly modulated by this interaction. If the atoms are arranged in a periodic fashion, as in crystals, the diffracted waves will consist of sharp interference maxima (peaks) with the same symmetry as in the distribution of atoms. Measuring the diffraction pattern therefore allows us to deduce the distribution of atoms in a material. It is to be noted here that, in diffraction experiments, only X-rays diffracted via elastic scattering are measured.

The peaks in an X-ray diffraction pattern are directly related to the atomic distance. Let us consider an incident X-ray beam interacting with the atoms arranged in a periodic manner as shown in two dimensions in Fig. 3.5. The atoms, represented as spheres in the illustration, can be viewed as forming different sets of planes in the crystal. For a given set of lattice planes with an inter-plane distance of d, the condition for a diffraction (peak) to occur can be simple written as

$$2d \sin n\theta = n\lambda \ , \qquad (3.1)$$

which is known as Bragg's law. In the equation, λ is the wavelength of the X-ray, θ is the scattering angle, and n is an integer representing the order of the diffraction peak. The Bragg's Law is one of the most important laws used for interpreting X - ray diffraction data. From the law, we find that the diffraction is only possible when $\lambda < 2d$ [3.15].

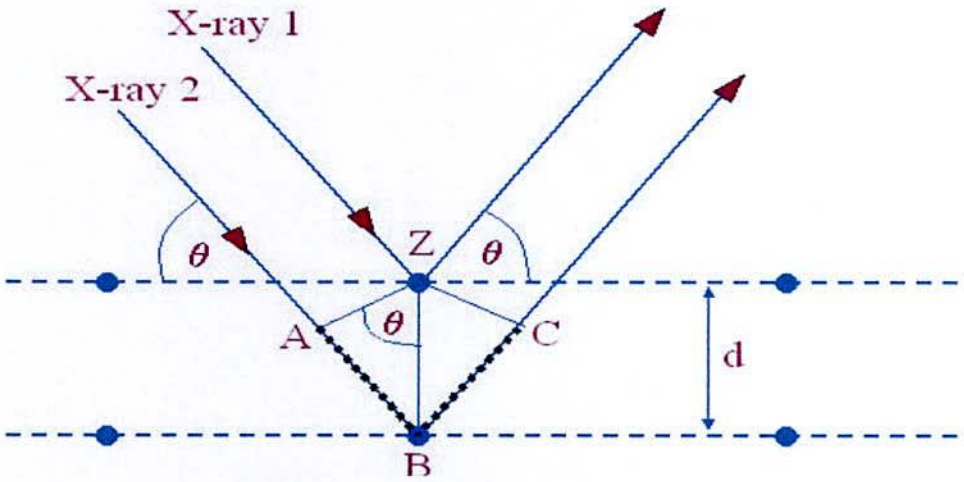

Fig. 3.5 Bragg's diffraction pattern

In the present work, A PHILIPS PW 3040 X'pert PRO X-ray diffractometer was used for the lattice parameter to study the crystalline phases of the prepared samples in the Materials Science division, Atomic Energy Centre, Dhaka. Fig. 3.6 shows the block diagram of X' pert XRD system.

The powder diffraction technique was used with a primary beam powder of 40 kV and 30mA for Cu-K_α radiation. A nickel filter was used to reduce Cu-K_β radiation and finally Cu-K_α radiation was only used as the primary beam. The experimental has been performed at room temperature. A 2θ scan was taken from 15° to 75° to get possible fundamental peaks of the samples with the sampling pitch of 0.02° and time for each step data collection was 1.0 sec. Both the programmable divergence and receiving slits were used to control the irradiated beam area and output intensity from the powder sample, respectively. An anti scatter slit was used just after the tube and in front of the detector to get parallel beam only. All the data of the samples were stored in the computer memory and later on analyzed them using computer "software, X' PERT HJGHS CORE". For XRD experiment each sample was set on a glass slide and fixed the sample by putting adhesive typed the two ends of the sample.

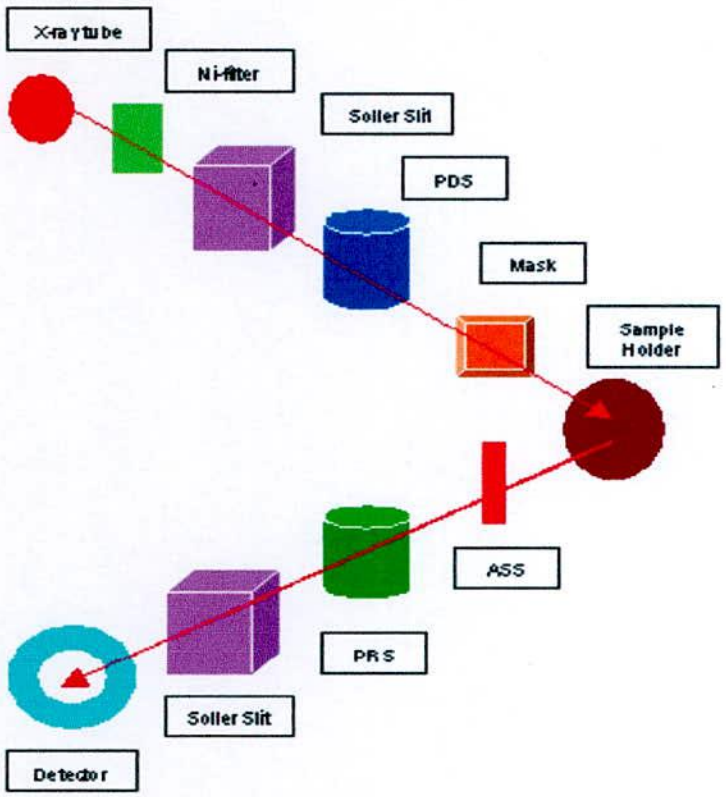

Fig. 3.6 Block diagram of the PHILIPS PW 3040 X' Pert PRO XRD system

For each composition, the cylindrical samples of weight more than 2 gm are converted into powder. For XRD experiment each sample was set on a glass slide and fixed the sample by putting adhesive tape at the two ends of the sample X-ray diffraction patterns were carried out to confirm the crystal structure. Instrumental broadening of the system was determined from θ–2θ scan of standard Si. At (311) reflection's position of the peak, the value of instrumental broadening was found to be 0.07°. This value of instrumental broadening was subtracted from the pattern. After that, using the X-ray data, the lattice constant (a) and hence the X-ray densities were calculated.

3.2.1 Different Parts of the PHILIPS X' Pert PRO XRD System

Fig. 3.7 shows the inside view of the X' pert PRO XRD system. A complex of instruments of X- ray diffraction analysis has been established for both materials research and specimen characterization.

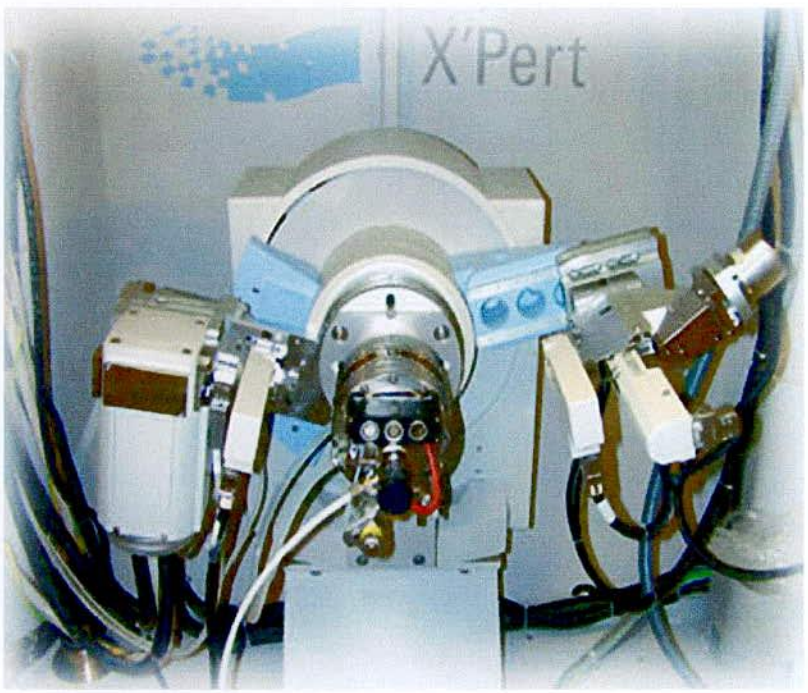

Fig. 3.7 Internal arrangement of a PHILIPS X' Pert PRO X-ray diffractometer

These include facilities for studying single crystal defects, and a variety of other materials problems.

The PHILIPS X' Pert PRO XRD system comprised of the following parts;

(i) "Cu-Tube" with maximum input power of 60 kV and 55 mA,

(ii) "Ni- Filter" to remove Cu-K_α component,

(iii) "Solar slit" to pass parallel beam only,

(iv) "Programmable Divergent slits" (PDS) to reduce divergence of beam and control irradiated beam area,

(v) "Mask" to get desired beam area,

(vi) "Sample holder" for powder sample,

(vii) "Anti Scatter slit" (ASS) to reduce air scattering back ground,

(viii) "Programmable Receiving slit" (PRS) to control the diffracted beam intensity and

(ix) "Solar slit" to stop scattered beam and pass parallel diffracted beam only.

3.2.2 Interpretation of the XRD data

The XRD data consisting of θ_{hkl} and d_{hkl} values corresponding to the different crystallographic planes are used to determine the structural information of the samples like lattice parameter and constituent phase. Lattice parameters of Co-ferrites samples were determined. Normally, lattice parameter of an alloy composition is determined by the Debye-Scherrer method after extrapolation of the curve. We determine the lattice spacing (interplaner distance), d using these reflections from the equation which is known as Bragg's Law.

$$2d_{hkl}\,\mathrm{Sin}\theta = n\lambda$$

$$\text{i.e. } d_{hkl} = \frac{n\lambda}{2\sin\theta} \quad , \tag{3.2}$$

Khulna University Central Library Bangladesh

where λ is the wavelength of the X-ray, θ is the diffraction angle and n is an integer representing the order of the diffraction.

The lattice parameter for each peak of each sample was calculated by using the formula:

$$a = d_{hkl} \times \sqrt{h^2 + k^2 + l^2} \quad , \tag{3.3}$$

where h, k, l are the indices of the crystal planes. We get d_{hkl} values from the computer using software "X' Pert HJGHS CORE". So we got ten 'a' values for ten reflection planes such as a a_1 , a_2 a_3 ..... etc. Determine the exact lattice parameter for each sample, through the Nelson-Riley extrapolation method. The values of the lattice parameter obtained from each reflected plane are plotted against Nelson-Riley function [3.9].The Nelson-Riley function F (θ), can be written as

$$F(\theta) = \frac{1}{2}\left[\frac{\cos^2\theta}{\sin\theta} + \frac{\cos^2\theta}{\theta}\right], \tag{3.4}$$

where θ is the Bragg's angle. Now drawing the graph of 'a' vs. F(θ) and using linear fitting of those points will give us the lattice parameter 'a_0'. This value of 'a_0' at F(θ) = 0 or $\theta = 90°$ .These 'a_0's are calculated with an error estimated to be ± 0.0001Å.

3.2.3 X-ray Density and Bulk Density

X-ray density, d_x was also calculated usual from the lattice constant. The relation between d_x and 'a' is as follows,

$$d_x = \frac{ZM}{Na^3}, \tag{3.5}$$

where M is the molecular weight of the corresponding composition, N is the Avogadro's number ($6.023X10^{23}$ $mole^{-1}$), 'a' is the lattice parameter and Z is the number of molecules per unit cell, (Z = 8 for the spinel cubic structure). The bulk density was calculated considering a cylindrical pellet of mass (m) and volume (V) of the pellets using the relation

$$d_B = \frac{m}{V} = \frac{m}{\pi r^2 h}, \tag{3.6}$$

where m is the mass of the pellet sample, r is the radius and h is the thickness of the pellet.

3.2.4 Porosity

Porosity is a parameter which is inevitable during the process of sintering of oxide materials. It is noteworthy that the physical and electromagnetic properties are strongly dependent on the porosity of the studied samples. Therefore an accurate idea of percentage of pores in a prepared sample is prerequisite for better understanding of the various properties of the studied samples to correlate the microstructure property relationship of the samples under study. The porosity of a material depends on the shape, size of grains and on the degree of their storing and packing. The difference between the bulk density d_B and X-ray density d_x gave us the measure of porosity. Percentage of porosity has been calculated using the following relation [3.10]

$$P = (1 - \frac{d_B}{d_x}) \times 100\% \tag{3.7}$$

3.3 Permeability Measurement

3.3.1 Agilent Precision Impedance Analyzer (Agilent, 4192A)

Curie temperature measurements were done by using Hewlett Packard 4192A LF Impedance Analyzer shown in Fig. 3.8. Impedance parameters absolute value of impedance ($|Z|$), absolute value of admittance ($|Y|$), phase angle (θ), resistance (R), reactance (X), conductance (G), susceptance (B), inductance (L), capacitance (C), dissipation (D) and quality factor (Q). Measurement range of $|Z|$ / R / X is 0.1mΩ to 1.2999 MΩ, $|Y|$/G/B is 1 ns to 12.999 s; θ is -180° to +180°; L is 0.1mH to 1.000 kH; C is 0.1PF to 100.0 mF, D is 0.0001 to 19.999; Q is 0.1 to 1999.9. All have a basic accuracy of 0.1% and resolution of $4\frac{1}{2}$ digits. Number of display digits dependence on measuring frequency and OSC level setting. We made use of the excellent experimental facilities available at the Materials Science Division, Atomic Energy Centre, Dhaka.

Moreover, the 4192A's high measurement performance and capable functionality delivers a powerful tool to circuit design and development as well as materials research and development (both electronic and non electronic materials) environments:

*Accurate measurement over wide impedance range and wide frequency range.

* Powerful impedance analysis function.

* Ese of use and versatile PC connectively.

The following are application examples;

- Impedance measurement of two terminal components such as capacitors, inductors, ferrite beads, resistors, transformers, crystal/ceramic resonators, multi-chip modules or array/network components.

Semiconductor components

- C – r characteristic analysis of varac for diodes.
- Parasitic analysis of a diode, transistor or IC package terminal/leads.
- Amplifier input/output impedance measurement.
- Impedance evaluation of printed circuit boards, relays, switches, cables, batteries etc.

Dielectric materials

- Permittivity and loss tangent evaluation of plastics, ceramics, printed circuit boards and other dielectric material

Magnetic materials

- Permeability and loss tangent evaluation of ferrite, amorphous and other magnetic materials.

Semiconductor material

- Permittivity, conductivity and C – V characteristics of semiconductor materials.

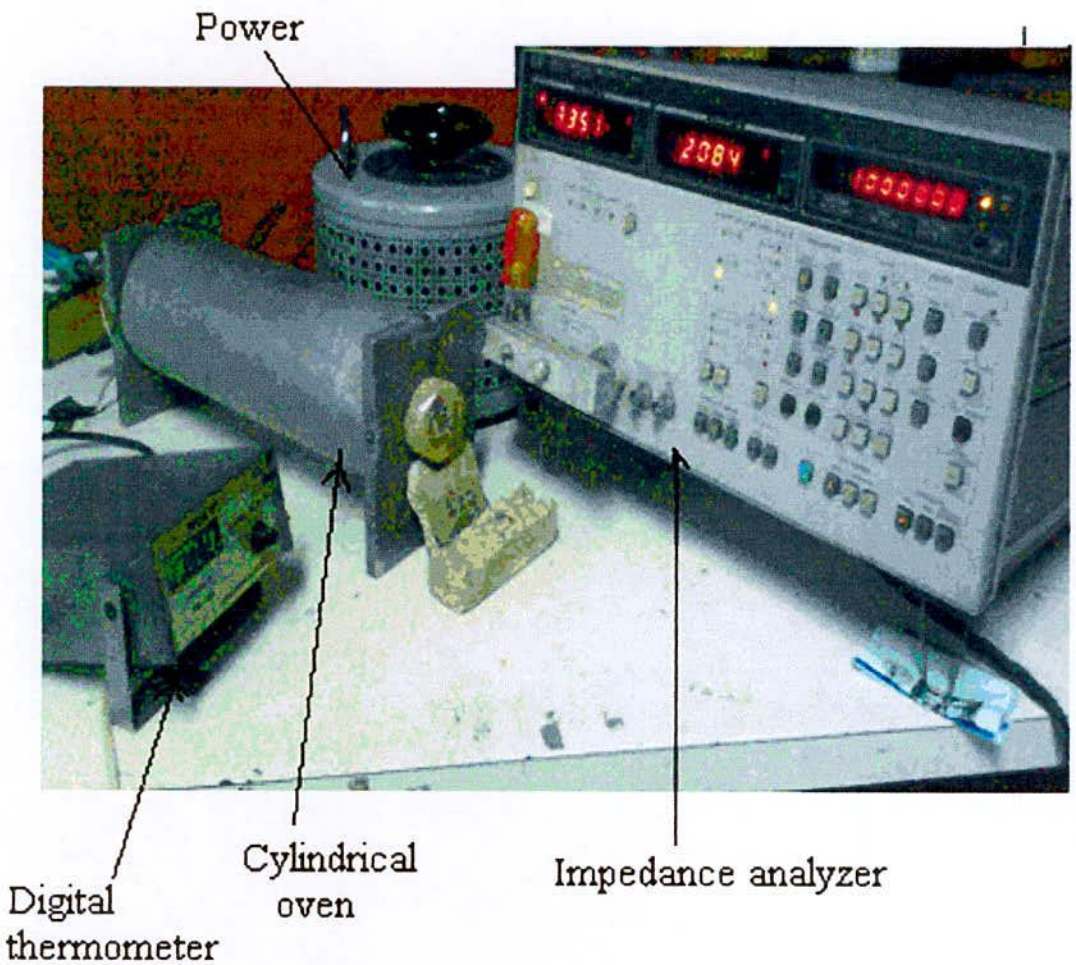

Fig. 3.8 Impedance Analyzer Model-Hewlett-Packard 4192A

3.3.2 Curie Temperature

Curie temperature measurement is one of the most important measurements because it provides substantial information on magnetic status of the substance in respect to the strength of exchange interaction. Above Curie temperature spontaneous magnetization vanishes and ferromagnetic materials behave like paramagnetic materials. So the determination of Curie temperature accurately is of great importance. The temperature dependence properties of ferrite materials depend upon its sublattice distribution and spin orientations of the metal ions and we can predict about the sublattice magnetization by measuring the Curie temperature.

There are several processes of measuring the Curie temperature; these are

(i) by measuring magnetization against temperature,

(ii) by measuring variation of initial permeability against temperature,

(iii) by measuring susceptibility against temperature and

(iv) by measuring the variation of resistivity of the sample against temperature.

In our present research work, we measured the Curie temperature of the samples by observing the variation of initial permeability of the ferrite samples with temperature and magnetization against temperature.

3.3.3 Measurement of Curie Temperature by Observing the Variation of Initial Permeability with Temperature

For ferrimagnetic materials in particular, for ferrite it is customary to determine the Curie temperature by measuring the permeability as a function of temperature. According to Hopkinson effect [3.11] which arises mainly from the intrinsic anisotropy of the material has been utilized to determine the Curie temperature of the samples. According to this phenomenon, the permeability increases gradually with temperature and reaching to a maximum value just before the Curie temperature.

The temperature dependent permeability was measured by using induction method. The specimen formed the core of the coil. The number of turns in each coil was 5. We used a constant frequency (100 kHz) of a sinusoidal wave, AC signal of 100mV. HP 4192A impedance analyzer with continuous heating rate of ≈ 5 K / min with very low applied ac field of ≈ 10^{-3}Oe. By varying temperature, inductance of the coil as a function of temperature was measured. Dividing this value of L_o (inductance of the coil without core material), we got the permeability of the core i.e. the sample. When the magnetic state inside the ferrite sample changes from ferromagnetic to paramagnetic, the permeability falls sharply. From this sharp fall at specific temperature the Curie temperature was determined. For the measurement of Curie temperature, the sample was kept inside a cylindrical oven with a thermocouple placed at the middle of the sample. The thermocouple measures the temperature inside the oven and also of the sample.

The sample was kept just in the middle part of the cylindrical oven in order to minimize the temperature gradient. The temperature of the oven was then raised slowly. If the heating rate is very fast then the temperature of the sample may not follow the temperature inside the oven and there can be misleading information on the temperature of the samples. The thermocouple showing the temperature in that case will be erroneous. Due to the closed winding of wires the sample may not receive the heat at once. So, a slow heating rate can eliminate this problem. The cooling and heating rates are maintained as approximately 0.5°C min^{-1} in order to ensure a homogeneous sample temperature. Also a slow heating ensures accuracy in the determination of Curie temperature.

The oven was kept thermally insulated from the surroundings. The temperature was measured with a digital thermometer attached close to the sample and put inside the furnace where the temperature fluctuation is almost negligible. Then the permeability versus temperature curve was plotted from which the Curie temperature was calculated.

3.3.3 Permeability

From the frequency dependence of complex permeability, evolution of permeability and magnetic loss component at different stages of ferrite sample as affected by thermal treatment at different temperature was determined using toroids shape sample prepared

with insulating Cu wire. The 4192 LF Impedance analyzer directly measure the value of inductance, L and loss factor.

$$D = \tan\delta \tag{3.8}$$

From inductance the value of real part of complex permeability, μ' can be obtained by using the relation

$$\mu' = \frac{L}{L_0}, \tag{3.9}$$

where L is the inductance of the toroid and L_o is the inductance of the coil of same geometric shape in vacuum, L_o is determined by using the relation,

$$L_0 = \frac{\mu_0 N^2 S}{\pi \bar{d}} \tag{3.10}$$

Here μ_o is the permeability of the vacuum, N is the number of turns (here N = 5), S is the cross-sectional area of the toroid shaped sample, S = dh, where, $d = \frac{d_1 \sim d_2}{2}$ and $\bar{d}$ is the average diameter of the toroid sample given as

$$\bar{d} = \frac{d_1 + d_2}{2}, \tag{3.11}$$

where, d_1 and d_2 are the inner and outer diameter of the toroid samples.

3.3.4 Mechanisms of Permeability

Mechanisms of permeability can be explained as the following way: a demagnetized magnetic material is divided into number of Weiss domains separated by block walls. In each domain all the magnetic moments are oriented in parallel and the magnetization has its saturation value M_s. In the walls the magnetization direction changes gradually from the direction of magnetization in one domain to that in the next. The equilibrium

positions of the walls results from the interactions with the magnetization in neighboring domains and from the influence of pores; crystal boundaries and chemical in homogeneities which tend to favor certain wall positions.

3.3.5 Technique of Measurements of Permeability

Measurements of permeability normally involve the measurements of the change in self inductance of a coil presence of the magnetic core. The behavior of a self inductance can now be described as follows. Suppose we have an ideal lossless air coil of inductance L_o. On insertion of magnetic core with permeability μ, the inductance will be μL_o. The complex impedance Z of this coil can be expressed as,

$$Z = R + jX = j\omega L_o(\mu' - j\mu''), \tag{3.12}$$

where the resistive part is

$$R = \omega L_o \mu', \tag{3.13}$$

and the reactive part is

$$X = \omega L_o \mu'' \tag{3.14}$$

The radio frequency (RF) permeability can be derived from the complex impedance of a coil Z (Eq^n. 3.12). The core is usually toroidal to avoid demagnetization effects. The quantity L_o is derived geometrically.

3.3.6 Frequency Characteristic of Ferrite Samples

The frequency characteristics of the cubic ferrite sample i.e. the permeability spectra were investigated using a Hewlett Packard Impedance Analyzer of Model No.4192A provide the value of inductance, L and loss factor, D = tanδ. The measurements of inductances were taken in the frequency range of 1 kHz to 13 MHz. The values of measured parameters obtained as a function of frequency and the real (μ') and imaginary

part (μ'') of permeability and the loss factor are calculated. μ' is calculated by using the Eq^n.3.9 and Eq^n.3.10 and μ'' is calculated by using the following equation

$$\mu'' = \mu' \tan\delta \qquad (3.15)$$

3.4 Low Field Hysteresis graph

Hysteresis is well known in ferromagnetic materials. When an external magnetic field is applied to a ferromagnet, the atomic dipoles align themselves with the external field. Even when the external field is removed, part of the alignment will be retained: the material has become magnetized.

A general view of the B - H loop tracer with its system components is shown in Fig. 3.9. A hysteresisgraph or B - H Meter allows for the magnetic properties of soft magnetic materials to be measured. A schematic diagram of commercial hysteresisgraph has been presented Fig. 3.10. A hysteresisgraphhas two major functions. It produces current to produce a magnetic field, and measures voltage over time to measure magnetic induction. By determining the induction response of the test sample to the applied current, the magnetic properties of the material is determined. Most soft magnetic materials are measured using ring geometry. Two coils of wire are wound around the sample.

A current from a bi-polar power supply is passed through the primary coil to generate a magnetic field in the ring. The applied magnetic field is proportional to the current. As the sample magnetic induction changes in response to the applied magnetic field, a voltage is induced in the secondary windings. This induced voltage is integrated over time with a circuit often called a fluxmeter, as it is used in many applications to measure magnetic flux. The integrated voltage is proportional to the magnetic induction of the test samples. The current in the primary coil is determined by measuring the voltage across a resistor. All the data of the samples were analyzed using computer software to control the applied field and measure both B and H simultaneously.

Fig. 3.9 B - H loop tracer

3.4.1 Measurement of an Initial B - H Curve

As these are important curves for magnetic design, these curves are measured using a hysteresis graph. For accurate initial curves, the sample must be demagnetized prior to the measurement. This demagnetization can be performed either externally, or in many cases, the sample can be demagnetized by the hysteresis graph. Residual magnetization can greatly distort the response of a soft magnetic material near zero field.

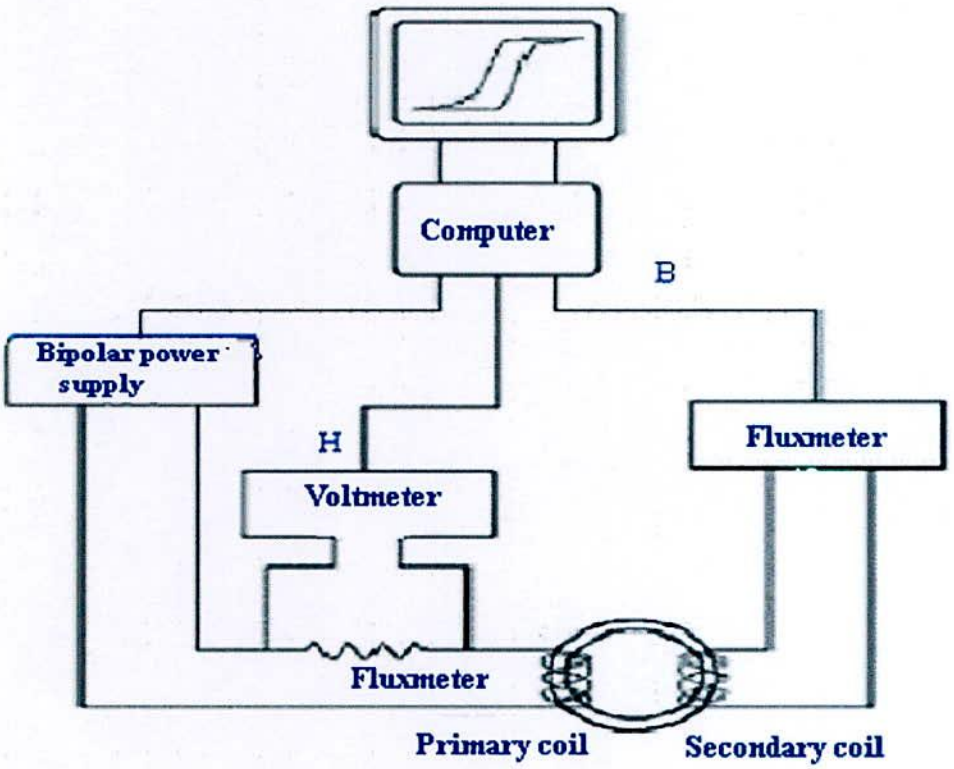

Fig. 3.10 Schematic diagram of commercial hysteresis graph

3.4.2 AC B - H Curve Measurement

In many applications, soft magnetic materials are subjected to cyclical magnetic field. The response of a soft magnetic material can be very complicated in this case, and is determined by both material parameters, such as sample permeability and material geometry. It can be exceedingly difficult to make accurate predictions of material performance through computer models. Therefore, the best way to determine the performance of these materials is to measure the B – H curve under cyclical applied magnetic fields. This can be performed using a hysteresis graph. The bi-polar power is driven at the test frequency, and the fluxmeter can measure the varying magnetic induction of the material. The resulting BH-curves are called AC B – H curves, and yield important information in regards to the material such as AC permeability and core loss.

For these types of measurements, it is important that the hysteresis graph components have the appropriate frequency response to measure the AC B – H curve properly.

3.4.3 Materials Geometry

The AMH-series permeameter measures characteristics of soft magnetic materials, according to the IEC 60404-4 and IEC 60404-6 standards. The ideal sample geometry of soft magnetic material is a ring. Thus shape is preferable because ring shape eliminates factors that can distort the magnetic test results. The main source of distortion of test data on soft magnetic materials is usually from air-gaps present in the magnetic test circuit. These air gaps lower the apparent permeability of the material, and can be difficult to control. As ring geometry is continuous path, the magnetic circuit is closed, without any air gaps that cause distortion. In addition, the magnetic path length, which is required to convert the applied current in the sense windings into applied magnetic field, is easy to calculate an unambiguous for ring samples. In ring shaped samples, primary winding are wound on the ring to generate a magnetic field in the sample via applied current to the primary windings. A secondary coil is also wound onto the ring to inductively measure the magnetic induction of the sample. If this machining process is on a sample must be form of ring can be made in different methods:

(i) made as an unique dense piece of material, obtained by mechanical works or by casting, sintering, etc.

(ii) made by stacking several disks with the same internal and external diameter, that can be obtained by punching, laser cutting, etc.

(iii) made by a unique thin strip wound as a clock-spring.

The external diameter D_e should be higher than 1.4 times the internal diameter D_i. The cross section A of the sample is calculated by the geometrical relation

$$A = \frac{(D_e - D_i)h}{2}, \tag{3.16}$$

where h is the thickness of the sample. The thickness can be measured normally with a gauge if the sample is a solid ring. If it is made by stacked rings, sometimes it is preferred

to use the mass and the density, calculating the thickness h with the formula:

$$h = \frac{4m}{\rho\pi(D_e^2 - D_i^2)}, \tag{3.17}$$

where ρ is the density of the material.

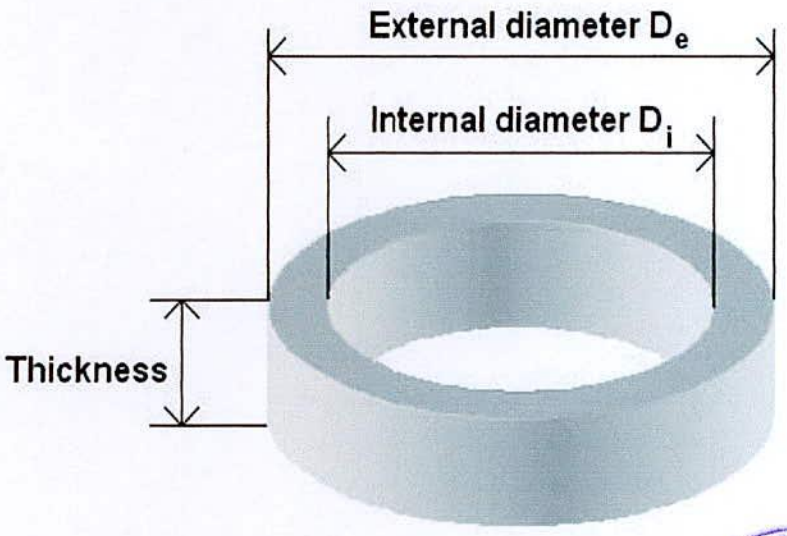

Fig. 3.11 Sample geometry

Khulna University of Engineering & Technology
Khulna
Bangladesh
Central Library

3.4.4 Windings

In these instances accurate magnetic measurements can still be performed, since the sample geometry creates a closed magnetic circuit. For these measurements, primary and secondary coils are wound onto the sample, as with ring measurement. The magnetic path length of the test circuit must be either determined or known in order to convert the applied primary current into applied magnetic field.

Two types of windings are necessary for the measure:

(i) Magnetization winding (N_H number of turns) and

(ii) Measuring winding (N_B number of turns)

The magnetization winding consists of a suitable number of turns N_H in which flows the magnetization current, *i*. The current produces the magnetic field H following the

relationship:

$$H = \frac{N_H i}{l_m} \quad , \tag{3.18}$$

where l_m is the mean magnetic path length. If D_e does not exceed D_i more than 10 %, we can approximate l_m with the mean circumference:

$$l_m = \pi \frac{D_e + D_i}{2} \tag{3.19}$$

If $D_e >> D_i$, then it is preferable to use the

$$l_m = \pi \frac{D_e - D_i}{\ln(\frac{D_e}{D_i})} \tag{3.20}$$

The value of l_m is automatically calculated by the software.

The magnetic flux induced in the sample under test is measured using a computer-controlled integrating fluxmeter attached to the secondary winding. The secondary winding produces the induced voltage V_2 from which the magnetic flux Φ is obtained:

$$\Phi = - \int V_2 dt \, , \tag{3.21}$$

The integrating fluxmeter is the preferred method of measuring induced magnetic flux when the H field is being varied at frequencies from DC (typically 0.01Hz) to 10 kHz and numerically by the computer controlled software for AC measurements. The common method for implementing an electronic integrator consists of a DC amplifier with resistive–capacitive feedback and the magnetic induction, B is then obtained by the flux by the relationship:

$$B = \frac{\Phi}{N_B A} \quad , \tag{3.22}$$

3.4.5 DC Measurement

DC measurements are made using a field that change very slowly, and that can be considered quasi-static. Since the variation of H, and in general the variation of B, is very slow, the inducted voltage is very small, and a numerical integration will give inaccurate results. The integration of the inducted voltage is performed by the flux meter, which is more precise and can follow very well the variation of B at such slow rate. After winding, the ring must be connected to the flux meter through the special cable for DC measure shown in Fig.3.12. This cable is simply an extension that takes signal from measuring connection to flux meters inputs. For devices with two flux meters, use the $\left(\frac{B}{J}\right)$ flux meter. This flux meter is then connected by the analog output (in the back panel) to the PC boards. A 4-poles connector permits the connection to auxiliary optional devices connect the H-turns to magnetization connectors and the B turnc in the connection in DC cable. Then connect the other terminals to the flux meter shown in Fig 3.13. The sample put on the fan grid.

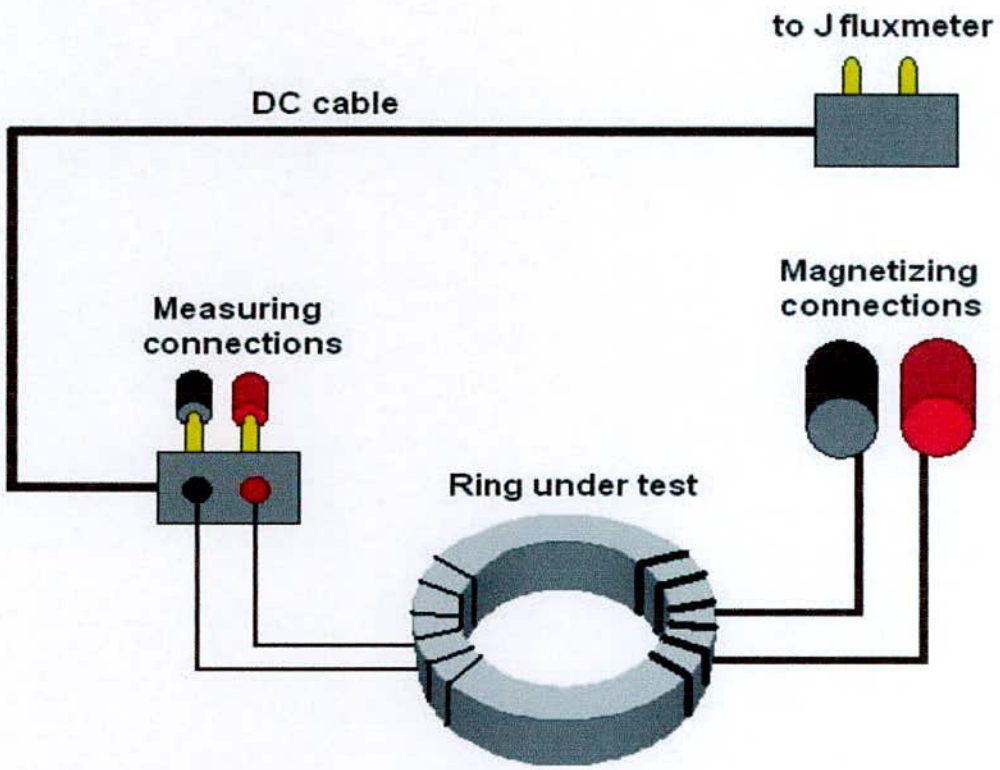

Fig. 3.12 DC measuring cable

AC/DC hysteresis graph for hard and soft magnetic materials of the prepared samples measured AMH-1K-1800-HS B-H loop tracer in the Materials Science division, Atomic Energy Centre, Dhaka. In DC conditions, H and B are always in phase, and the max value of H corresponds to the max value of B. The Hysteresis cycle always has some sharp vertex. The DC normal magnetization curve is the set of all the vertex of different amplitude. The ratio between B and $\mu_0 H$ is a ratio between two simultaneous values, and it is called relative permeability.

3.5 Transport Property

3.5.1 DC and AC Resistivity

Resistivity is an intrinsic property of a material .The technical importance of ferrites lies primarily in their high resistivity. Technical ferrites are resistivity of 1 to 10^{12} Ω-cm. In magnetic material to low resistivity gives raise T_c eddy current losses. The losses are inversely proportional to the resistivity. So measurement of resistivity is very crucial for ferrite material. The electrical resistivity measurements carried out by a two probe method on silver painted sample a Keithley Electrometer using pellet samples of diameter 8.3-8.8mm and of thickness 1.2 - 2.5 mm by applying silver electrodes on the surfaces. Samples were prepared by sintering the samples at 1100°C to 1200°C for Ni-Cu-Zn ferrites for 3hours. The samples were polished using metallurgical polishing machine with the help of silicon carbide papers with grit size 600. After that the samples were clean with acetone and then again polished with special velvet type polishing cloth named as α-gam, for finer polishing using fine alumina powder of grain size 0.05 micron dispersed in a liquid.

The powders were of various sizes starting with 1 micron to 0.05 micron. Samples are then cleaned in a ultrasonic cleaner and dried in surface at 150°C for several hours. Then the samples are again cleaned with acetone and silver paste was added to both the sides of the polished pellet samples together with two thin copper wires of 100 micron diameter for conduction. Again the samples are dried at 150°C to eliminate any absorbed moisture.

The DC and AC resistivity were measured as a function of frequency in the range 1 kHz-13MHz at room temperature by Electrometer Keithley model 6514 and impedance analyzer. The electrical resistivity has been calculated using the formula:

$$\rho = \frac{RA}{l} = \frac{\pi r^2 R}{l}, \quad \left[\because A = \pi r^2\right] \tag{3.23}$$

where R is the resistance of the Pellet, r is the radius of the pellet and l is the thickness of the pellet . Sintered ferrite pellet specimens were used to determine resistivity. Electrodes were painted on the surface of the sample using a conducting silver paste. The AC resistivity ρ was calculated using the formula

$$\rho = \frac{1}{\omega \varepsilon_0 \varepsilon' \tan\delta} = \frac{A}{2\pi f \tan\delta C t}, \tag{3.24}$$

Where ε_0 is the permittivity of free space, ε' is relative dielectric constant, tanδ is the dissipation or loss factor, ω is the angular frequency, C is the capacitance, A and t are the area and thickness of the sintered pellet respectively.

Ferrites are semiconductors and their resistivity decreases with increasing temperature according to the relation

$$\rho = \rho_\alpha e^{E_p / KT}, \tag{3.25}$$

where K the Boltzmann constant, T is the absolute temperature, E_p represents an activation energy which according to Verway and De Boer is the energy needed to release an electron from the ion to jump to the neighboring ion, thus giving rise to electrical conductivity. If we plot log ρ vs $\frac{1}{T}$ for various ferrites, a straight line is found in a wide temperature range with a slope corresponding to E_p according to the relation

$$E_p = 0.198 \times 10^{-3} \frac{d(\log \rho)}{d(1/T)} \tag{3.26}$$

3.5.2 Dielectric Properties

Ceramics are mostly covalently bonded material hence electrically non conductive or insulator. Importance of particular property depends on the application demand. For instance, dielectric strength is an important parameter for application of ceramic as insulators used in power transmission line, load bearing general insulators, in house hold appliances etc. In this kind of applications where frequency do not exceed

1kHz, the break down strength, measured in kV/cm, together with mechanical strength are important factors. The dielectric constant (ε') or loss factor (ε'') does not matter much. On the other hand, for capacitors and electronics application just the opposite required. The values of ε' and ε'' are of prime importance, not only their room temperature values but also as function of frequency. These are intrinsic properties of material, especially of polycrystalline ceramic can be modified by doping, micro structural variation.

3.5.2.1 Dielectric Constant

Dielectric constant measurements were done by using WAYNE KERR INDUCTANCE ANALYZER 3255B. The overall dielectric constant (ε') of an insulator material as given by the relation:

$$D = \varepsilon_0 E = \varepsilon_0 \varepsilon' E \tag{3.27}$$

D represents the electric displacement, E the electric field in the dielectric, ε' the dielectric constant and ε_0 permitivity of the vacuum. The electric displacement describes the extent to which the electric field has been altered by the presence of the dielectric material. The dielectric constant ε' is an intrinsic property of a material and a measure of the ability of the material to store electric charge relative to vacuum.

It is measured directly from the capacitance of a capacitor in which the material is used as electrode separator or dielectric. The capacitive cell, the dielectric constant (ε'), total charge (q) and capacitance © can be developed as follows:

$$\varepsilon' = \frac{D}{\varepsilon_0 E} = \frac{\frac{Q}{A}}{\frac{\varepsilon_0 V}{d}} \tag{3.28}$$

$$\therefore Q = \frac{\varepsilon_0 \varepsilon' A V}{d} = CV \tag{3.29}$$

Where $C = \frac{\varepsilon_0 \varepsilon' A}{d}$ (3.30)

Here A represents the area of the capacitive cell, d its thickness, C is the capacitance of the material, V the voltage across the cell and $\varepsilon_0\left(\frac{F}{m}\right)$ the material permittivity in vacuum.

Thus ε' represents the ratio of the permittivity or charge storage capacity relative to air or vacuum as dielectric

$$\varepsilon' = \frac{cd}{\varepsilon_o A}, \tag{3.31}$$

where c is the capacitance of the pellet in Farad, d the thickens of the pellet in meter , A the cross-sectional area of the flat surface of the pellet in m^2 and ε_o the constant of permittivity for free space. Dielectric measurement as a function of frequency in the range 100Hz-13MHz at room temperature were carried out by using Hewlett Packrat impedance analyzer in conjunction with a laboratory made furnace which maintain the desired temperature with the help of a temperature controller.

3.6 Magnetization Measurement Techniques

In the present study magnetization has been performed using a Vibrating Sample Magnetometer (VSM).

3.6.1 Vibrating Sample Magnetometer (VSM)

A vibrating sample magnetometer (VSM) operates on Faraday's Law of Induction, which tells us that a changing magnetic field will produce an electric field. This electric field can be measured and can tell us information about the changing magnetic field. A VSM is used to measure the magnetic behavior of magnetic materials. Vibrating Sample Magnetometer is a versatile and sensitive method of measuring magnetic properties developed by S. Foner [3.12] and is based on the flux change in a coil when the sample is vibrated near it. The Vibrating Sample Magnetometer (VSM) is designed to continuously measure the magnetic properties of materials as a function of temperature and field. In this type of magnetometer, the sample is vibrated up and down in a region surrounded by several pickup coils. The magnetic sample is thus acting as a

time-changing magnetic flux, varying inside a particular region of fixed area. From Maxwell's law it is known that a time varying magnetic flux is accompanied by an electric field and the field induces a voltage in pickup coils. This alternating voltage signal is processed by a control unit system, in order to increase the signal to noise ratio. The result is a measure of the magnetization of the sample.

3.6.2 Principle of VSM

If a sample is placed in a uniform magnetic field, created between the poles of a electromagnet, a dipole moment will be induced. If the sample vibrates with sinusoidal motion a sinusoidal electrical signal can be induced in suitable placed pick-up coils. The signal has the same frequency of vibration and its amplitude will be proportional to the magnetic moment, amplitude, and relative position with respect to the pick-up coils system. Fig 3.15 shows the block diagram of vibrating sample magnetometer.

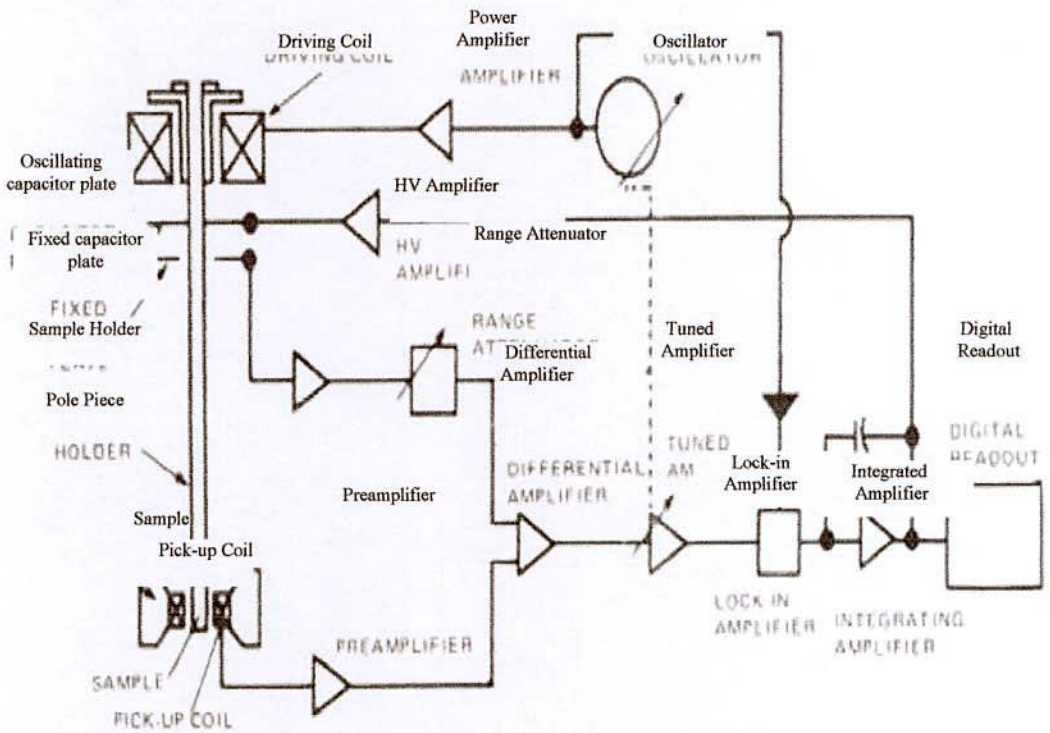

Fig. 3.13 Block diagram of vibrating sample magnetometer

The sample is fixed to a sample holder located at the end of a sample rod mounted in a electromechanical transducer. The transducer is driven by a power amplifier which itself is driven by an oscillator at a frequency of 90 Hz. So, the sample vibrates along the Z axis perpendicular to the magnetizing field. The latter induced a signal in the pick-up coil system that is fed to a differential amplifier. The output of the differential amplifier is subsequently fed into a tuned amplifier and an internal lock-in amplifier that receives a reference signal supplied by the oscillator.

The output of this lock-in amplifier, or the output of the magnetometer itself, is a DC signal proportional to the magnetic moment of the sample being studied. The electromechanical transducer can move along X, Y and Z directions in order to find the saddle point. Calibration of the vibrating sample magnetometer is done by measuring the signal of a pure Ni standard of known saturation magnetic moment placed in the saddle point. The basic instrument includes the electromechanical system and the electronic system (including a personal computer). Laboratory electromagnets or superconducting coils of various maximum field strengths may be used.

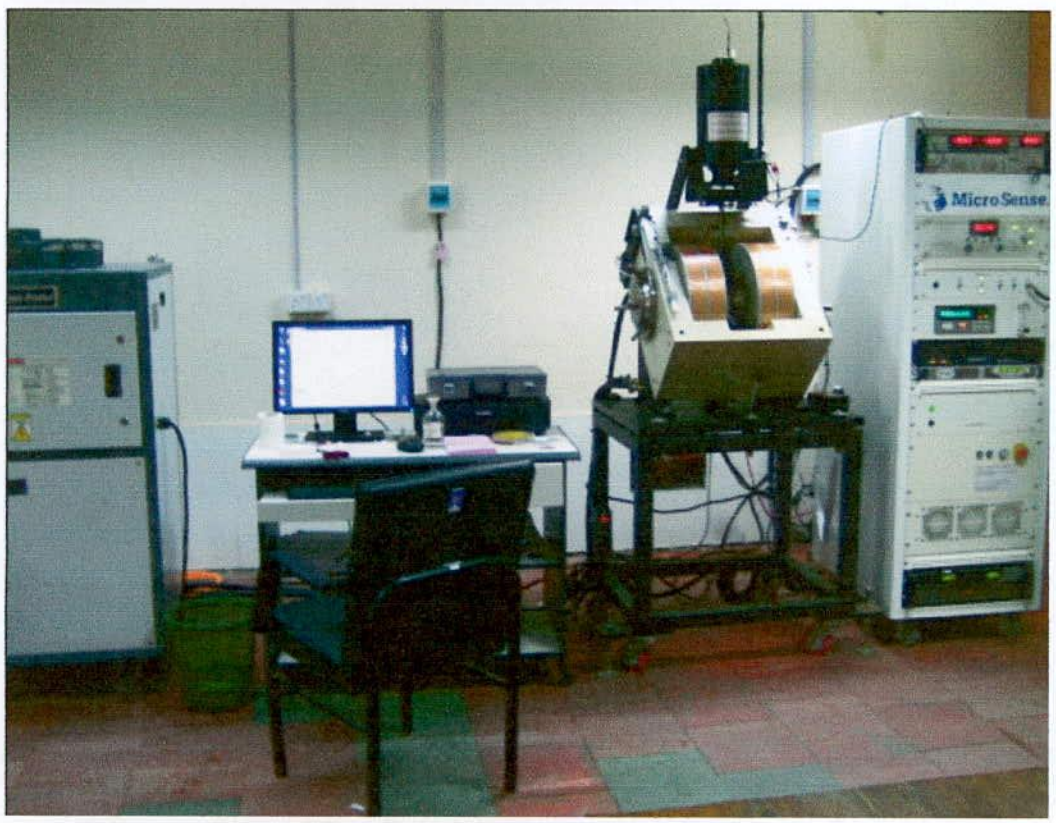

Fig. 3.14 Vibrating sample magnetometer

Chapter - IV

Results and Discussion

Chapter-IV Result and Discussions

4.0 Introduction

$(Ni_{0.28}Cu_{0.10}Zn_{0.62}O)(Fe_2O_3)_{1-x}$ ferrites where x = 0.00, 0.02, 0.04, 0.06 and 0.08 were investigated to optimize Fe-deficient. Structural characterization and identification of phases is a prior necessity for the study of ferrites. Optimum magnetic and electrical transports properties of the ferrites necessitate have been investigated with variation Fe-deficient in Ni-Cu-Zn ferrites. Optimization of Fe-deficient with respect $(Ni_{0.28}Cu_{0.10}Zn_{0.62}O)(Fe_2O_3)_{1-x}$ will be investigated to achieve high permeability as well as high resistivity in the ferrites.

4.1 X-Ray Diffraction Analysis

X-ray neutron and electron diffraction are useful techniques to evaluate the various phases of the synthesized ferrites as well as their unit cell parameters. In the present study X-ray diffraction technique has been utilized to discern these parameters X-ray diffraction (XRD) studies of the samples were performed by using Philips PERT PRO X-ray Diffraction using Cu-K_α radiation in the range of $2\theta = 20^0$ to 65^0 in steps of 0.02^0.

4.1.1 Phase Analysis

The phase formation behavior of $(Ni_{0.28}Cu_{0.10}Zn_{0.62}O)(Fe_2O_3)_{1-x}$ ferrites where x = 0.00, 0.02, 0.04, 0.06 and 0.08 sintered at 1100^0C were studied by XRD. All the samples show crystallization with we defined diffraction patterns exhibited that all the samples were identified as a single phase of cubic spinel structure. The XRD patterns for all the samples were indexed for fcc spinel structure and the Bragg planes are shown in the patterns. The XRD patterns of the samples are given in Fig.-4.1.The peaks (220), (311), (222), (400), (422), (551) and (440) correspond to spinel phase which are characteristic of spinel structures with a single phase. The lattice parameter 'a' corresponding to each

plane was calculated by using the X-ray data. The average values of 'a' were found by plotting a against Nelson-Riley function.

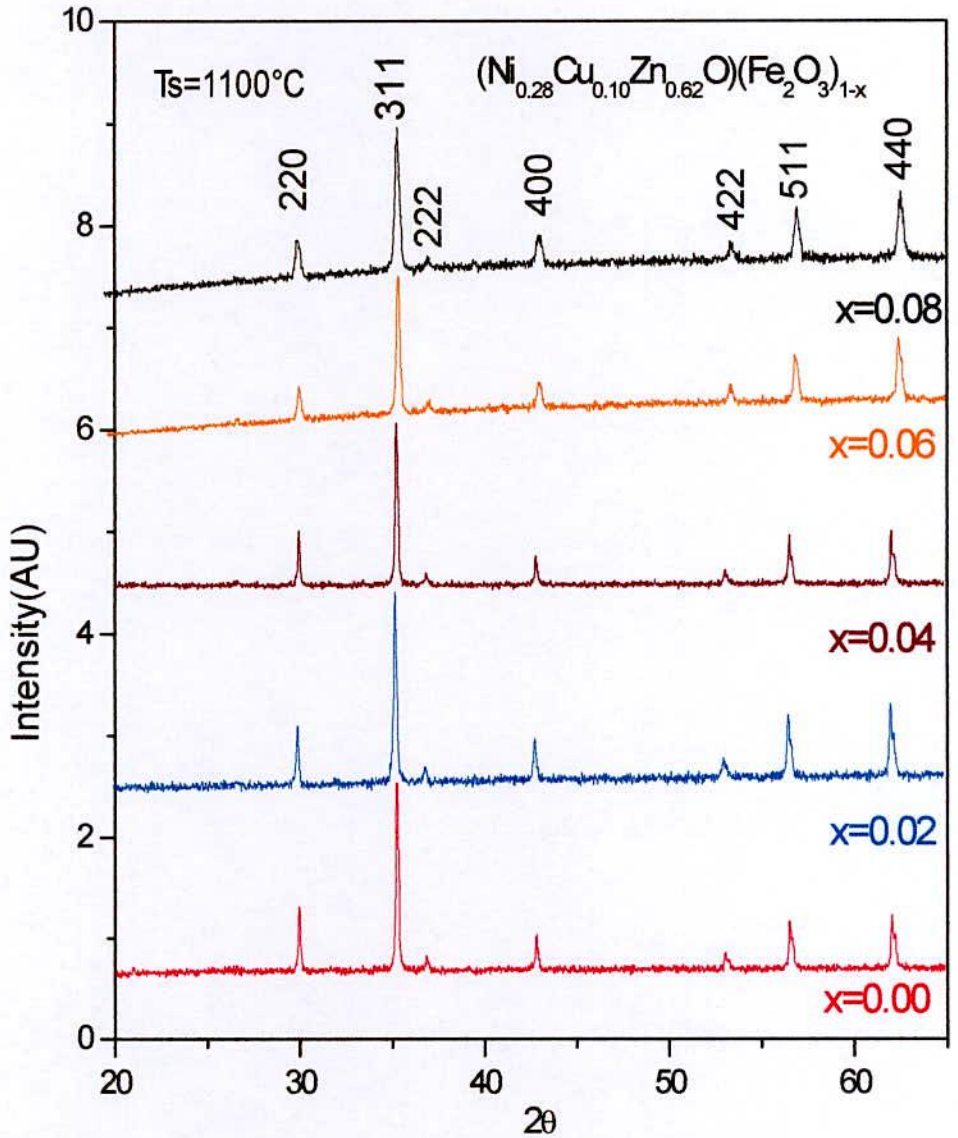

Fig.-4.1 X-ray diffraction patterns of $(Ni_{0.28}Cu_{0.10}Zn_{0.62}O)(Fe_2O_3)_{1-x}$ ferrites sintered at 1100^0C for 2hrs.

4.1.2 Lattice Parameters

The lattice parameter is plotted against the concentration x in Fig.-4.2. The values of the lattice parameter obtained from each plane are plotted against Nelson-Riley function [4.1] $F(\theta)=\frac{1}{2}\left[\frac{Cos^2\theta}{Sin\theta}+\frac{Cos^2\theta}{\theta}\right]$, where θ is the Bragg's angle. A decrease in lattice constant is observed with the increasing of Fe-deficient content (x), in the lattice. This is indicates that the present system obeys the Vegard's law [4.2]. This may be due to Fe^{3+} ions having smaller ionic radius (0.69 $A°$) [4.3] than that of Ni^{+2}, Cu^{+2} and Zn^{+2} ions of ionic radius 0.78 $A°$, 0.70 $A°$ and 0.82 $A°$ respectively [4.4], which when Zn^{+2} substituted resides on A-site and displaces all small ions from A site to B-site. This decrease can be attributed to the vacancy created by Fe^{3+} deficiency with increasing its content. The unit cell is expected to reduce its size by contraction of the lattice resulting in decrease of lattice parameter gradually.

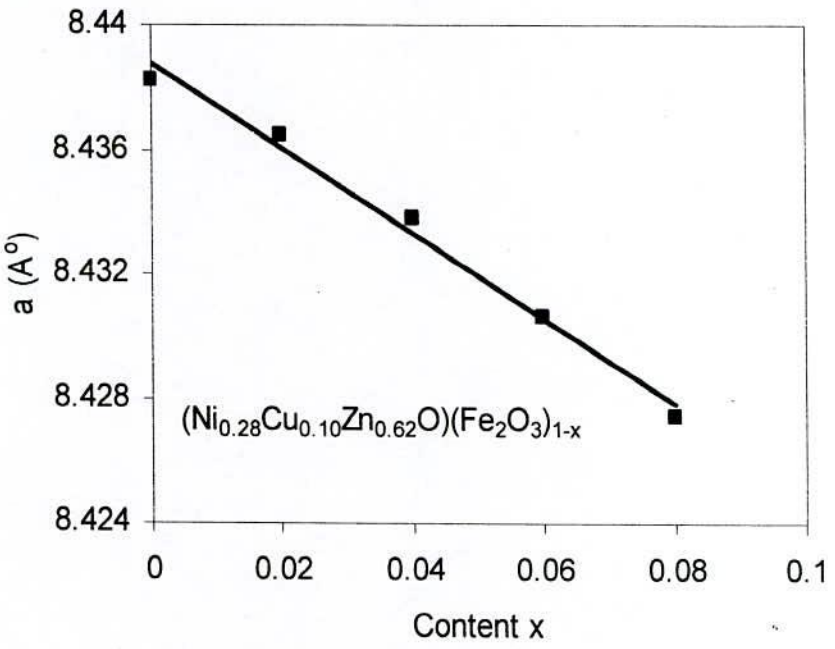

Fig.-4.2 Variation of lattice parameter 'a' as a function of content (x).

4.1.3 Density and Porosity

Variation of bulk density and X-ray density with Fe-deficiency is shown inFig.-4.3. The bulk density (d_B) was measured by usual mass and dimensional consideration whereas X-ray density (d_x) was calculated from the molecular weight and the volume of the unit cell for each sample by using the eq^n (4.1) and (4.2).

$$d_B = \frac{m}{V} = \frac{m}{\pi r^2 h} \tag{4.1}$$

$$d_x = \frac{8M}{Na^3} \, gm/cm^3 \tag{4.2}$$

The calculated values of the bulk density and theoretical (or X-ray) density of the present ferrite system are listed in Table- 4.1. It is observed that bulk density is lower than the X-ray density shown in Fig.-4.3. This may be due to the existence of pores which were formed and developed during the sample preparation or sintering process. The X-ray density slightly decreases with increasing Fe-deficiency and the bulk density increases continuously with increasing x-content.

The enhancement of bulk density is due to activated diffusion process triggered by the excess vacancies created by Fe^{3+} deficiency. It may be also be mentioned that reduction Fe^{2+} due to Fe^{3+} deficiency is expected to increase the resistivity of the samples. This density plays an important role on the magnetic properties especially on the structure sensitive property such as permeability and flux density. Table-4.1 shows the results of lattice parameter, theoretical density, and bulk density calculated porosity. It is observed from the Table-4.1 that porosity decreases monotonically with increasing Fe-deficiency in constant with bulk density which shows reverse behavior shown in Fig.4.4.

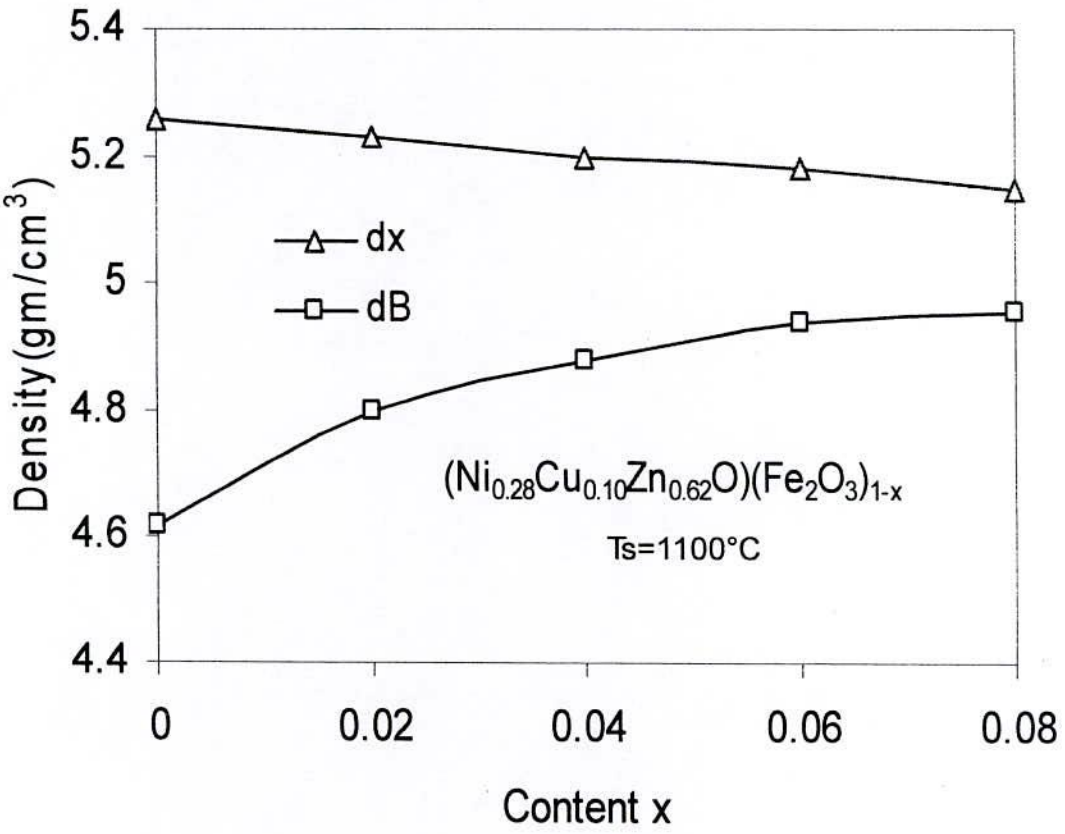

Fig.-4.3 Variation of bulk density and X-ray density as a function of Fe-deficient content (x).

Table- 4.1 Data of the lattice parameter (a), X-ray density (d_x), bulk density (d_B), porosity (P%), molecular weight (M) of $(Ni_{0.28}Cu_{0.10}Zn_{0.62}O)(Fe_2O_3)_{1-x}$ samples sintered at 1100°C for 2hrs

Fe-deficient content (x)	a (Å)	d_x (g/cm^3)	d_B (g/cm^3)	P%	M (g)
0.00	8.4382	5.21	4.52	13.24	239.02
0.02	8.4365	5.25	4.62	12	237.42
0.04	8.4338	5.22	4.80	8.04	235.82
0.06	8.4307	5.19	4.88	4.045	234.23
0.08	8.4275	5.16	4.93	4.04	232.63

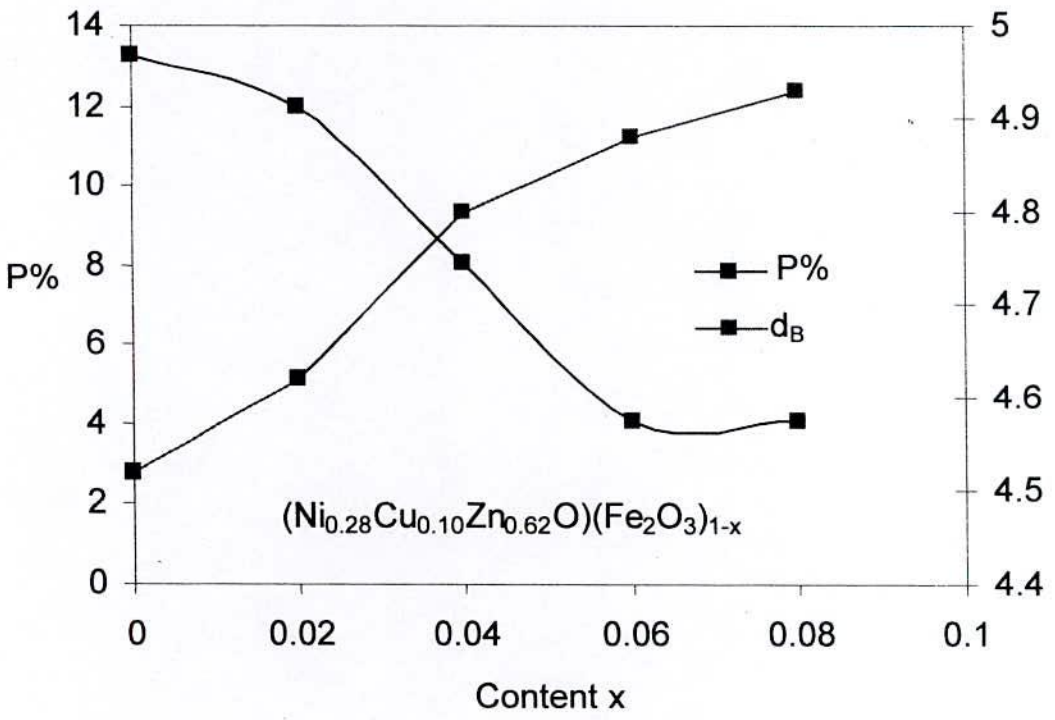

Fig.-4.4 Bulk density and porosity as a function of Fe- deficient content (x)

The density of Fe, Ni, Cu and Zn are 7.87gm/c.c., 8.91gm/c.c. and 7.14gm/c.c. respectively. Zn acts as densification. It is known that Ni reduces densification rate of Ni-Cu-Zn ferrites; while Cu helps its densification [4.5]. This increase in densification is mainly due to decreasing of lattice parameter. Another reason might be due to the liquid phase formation in the ceramic promoted material or atomic diffusion in the crystal [4.6]. The porosity which is intrinsic for any oxide material plays an important role in the deciding the magnetic and electrical properties.

4.2 Magnetic Properties

4.2.1 Temperature Dependence of Initial Permeability

Fig.-4.5 shows the temperature dependence of initial permeability, μ', for the toroid shaped samples $(Ni_{0.28}Cu_{0.10}Zn_{0.62}O)$ $(Fe_2O_3)_{1-x}$ ferrites where x = 0.00, 0.02, 0.04, 0.06 and 0.08 sintered at 1100°C for 2hrs, which is measured at a constant frequency (100kHz) of an AC signal by using Impedance Analyzer. It is observed that the initial permeability increase with the increase in Fe-deficiency throughout the entire range of compositions, while it falls abruptly close to the Curie point. This because Fe in these compositions not only increases the magnetic moments and but also lower anisotropy K_1 [4.7]. On the other hand, permeability increases with the decrease of K_1 as the temperature increases according to the relation $\mu' \propto \frac{M_S^2 D}{\sqrt{K_1}}$ [4.8 - 4.9]. It is observed from Fig.-4.5 that the permeability falls sharply when the magnetic state of the ferrite samples changes from ferromagnetic to paramagnetic.

Fig.-4.6 shows the variation of Curie temperature (T_C) with Fe-deficiency of $(Ni_{0.28}Cu_{0.10}Zn_{0.62}O)$ $(Fe_2O_3)_{1-x}$ ferrites and the values are taken during the heating the sample. T_C is the transition temperature above which the ferrite material losses its magnetic properties. The T_C gives an idea of the amount of energy required to break up the long range ordering in the ferromagnetic material. The T_C mainly depends upon the strength of A – B exchange interaction. From the Fig.-4.6 it is observed that T_C slowly and gradually increases with increasing of Fe deficiency.

It is known that at T_C, the thermal energy wining over the exchange energy which results to disorder the system from an ordered one i.e. a ferromagnetic substance transforms to a paramagnetic one. T_C of ferrites is dependent on the strength of A –B exchange interaction [4.10]. As the Fe – deficiency is increased in the sample, the strength of the interaction of between the tetrahedral A –site and octahedral B-site might be increased which enhances the T_C.

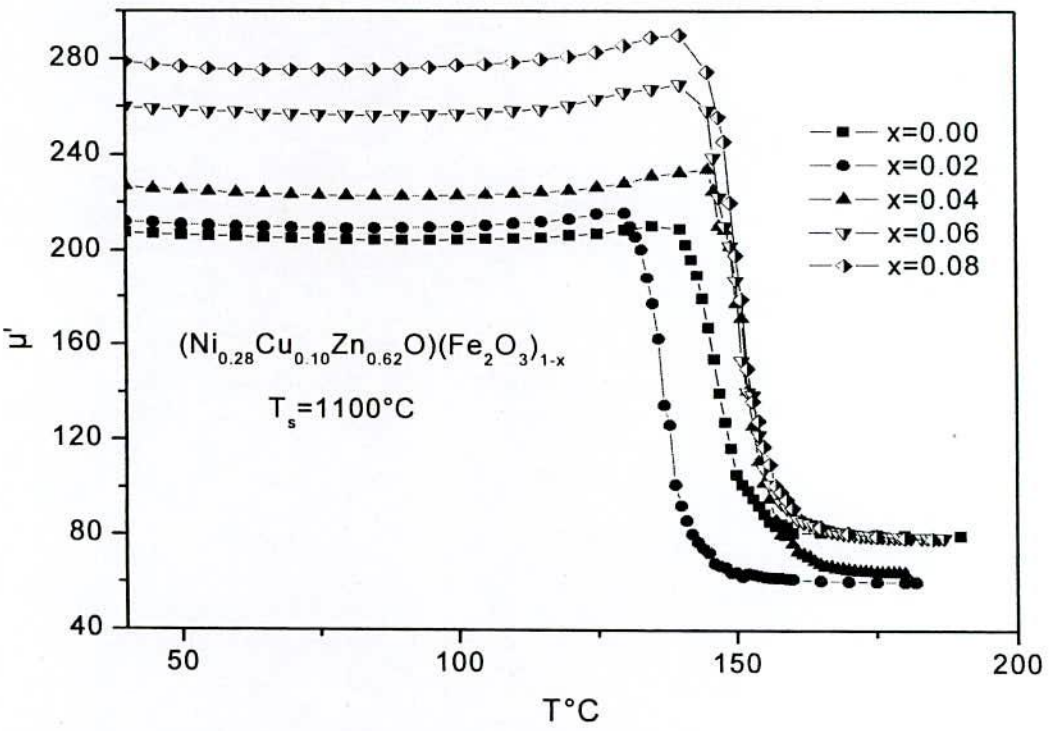

Fig. 4.5 Variation of real part of permeability,μ′ with temperature of $(Ni_{0.28}Cu_{0.10}Zn_{0.62}O)\ (Fe_2O_3)_{1-x}$ ferrites sintered at 1100°C for 2hrs.

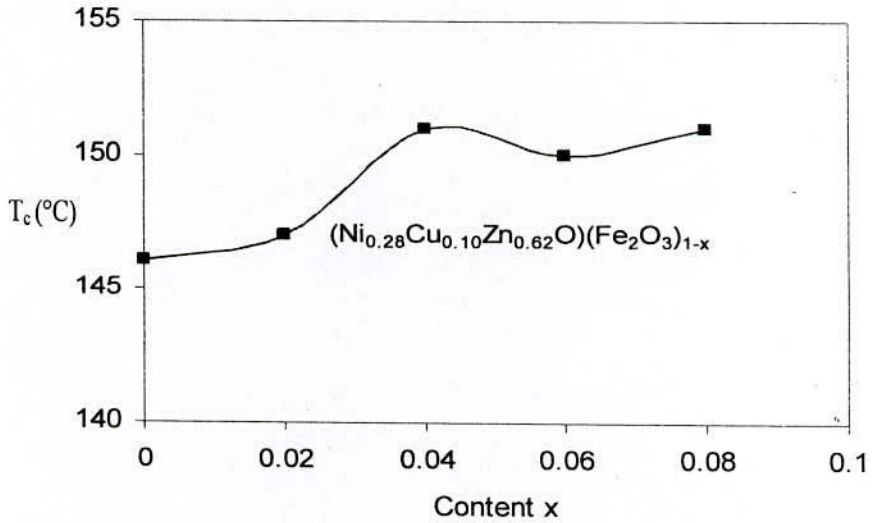

Fig.-4.6 Variation of T_C with Fe-deficient (x) of $(Ni_{0.28}Cu_{0.10}Zn_{0.62}O)\ (Fe_2O_3)_{1-x}$ ferrites

Table - 4.2 Data of Curie temperature (T_C) $(Ni_{0.28}Cu_{0.10}Zn_{0.62}O)(Fe_2O_3)_{1-x}$ ferrites

Fe- deficient Content X	T_s=1100°C
	T_c (°C)
0.00	146
0.02	147
0.04	151
0.06	150
0.08	151

Khulna University Library
KUET
Bangladesh
Central Library

4.2.2 Frequency Dependence of Complex Permeability

The complex permeability is given by $\mu = \mu' - i\mu''$, μ' is the real permeability (in phase) and μ'' the imaginary permeability (90^0 out of phase). Complex permeability has been determined as a function of frequency, f up to 13MHz at room temperature for all the samples of series $(Ni_{0.28}Cu_{0.10}Zn_{0.62}O)(Fe_2O_3)_{1-x}$ ferrites by using the conventional technique based on the determination of the complex impedance of circuit loaded with toroid shaped sample. Fig.-4.7 represents the results of the real part of the permeability μ' and Fig.-4.8 imaginary part, μ'' as a function of frequency for the whole series of ferrite samples at 1100^0C for 2hrs.

From Fig.-4.7 it is noticed that the real component of permeability, μ' is fairly constant with frequency up to certain frequency range and then falls rather rapidly to very low value at higher frequency. The permeability of composition with x = 0.00 to 0.08 were stable up to 2 – 3 MHz and the cut off frequencies of samples were evident from these figures that the initial permeability as a function of frequency increases with fe-deficiency (x-content), i.e. the permeability μ' increases monotonically with x – content. The constant value of permeability over a wide frequency range, which is named the zone of utility of ferrites, is desirable over various applications such a broad band transformer and wide band read-writes head for video recording [4.11]. From Fig.-4.6 the range of operating frequency in the x = 0.04 and 0.06 samples are wider than that in the others which shows the compositional stability and quality of the ferrites samples.

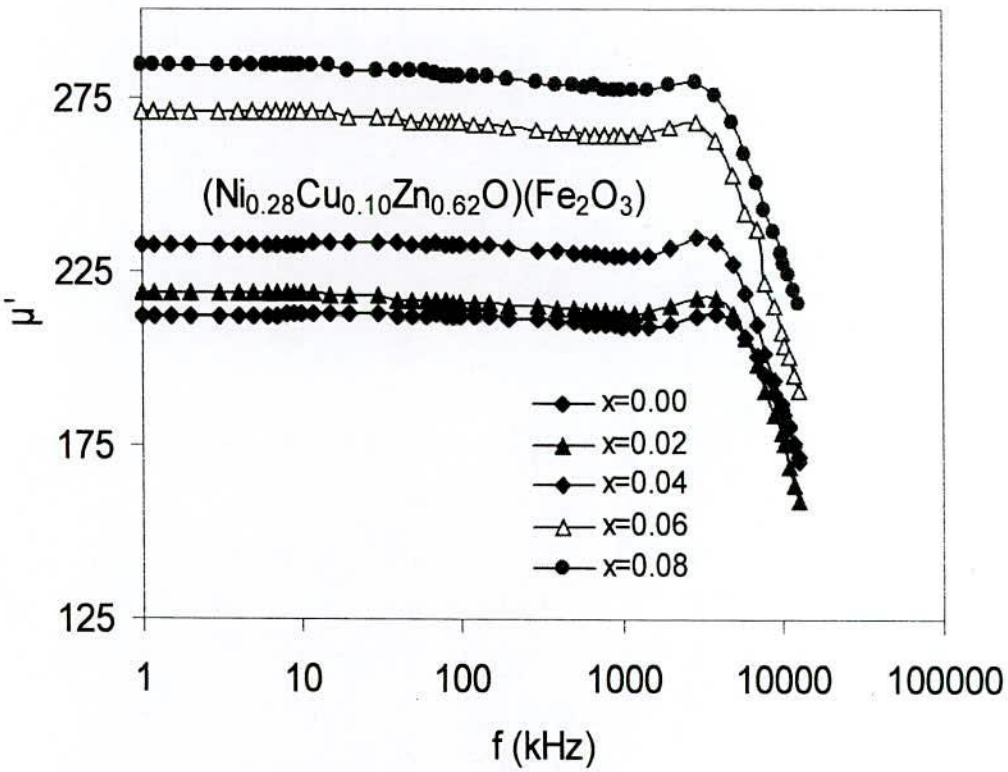

Fig.-4.7 Variation of initial permeability with frequency of $(Ni_{0.28}Cu_{0.10}Zn_{0.62}O)(Fe_2O_3)_{1-x}$ ferrites sintered at 1100^0C for 2hrs.

From the Fig.-4.8, the imaginary permeability, μ'' first rises slowly and then increases quite abruptly making a peak at a certain frequency (called resonance frequency f_r), where the real component μ' is failing sharply. This phenomenon is attributed to the ferromagnetic resonance. Resonance frequency (f_r) was determined from the maximum of imaginary permeability of the ferrites. It is observed from the Fig.-4.8 that the higher the permeability the lower the resonance frequency of the material. This really confirms with Snoek's limit [4.12]

$$f_r(\mu_i - 1) = \left(\frac{4}{3}\right)\gamma M_S \,, \qquad (4.3)$$

Where, f_r is the resonance frequency for domain wall motion, γ is the gyro magnetic ratio and M_S the saturation magnetization. This means that there is effective peaks are the results of the absorption of energy due to matching of the oscillation frequency of the magnetic dipoles and the applied frequency. Since the starting point of resonance frequency determine the upper limit of the operational frequency of any device, it predicts that the operational frequency range of the samples is greater than 6MHz. The resonance frequencies along with the permeability of the samples are listed in Table-4.2.

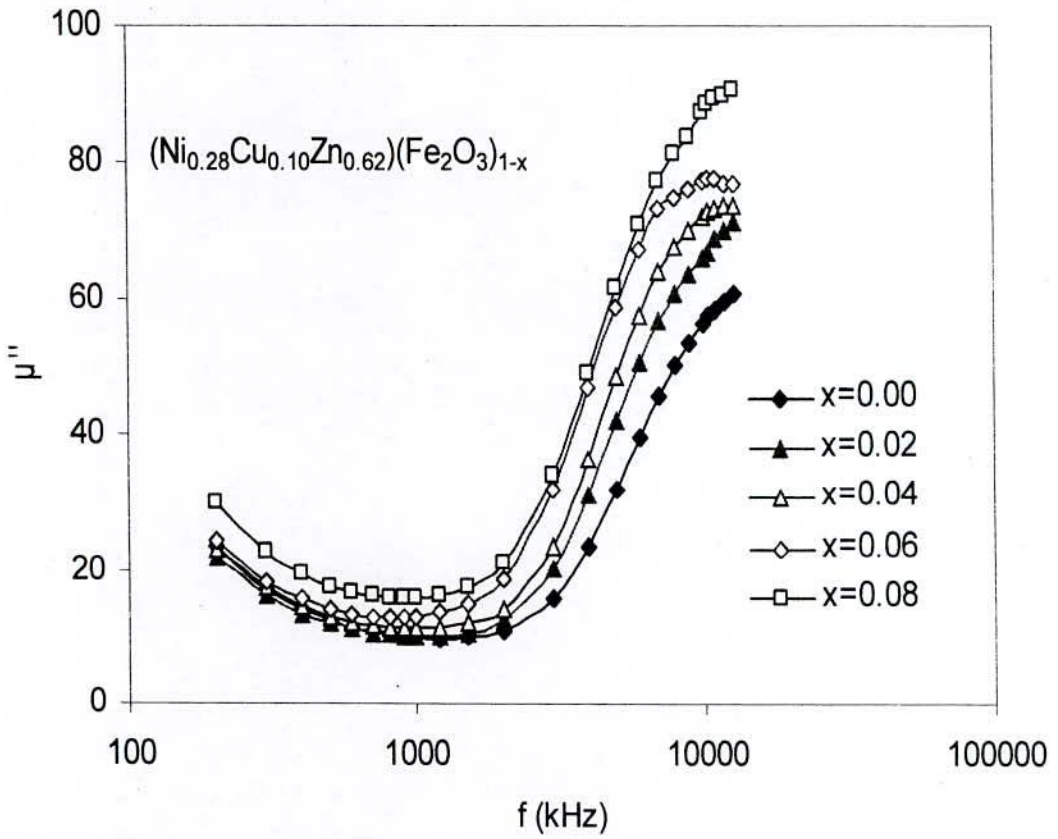

Fig.-4.8 Complex imaginary permeability μ'' with frequency of $(Ni_{0.28}Cu_{0.10}Zn_{0.62}O)(Fe_2O_3)_{1-x}$ ferrites sintered at 1100^0C for 2hrs.

Fig.-4.9 shows that the variation of initial permeability at frequency 10kHz with Fe-deficient $(Ni_{0.28}Cu_{0.10}Zn_{0.62}O)(Fe_2O_3)_{1-x}$ ferrites sintered at 1100^0C for 2hrs. It was observed that the permeability increases slowly with increase in Fe deficiency.

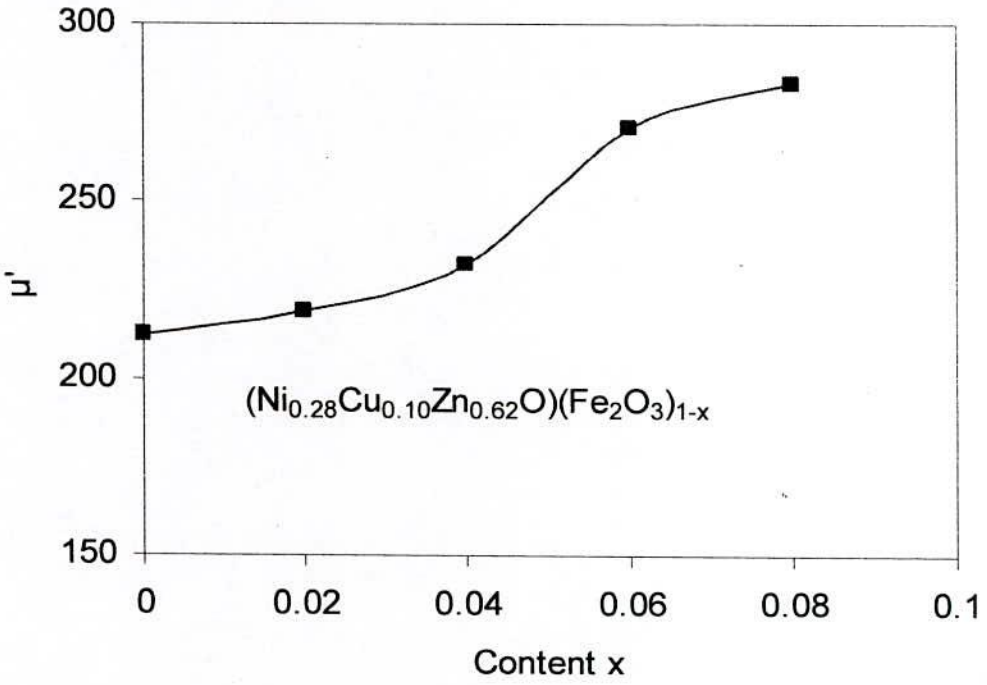

Fig.-4.9 Variation of initial permeability, μ' at frequency 10kHz with Fe-deficient of $(Ni_{0.28}Cu_{0.10}Zn_{0.62}O)(Fe_2O_3)_{1-x}$ ferrites sintered at 1100^0C for 2hrs.

The increase of permeability with Fe-deficient is connected with increased magnetization, density, grain size and possible reduction of anisotropy energy. The initial permeability is closely corrected to the densification. An increase in the density of ferrites not only results in the reduction of magnetization field due to the presence of pores but also raise the spin rotational contribution, which in turn increases the permeability [4.13].

Table-4.3 Data for permeability (μ'), resonance frequency (f_r) and Snoek's limit ($\mu'.f_r$) of $(Ni_{0.28}Cu_{0.10}Zn_{0.62}O)(Fe_2O_3)_{1-x}$ ferrites sintered at 1100^0C for 2hrs.

Fe-deficient content (x)	Ts=1100°C		
	μ' (10kHz)	f_r (MHz)	Snoek's $\mu.f_r$(GHz)
0.00	212	13	2756
0.02	219	12	2628
0.04	272	12	2784
0.06	271	10.5	2846
0.08	283	10	2830

4.2.3 Frequency Dependence of Quality Factor

Fig.4.10 show the frequency dependence of relative quality factor (RQF) of the samples sintered at 1100^0C. The variation of the relative quality factor with frequency showed a similar trend for all the samples. Q-factor increases with increases of frequency showing as peak and the decreases with further increase of frequency. It is seen that RQF deteriorates beyond 4.5MHz i.e., the loss tangent is minimum up to 4.5MHz and then it rises rapidly. The loss is due to lag of domain wall motion with respect to the applied alternating magnetic field and is attributed to various domain defects [4.14], which include non-uniform and non-repetitive domain wall motion, domain wall bowing, localized variation of flux density, nucleation and annihilation of domain walls. This phenomenon is associated with the ferromagnetic resonance within the domains [4.15] and at the resonance maximum energy is transferred from the applied magnetic field to the lattice resulting in the rapid decreases in RQF.

The peak corresponding to maxima in Q-factor shifts to lower frequency range as Fe-deficiency increases, sample with x = 0.00 posses the maximum value of quality factor.

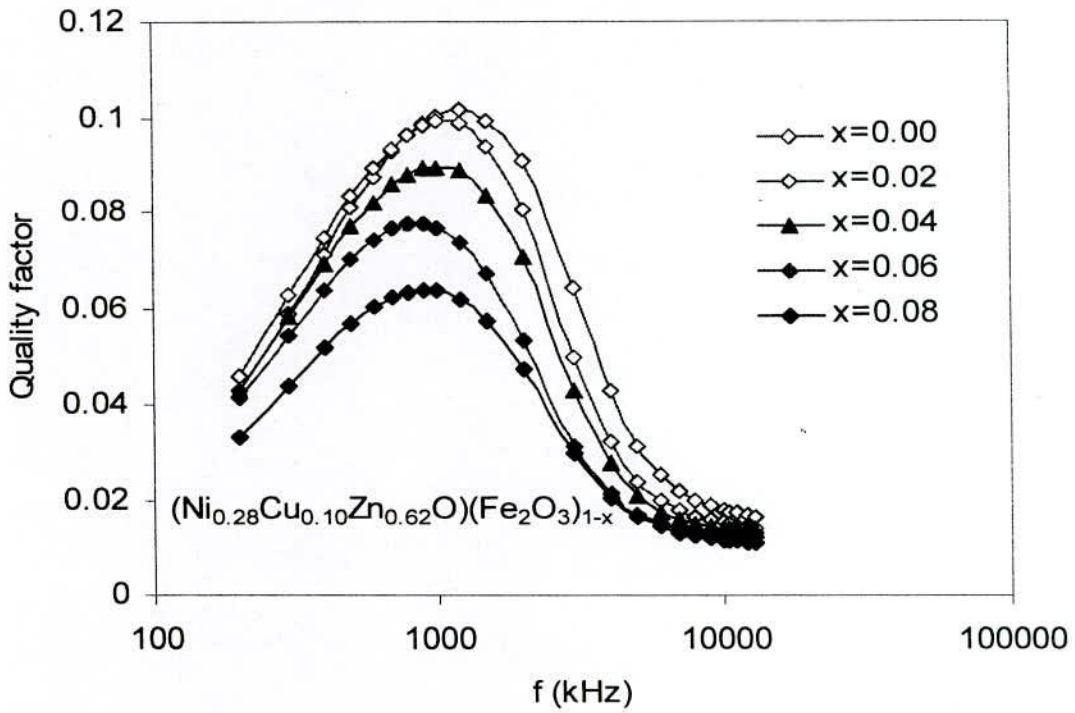

Fig.-4.10 Variation of RQF as a function of frequency of $(Ni_{0.28}Cu_{0.10}Zn_{0.62}O)(Fe_2O_3)_{1-x}$ ferrites sintered at 1100^0C for 2hrs.

4.2.4 Low Field B - H Loop at Room Temperature

Both ferro- and ferromagnetic materials differ widely in the case with which they can be magnetized. If a small applied field suffices to produce saturation the material is said to be magnetically soft. Saturation of some other material, which will in general have a different value of M_S, may require very large fields. Such a material is magnetically hard. Sometimes the same material may be either magnetically soft or hard, depending on its physical condition: thus curve (a) might relate to a well annealed material, and curve (b) to the heavily cold worked state.

Thus derivative $\left(\frac{dB}{dH}\right)$ is unity beyond the point B_S, called the saturation induction. However, the slope of these lines does not normally appear to be unity, because the B and H scales are usually quite different.

Fig.-4.11 represents the B - H loops at room temperature were measured with B - H loop tracer at constant frequency (f = 1kHz) and applied field H = 0 – 15Oe for the whole series of $(Ni_{0.28}Cu_{0.10}Zn_{0.62}O)(Fe_2O_3)_{1-x}$ ferrites where x = 0.00, 0.02, 0.04, 0.06 and 0.08 sintered at 1100^0C for 2hrs. From these loops the remanence induction (B_r), saturation induction (B_S) and the coercive force (H_C) were determined. These results are shown in Table-4.3.

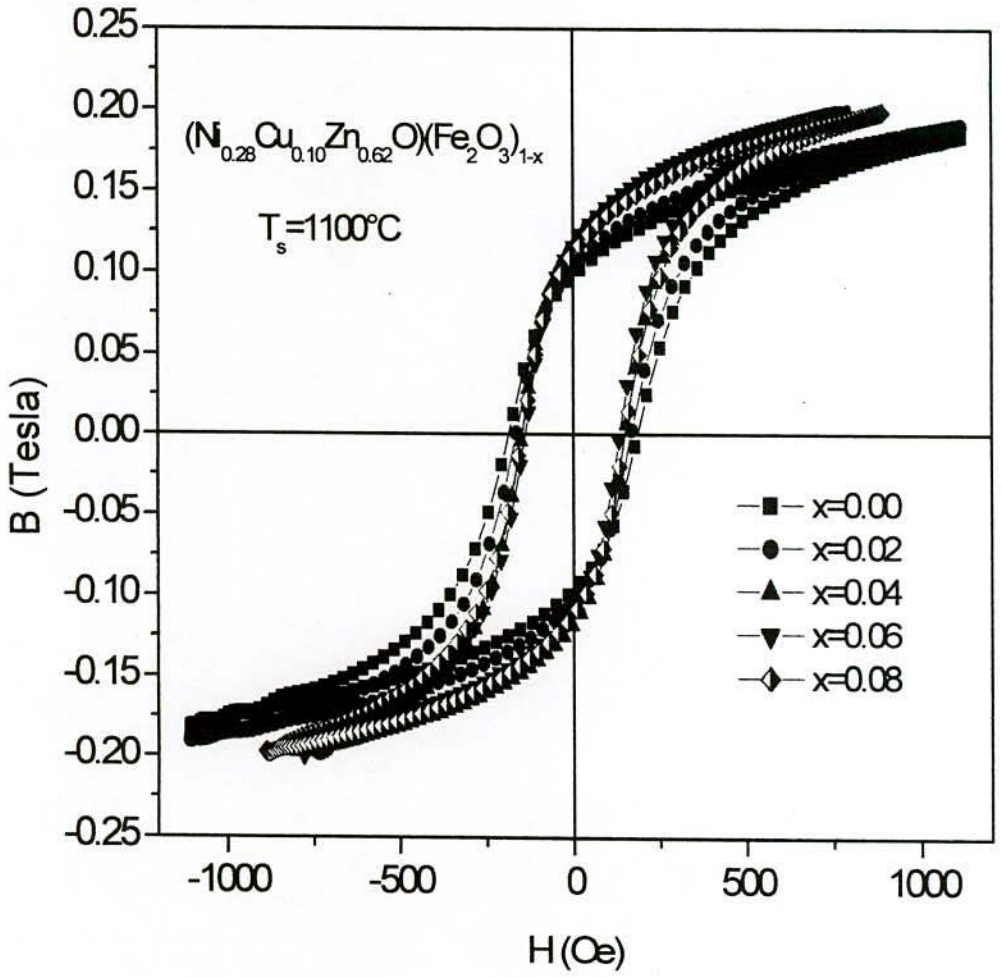

Fig.-4.11 Magnetic hysteresis graphs of $(Ni_{0.28}Cu_{0.10}Zn_{0.62}O)(Fe_2O_3)_{1-x}$ ferrites with x sintered at 1100^0C for 2hrs.

It is observed that the B_r and B_S both increase with x-content. For high permeability material a low coercivity is a prime requirement which is fulfilled in the present study. Since permeability is inversely related to coercivity i.e., $\mu' \propto \frac{1}{H_c}$. Again a high B_S is also a requirement for high permeability which is also manifested in the studied sample. Fig.-4.12 shows the dependence of permeability μ' and coercivity, H_c with x content. And excellent correlation between μ' and H_c is observed.

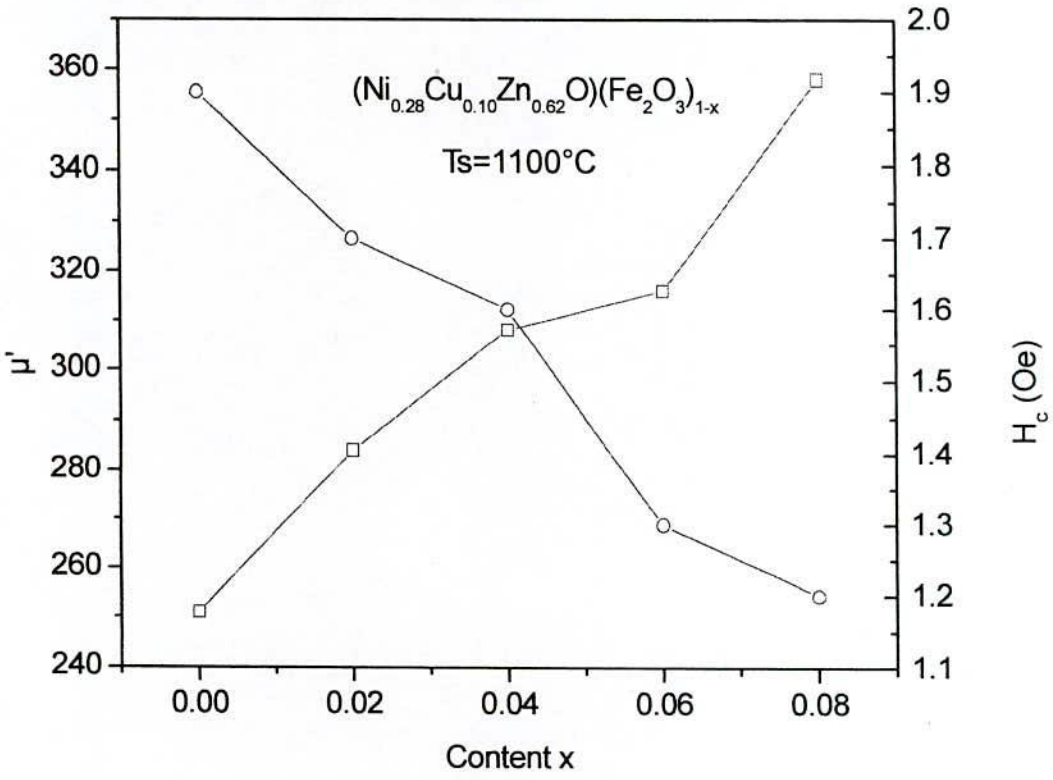

Fig.-4.12 Magnetic hysteresis graph of $(Ni_{0.28}Cu_{0.10}Zn_{0.62}O)(Fe_2O_3)_{1-x}$ ferrites with x sintered at 1100^0C for 2hrs at constant frequency f = 1kHz and μ' and H_c versus x-content.

The low coercive force and higher permeability confirms that the development of soft magnetic characteristic properties of Ni-Cu-Zn ferrite with increasing Fe-deficiency, which is well known as soft magnetic materials from application point of view. The increase of Fe-deficiency decreased the coercive field and the hysteresis losses, increase

the samples magnetization and permeability. B_s is found to increase with increasing Fe-deficient. The different values of retantivity and $\frac{B_r}{B_s}$ ratio observed are interpreted in a quantitative way by means of domain theory. The predominant losses in Ni-Cu-Zn ferrite are hysteresis and eddy current at operating frequencies lower than the relaxation frequency of the wall displacement. The values of maximum flux density, coercive field, and hysteresis loss of the system has been found with x = 0.08.

Table-4.4 The experimental values of coercive force (H_c), remanence induction (B_r), saturation induction (B_s), $\left(\frac{B_r}{B_s}\right)$ ratio and losses of ($Ni_{0.28}Cu_{0.10}Zn_{0.62}O$) $(Fe_2O_3)_{1-x}$ samples at room temperature with constant frequency (f = 1kHz) at sintering temperature 1100^0C for 2hrs.

Fe-deficient content (x)	H_C (Oe)	B_r (kG)	B_s (kG)	B_r/B_s	Losses (W/kg)
0.00	2.34	0.97	1.84	0.53	22.13
0.02	2.08	1.03	1.90	0.54	21.11
0.04	1.87	1.17	1.97	0.59	20.39
0.06	1.87	1.21	2.13	0.56	23.64
0.08	1.94	1.10	2.10	0.52	23.85

If H is reduced to zero after saturation has been reached in the positive direction, the induction in a ring specimen will decrease from B_s to B_r, called the retentivity or residual induction. If the applied field is then reversed, reversing the current in the magnetizing winding, the induction will decrease to zero when the negative applied field equals the coercivity, H_c. The B - H loop of this sample is wide and almost reversible.

4.2.5 Variation of Saturation Magnetization at Room Temperature

The room temperature magnetic hysteresis loop of the samples has been measured and is presented in Fig.-4.13. The hysteresis loops do not show any noticeable hysteresis effect. All samples exhibited low coercivity values inducting that all the samples being to the family of soft ferrites. Fig.-4.14 shows the variation of magnetization of the $(Ni_{0.28}Cu_{0.10}Zn_{0.62}O)(Fe_2O_3)_{1-x}$ ferrites as a function of applied magnetic field for various samples where x = 0.00, 0.02, 0.04, 0.06 and 0.08. It is observed from the Fig.-4.15 that virgin saturation magnetization M_s increases up to x = 0.06 and then decrease slightly with x content.

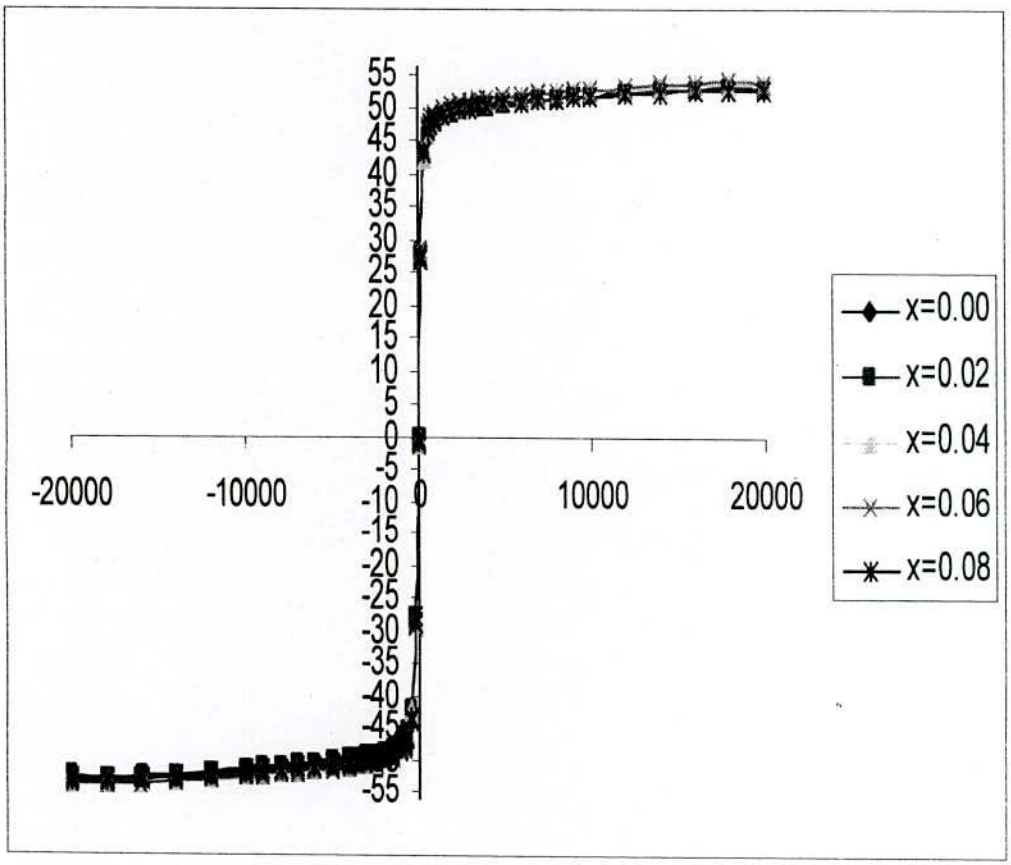

Fig.-4.13 Variation of magnetization at room temperature as a function of applied field on $(Ni_{0.28}Cu_{0.10}Zn_{0.62}O)(Fe_2O_3)_{1-x}$ ferrites where x = 0.00, 0.02, 0.04, 0.06 and 0.08.

The insignificant decrease of M_s may be experimental uncertainty. The observed variation in M_s can be explained on the basis of cation distribution and the exchange interactions between A and B sites. The initial increase in M_s with increased Fe-deficient is due to the increase of resultant sub lattice magnetic moment which can be explained on the basis of Neel's two sub lattice model. Neel [4.16] considered three types of exchange interactions between unpaired electron of two ions lying in A and B sites. In perfect ferrites, the A - A, B - B and A - B nearest neighbor exchange coupling are normally anti ferromagnetic and the A - B exchange coupling is usually heavily predominant.

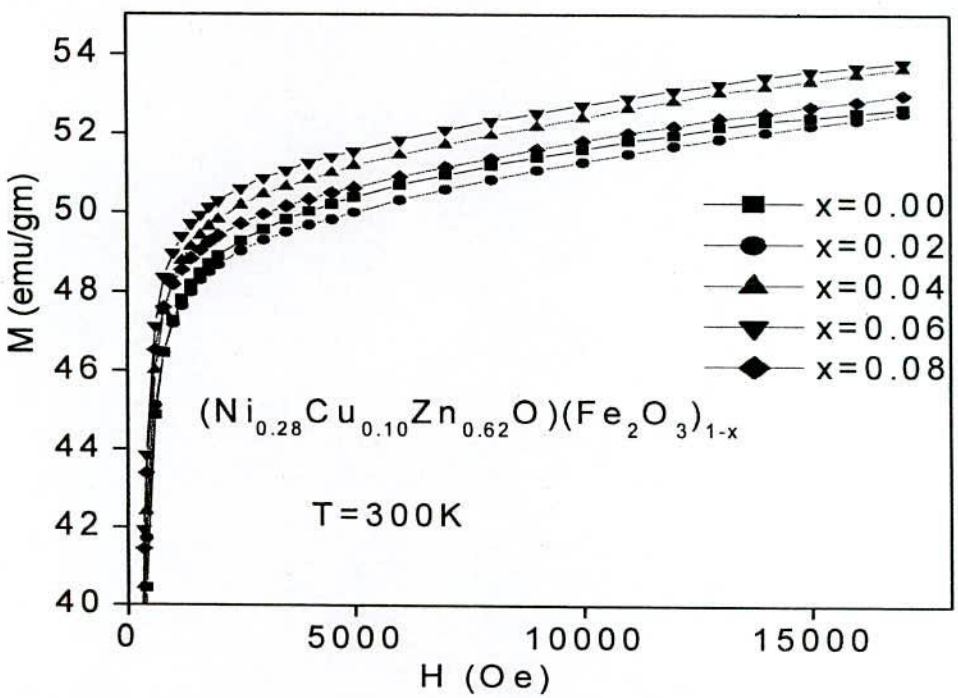

Fig.-4.14 Field dependence of magnetization at virgin state of $(Ni_{0.28}Cu_{0.10}Zn_{0.62}O)(Fe_2O_3)_{1-x}$ ferrites where x = 0.00, 0.02, 0.04, 0.06 and 0.08 sintered at 1100^0C for 2hrs at constant frequency f = 1kHz.

The net magnetization is therefore the difference between the magnetic moments of B and A sub lattices, i.e. $M = M_B - M_A$ and will normally be parallel to the B-sub lattice magnetization because the number of cations on B-sites is twice the number of cations on A-sites. The magnetization of each composition depends on the distribution of

Fe^{3+} ions between the two sub lattices A and B, where the Ni^{2+} and Zn^{2+} ions are non magnetic. It is mentioned that $CuFe_2O_4$ and $NiFe_2O_4$ ferrite are known as inverse ferrite, where Cu^{2+} and Ni^{2+} ions are located on B-sites.

The substitution will lead to increase Fe^{3+} ions on the B-sites and consequently the magnetization of the B-sites will increase. At the same time the magnetization of A-site will decrease according to the decrease of the Fe^{3+} ions on A-site. So the net magnetization will increase accordingly up to x = 0.06 as shown in Fig.-4.15.

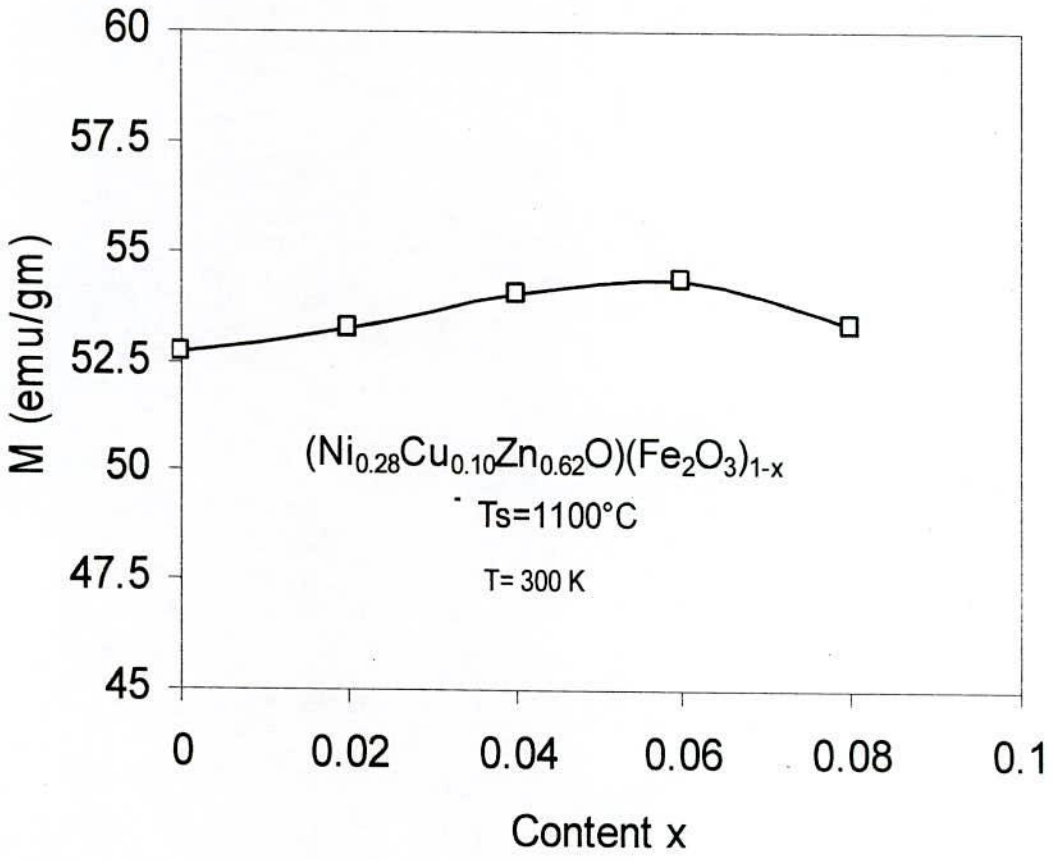

Fig.-4.15 Saturation magnetization (M_s) versus Fe-deficient in $(Ni_{0.28}Cu_{0.10}Zn_{0.62}O)(Fe_2O_3)_{1-x}$ ferrites

Fig.-4.16 shows the temperature dependence of saturation magnetization measured with an applied magnetic field of H = 5kOe. It is observed that magnetization,

M_s decreases monotonically with increasing temperature and finally tends toward zero above the Curie temperature, T_c . The show decreases of magnetization unlike ferromagnet where much sharper fall of M_s is observed that at $T = T_c$. From the Fig-4.16, it is observed that at low temperature magnetization increases slightly with increasing x-content.

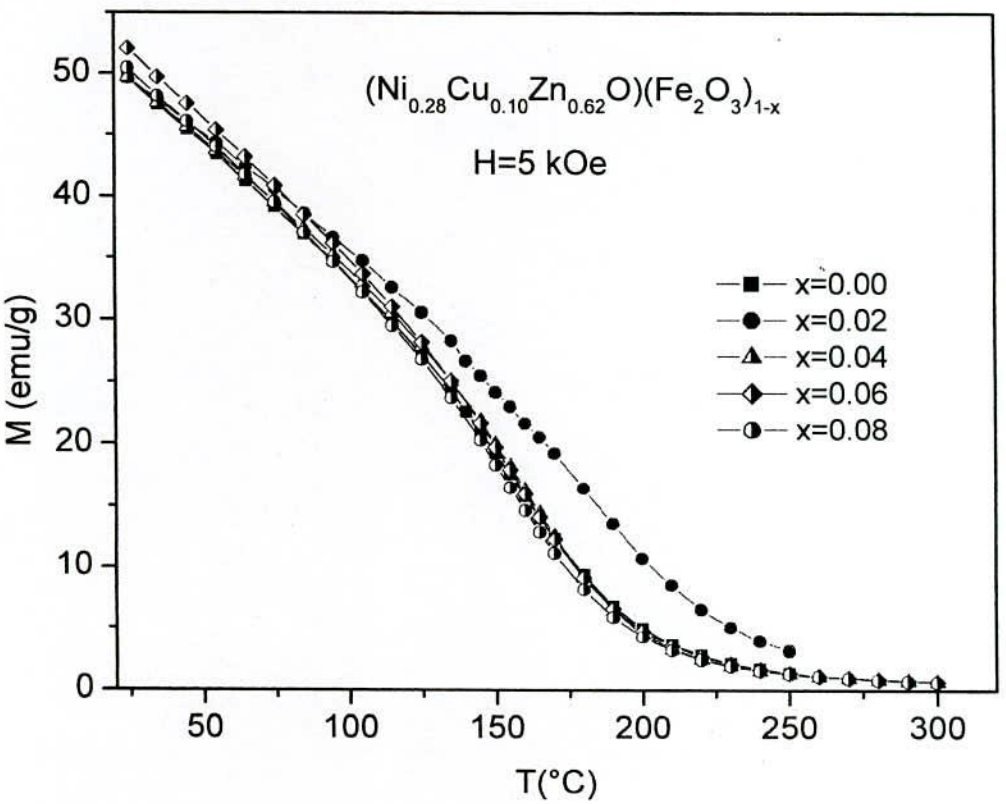

Fig.-4.16 Temperature dependences of magnetization of $(Ni_{0.28}Cu_{0.10}Zn_{0.62}O)(Fe_2O_3)_{1-x}$ ferrites with an applied field 5kOe

4.3 Electrical Transport Property

4.3.1 Compositional Dependence of DC Electrical Resistivity

Electrical DC resistivity is an important electrical property of ferrites in high frequency application. Fig.-4.17 shows the room temperature values of resistivity versus

Fe-deficient of samples of series $(Ni_{0.28}Cu_{0.10}Zn_{0.62}O)(Fe_2O_3)_{1-x}$ ferrites by using a keithely Electrometer. For measurements, the pellet shaped samples were coated with silver paint on the both surfaces of each sample to obtain good ohmic contact. The DC resistivity is found to increase vary fast up to x = 0.02 with Fe-deficient. Resistivity is found to increase slowly with further addition of Fe-deficient. Resistivity is found to decrease with further increase of Fe-deficient. This decrease of resistivity may be attributed to the entrapped of intragranular porosity. Sankpul et. al. and Shaikh et. al. measured resistivity as a function of composition in their work on Ni-Cu and Li-Cu ferrites [4.17 – 4.18].

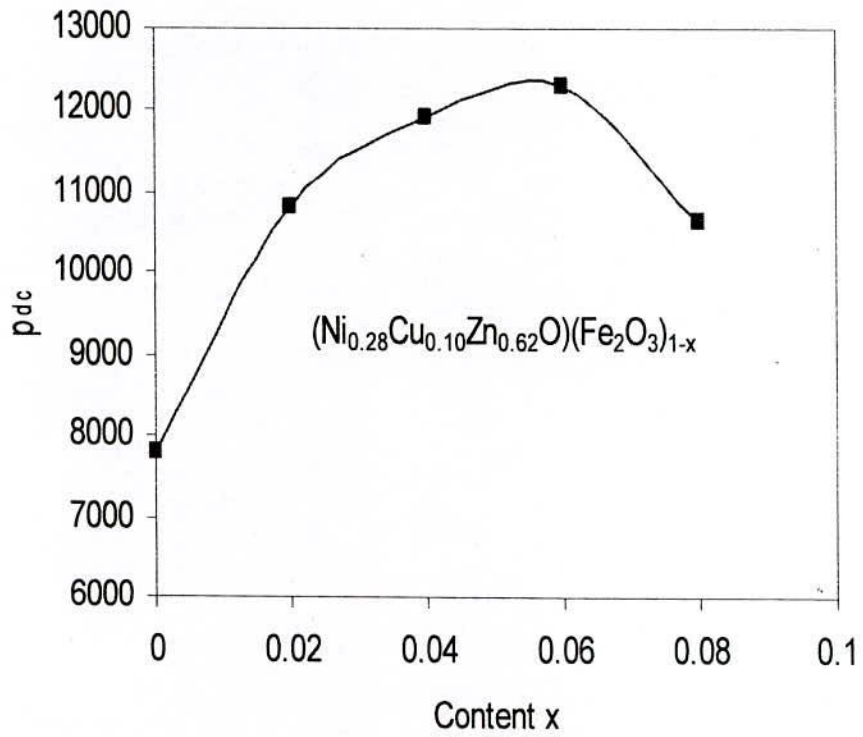

Fig.-4.17 Room temperature DC resistivity as a function of Fe-deficient content (x) of $(Ni_{0.28}Cu_{0.10}Zn_{0.62}O)(Fe_2O_3)_{1-x}$ ferrites sintered at 1100^0C for 2hrs.

The highest value of DC resistivity for x = 0.06 same is observed 12.3×10^3 Ω-cm and values are shown in Table-4.4. The observed decrease in resistivity with the increase

of Fe-deficient has been related to the decrease of porosity since pores are non-conductive. This trend could be attributed to the high activation energy, which is associated with high resistivity at room temperature.

4.3.2 Frequency Dependence of Resistivity

This very large resistivity means in turn that an applied alternating magnetic field will not induce eddy currents in a ferrite. This property makes ferrite the best magnetic materials for high frequency applications where power losses from eddy currents must be minimized. Fig.-4.18 shows the frequency dependence of AC resistivity and values are shown in table-4.4. A large decrease in resistivity was found with increasing Fe-deficient. All the samples show the significant dispersion with frequency which is the normal ferromagnetic behavior. The AC resistivity of the composition also decreased due to enhancement of Fe^{2+} ion concentration. It means that the decrease in AC resistivity with Fe-deficient was due to the increase of electrons in the ferrites.

Table-4.5 AC and DC resistivity at 100kHz of $(Ni_{0.28}Cu_{0.10}Zn_{0.62}O)(Fe_2O_3)_{1-x}$ ferrites sintered at 1100^0C for 2hrs.

X	DC Resistivity ρ_{dc} Ω-cm	AC Resistivity	
		ρ_{ac}, Ω-cm 1kHz	ρ_{ac} Ω-cm 100kHz
0	7.8×10^3	3.1×10^4	1.4×10^3
0.02	10.8×10^3	6.3×10^4	2.3×10^3
0.04	11.9×10^3	7.7×10^4	3.7×10^3
0.06	12.3×10^3	9.1×10^4	5.6×10^3
0.08	10.6×10^3	3.7×10^4	4.1×10^3

The resistivity of all the composition decreased with the increasing frequency. The resistivity (ρ_{ac}) was calculated as per equation (4.4)

$$\rho_{ac} = \frac{1}{\omega \varepsilon_0 k' \tan \delta}$$

$$\rho_{ac} = \frac{A}{2\pi f \tan \delta C t} \qquad (4.4)$$

The resistivity was primarily dependent on the frequency and was found to be inversely proportional that was why resistivity decreases with the increase in frequency. The low frequency region corresponds to high resistivity due to grain boundaries whereas high frequency ranges corresponds to low resistivity due to the grains [4.19].

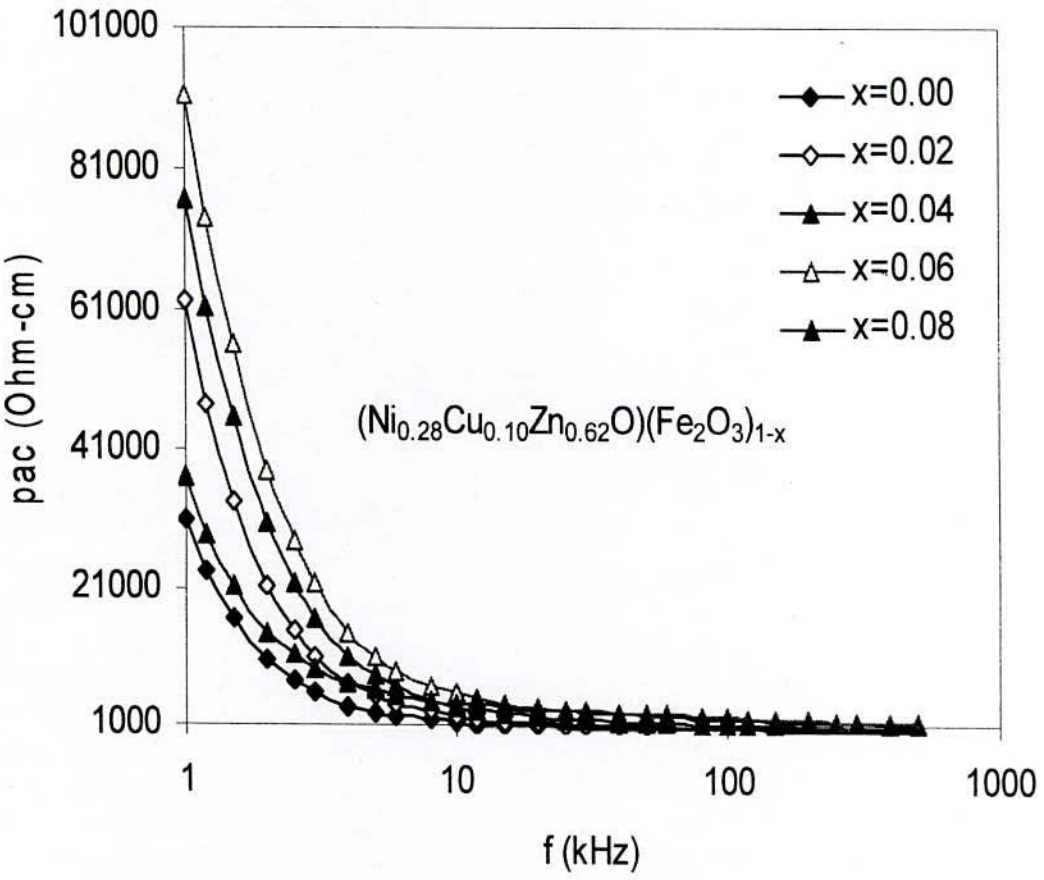

Fig.-4.18 AC resistivity as a function of frequency of $(Ni_{0.28}Cu_{0.10}Zn_{0.62}O)(Fe_2O_3)_{1-x}$ ferrites sintered at 1100^0C for 2hrs.

4.3.3 Frequency Dependence of Dielectric Constant

Fig.-4.19 shows the variation of dielectric constant, ε' with frequency for different composition of $(Ni_{0.28}Cu_{0.10}Zn_{0.62}O)(Fe_2O_3)_{1-x}$ ferrites sintered at 1100^0C/2hrs for 1kHz to 13MHz at room temperature. It can be seen from the figure that the dialectric constant is found to decrease continuously with increasing frequency for all the specimens exhibiting a normal dielectric behavior of ferrites. The dielectric dispersion is rapid at lower frequency region and it remains almost independent at high frequency side. The incorporation of Fe into these ferrites has no pronounced effect on the dielectric constant in high frequency, but significantly decreases the dielectric constant in the low frequency range.

The type of behavior was observed in a number of ferrites such as Li- Co ferrites [4.20], Cu – Cd ferrites [4.21], Ni–Cu–Zn ferrites [4.22], Mg–Cu–Zn ferrites [4.24-4.25]. The dielectric behavior of ferrites may be explained on the basis of the mechanism of the dielectric polarization process and is similar to that of the conduction process. The electronic $Fe^{2+} \leftrightarrow Fe^{3+}$ gives the local displacement of electrons in the direction of applied electric field, which induces the polarization in ferrites [4.25].

The magnitude of exchange depends on the concentration Fe^{2+}/Fe^{3+} in pairs present on B-site for the present ferrite. All the samples have high value of ε' in the order of 10^5 at low frequencies. This could be explained using Koop's phenomenological theory [4.26] which was based on the Maxwell-Wagner model [4.27 – 4.28] for the inhomogeneous double layer dielectric structure. The first layer is the fairly well conducting large ferrite grain which is separated by the second thin layer of the poorly conducting grain boundaries. The grain boundaries of the lower conductivity were found to be ferrite at lower frequencies while ferrite grains of high conductivity are effective at high frequency.

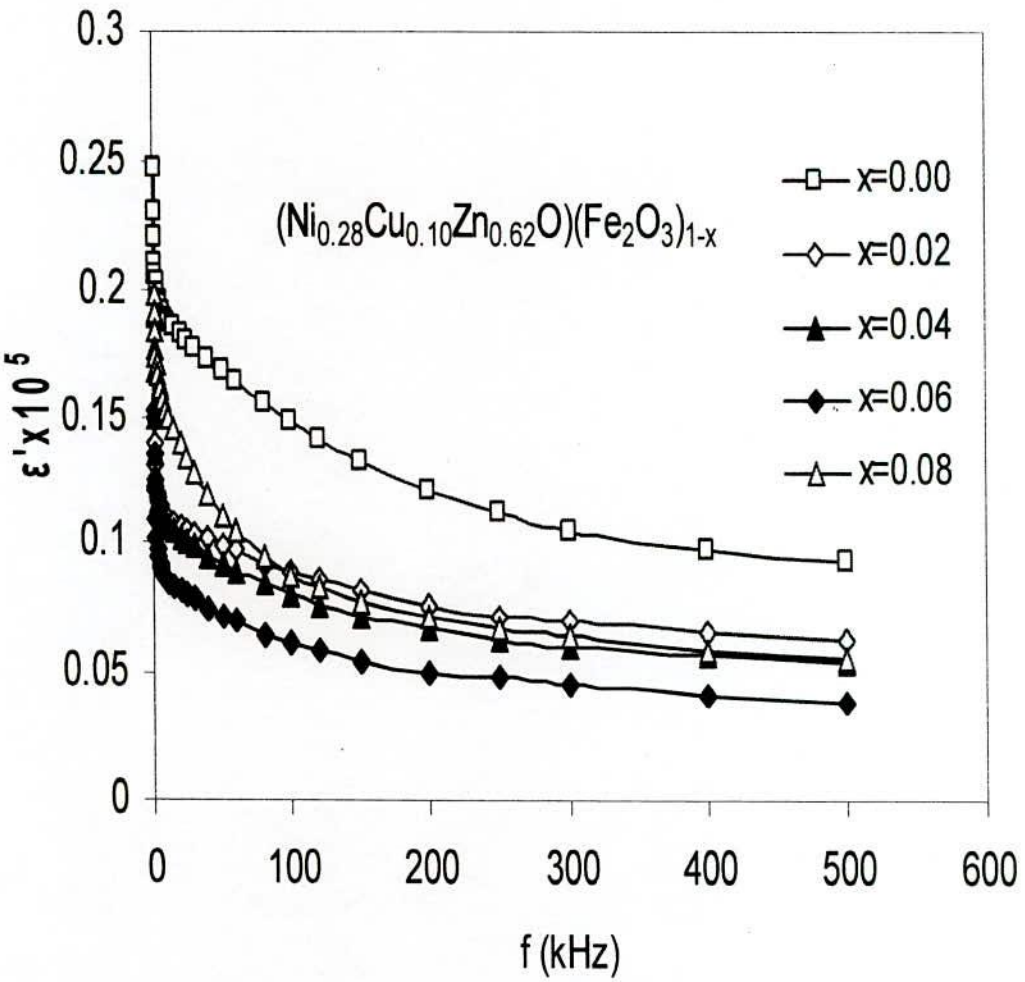

Fig.-4.19 Dielectric constant as a function of frequency of the ferrite system of $(Ni_{0.28}Cu_{0.10}Zn_{0.62}O)(Fe_2O_3)_{1-x}$ ferrites sintered at 1100^0C for 2hrs.

CHAPTER - V

Conclusions

Conclusions

5.1 Conclusions

The present work is focused on the synthesis, characterization and detail study of structure, electrical and transport magnetic properties of Fe-deficient of $(Ni_{0.28}Cu_{0.10}Zn_{0.62}O)(Fe_2O)_{1-x}$ ferrites where x = 0.00, 0.02, 0.04, 0.06 and 0.08 samples using standard double sintering ceramic method, sintered at 1100^0C for two hours. The X-ray diffraction confirmed the single phase cubic spinel structure of the samples. The lattice constant decreases with increasing Fe-deficient content obeying Vegard's law. Bulk density is found to increase while porosity decreases with decreasing Fe-deficient content.

Curie temperature slightly increases linearly with the addition of Fe-deficient content possibly due to weakening of A–B exchange interaction. This happened due to increase linkage between the magnetic ions and exchange coupling that determines the magnitude of the Curie temperature. The initial permeability gradually increases with increasing x-content at constant sintering temperature 1100^0C for 2hrs. The initial permeability is constant up to 2 – 4.5MHz region dependent on sintering temperature. Grain size has a great influence on the domain wall contribution and hence on permeability is constant up to 2 - 3 MHz region dependent on sintering temperature. Ferromagnetic resonance f_r shifts to lower frequency with increasing of permeability validating Snoek's relation $\mu_i.f_r$ = constant.

Saturation magnetizations are found to increase with increasing Fe-deficient. This may be due to modified cation distribution on two sub lattice. The low field hysteresis parameter such as coercivity (H_c) decreases with increasing Fe-deficiency. The remanance (B_r) and flux density (B_s) increases gradually with Fe-deficient. Increase of H_c comes from the enhancement of pinning force between domain walls and grain boundaries resulting from smaller grain size. The DC electrical resistivity increases with increasing Fe-deficient content up to x = 0.06 and thereafter decreases. The AC electrical

resistivity decrease with increase in frequency. Dielectric constant decreases with increasing frequency exhibiting normally dielectric behavior of ferrites. Based on the experimental results in terms of soft magnetic properties it may be concluded that optimum composition of Fe-deficient $(Ni_{0.28}Cu_{0.10}Zn_{0.62}O)(Fe_2O)_{1-x}$ ferrites series x = 0.06 sintered at 1100^0C for 2hrs with high initial permeability of 271, low H_c of 1.87Oe and minimum hysteresis loss of 23.64W/kg.

Finally Soft ferrite materials are extensively used in inductor cores which form a basic requirement in modern technology. Ni–Cu-Zn ferrites are suitable for these devices for future. Fabrication and characterizations of multilayer chip inductor using improved Ni-Cu-Zn ferrites is of high demand.

5.2 Scope for Future Work

With the development and advancement of nanotechnology a tremendous growth in research on miniaturization and high efficiency electronic devices is taking place. For these efficient miniaturized devices we need soft magnetic materials as its basic magnetic component. Soft ferrites are extensively used in inductor cores which form a basic requirement in modern technology. Ni-Cu-Zn ferrites are suitable for these devices for future advanced technology. Fabrication and characterizations of multilayer chip inductor using improved Ni-Cu-Zn ferrites is of high demand.

References

References

Chapter – I

1.1 "The Encyclopedia of Chemical Technology", 8, 881 (1998).

1.2 S. Hilpert; Ber. Deutseh Chem. Gas. Bd2, 42, 2248, 1909.

1.3 A Verma, T. C. Goel, R. G. Mendiralta, R. G. Gupta; 1999, "High-resistivity Nickel-Zinc ferrites by the Citrate precursor method"; J. Magn. Magn. Mater. Vol.192, pp.271-276.

1.4 T. Nakamura, T. Miyaonoto, Y. Yamada; 2003, "Complex Permeability Spectra of Polycrystalline Li-Zn ferrite and application of EM-Wave absorber"; J. Magn. Magn. Mater. Vol.256, pp.340-347.

1.5 A. Lakshman, K. H. Rao, R. G. Mendiratta; 2002, "Magnetic Properties of In^{3+} and Cr^{3+} substituted by Mg-Mn ferrites"; J. Magn. Magn. Mater. 235 (2001) 159.

1.6 J. Kulikowski; 1984, "Soft Magnetic Ferrites development or stagnations'; J. Magn. Magn. Mater. Vol.41, pp.56-62.

1.7 J. L. Snoek; "New Development Ferromagnetic materials'; Elsevier Publ. Co. N. Y. (1947).

1.8 L. Neel; "Properties Magnetique des ferrites: Ferimagnetism et Antiferromagnetism"; Annels de Physique, 3(1948) 137.

1.9 M. Manjurul Haque, M. Huq and M. A. Hakim; "Influence of CuO and sintering temperature on the microstructure and magnetic properties of Mg-Cu-Zn ferrites"; J. Magn. Magn. Mater. Vol. 320, (2008) pp.2792-2799.

1.10 T. T. Ahmed, I. Z. Rahman and s. A. M. Tofial; "Effect of copper ion distribution on the magnetization of nano scaled Ni-Zn ferrite"; J. Magn. Magn. Mater., Vol.272-276 (2004) pp. 2250-2252.

1.11 P. K. Puri, V. K. Babbar; Solid State Physics, 3rd ed., Chand & Company LTD, New Delhi, 1997, p.229.

1.12 Toshiyuki Suzuki, Termitsu Tanaka, Kaoru Ikemizu; "High density recording capability for advanced particulate media"; J. Magn. Magn. Mater. 235 (2001) 159.

1.13 T. Gannakopoulou, L. Kompotiatis, A. Kontogeogakos, G. Kordas; "Microwave behavior of ferrites prepared via Sol-gel method"; J. Magn. Magn. Mater. 246 (2002) 360.

1.14 E. Olsen, J. Thonstad; "Nickel ferrites as inert anodes in aluminum electrodes; Part I Material fabrication and preliminary testing"; J. Mater. Sci. Lett 12 (1993) 383.

1.15 C. O. Augustin, D. Prabbakaran, L. K. Srinivasan; "Febrication and characterization of $NiCr_2O_4$ spinel'; J. Mater. Sci. Lett 12 (1993) 383.

1.16 Abdeen A. M. ; "Electrical conduction in Ni-Zn ferrites"; J. Magn. Magn. Mater., 185 (1998) 199.

1.17 M. A. Ahmed, E. Ateia, L. M. Salah, A. A. E. Gamal; Mat. Chem. Phys. 92 (2005) 310.

1.18 G. L. Sun, J. B. Li, J. J. Sun, X. Z. Yang; J. Magn. Magn. Mater. 281 (2004) 173.

1.19 M. Ajmal, A. Maqsood; J. All. Compd. (2008) 54.

1.20 T. Nakamura; "Low Temperature Sintering of Ni – Cu- Zn ferrite and its Permeability Spectra"; J. Magn. Magn. Mater. 168 (1997) 285 – 291.

1.21 T. Nakamura, T. Tsutaka, K. Hatake Yana; "Frequency dispersion of permeability in ferrite composite materials"; J. Magn. Magn. Mater, 138 (1994) 319.

1.22 S. M. Hoque, Md. A. Choudhury, Md. F. Islam; J. Magn. Magn, Mater. 251 (2002) 292.

1.23 M. M. Hoque, M. Huq, M. A. Hakim; Mat. Chem. Phys. 112 (2008) 580.

1.24 D. Banerjee, D. Bahadur, K. G. Suresh, A. K. Nigam; Physica B 378 – 380 (2006) 1091.

1.25 N. Rezescu, E. Reslescu, P. D. Popa, M. L. Craus, L. Rezlescu; J. Magn. Magn. Mater. 182 (1998) 199.

1.26 E. Rezlescu, N. Reszlescu, P. D. Popa, C. Pasnicu, M. L. Craus; Mat. Res. Bull. 33(6) (1998) 915.

1.27 K. O. Low, F. R. Sale; "Sintering of gel-derived Ni – Cu- Zn ferrites"; Ferrites Proceedings of ICF 8, Kyoto, Tokyo, Japan; The Japan Society of Power and Powder Metalurgy, 2000, pp. 548 – 550.

1.28 Kin O. Low, Frank R. Sale; "Electromagnetic properties of gel-dervied Ni- Cu-Zn ferrites"; J. Magn. Magn. Mater. 246 (2002) 30-35.

1.29 O. F. Caltun, L. Spinu, Al. Staneu, L. D. Thung, W. Zhou; J. Magn. Magn. Mater. 242 – 245 (2002) 160.

1.30 M. C. Dimri, A. Verma, S. C. Kashyap, D. C. Duba, O. P. Thakur, C. Prokash; Mat. Sci. Engg. B133 (2006) 42.

1.31 G. Goev, V. Masheva, L. Ilkov, D. Nihtianova, M. Mikhov; Proceedings of the 5th General Conference of the Balken Physical Union BPU – 5 (2003) 687.

1.32 K. O. Low, F. R. Sale; J. Magn. Magn. Mater. 256 (2003) 221.

Chapter – II

2.1 D. Hadfield; Lliffe Books, LTD, London, John Wiely and Sons, "Permanent Magnets and Magnetism", Inc., New York, 1961.

2.2 Rollin J. Parker and Robertj Studders; John Wiley and Sons, "Permanent Magnets and Their Applications"; Inc., New York, 1962.

2.3 Rollin J. Parker; John Wiley and Sons, "Advances in Permanent Magnetism"; Inc. New York, 199.

2.4 D. S. Parasnis, Harper and Brothers; "Magnetism From Lodestone to Polar Wandering"; New York, 1961.

2.5 Malcom Mc Caig; John Wiley and Sons, "Permanent Magnet in Theory and Practice", Inc., Toronto, 1977.

2.6 L. Neel; Ann. Phys. 3(1946) 137.

2.7 Y. Yafat and C. Kittel; "Antiferromagnetic arrangement in ferrites", Phys. Rev. 87 (1952) 290.

2.8 T. Ogasawara and M. A. S. Oliveira; J. Magn. Magn. Mater. 217 (2000 147.

2.9 N. H. Bragg; "The structure of magnetite and the spinels"; Nature, 95 (1915) 561.

2.10 Alex Goldmann; "Modern Ferrite Technology", Van Nostrand Reinhold, New York, (1940) p.15.

2.11 N. Spaldin; Magnetic Materials; Fundamentals and device applications Cambridge: Cambridge University Press, 2003.

2.12 Alex Goldmann; "Modern Ferrite Technology",Van Nostrand Reinhold, New York, (1940) p.15.

2.13 R. W. Cahn, P. Haasen, E. J. Kramer; "Materials Science and Technology", Vol. 3B, VCH Publishers Inc., New York, NY(USA) & Verlagsgesellschaft mbH Weinheim (Federal Republic of Germany), (1994).

2.14 D. J. Craik; 1975, Magnetic Oxide, Part1, John Wiley & Sons, Ltd, Bristol England.

2.15 E. J. W. Verwaw and E. L. Heilmann; T. Chem. Phys. 15(4), (1947) 174-180.

2.16 F. C. Romeign; Philips Res. Rep. 8, NR-5(1953), 304 – 342.

2.17 A. land, "Quantum Mechanics"; Pitman, London (1951).

2.18 J. H. VanVleck; "Theories of Electric and Magnetic Susceptibilities"; Clarendon Press, Oxford (1952).

2.19 P. Weiss; J. Phys. Theor. Appl. 6, 667 (1907).

2.20 Fowler, Michael; "Historical Beginning of Theories of Electricity and Magnetism"; Retrieved 2008.

2.21 Vowles, P. Hugh; "Early Evolution of Power Engineering"; Isis (University of Chicago Press) 17(2): (1932) 412.

2.22 A. A. Samokhvalov and A. G. Rustamov; SOV. Phys. Solid State, 6(1964) 749.

2.23 A. J. Bossmann and C. Crevecoeur, "Mechanism of the electrical conduction in Li-dopped NiO"; Phys. Rev. 144(1966) 763.

2.24 E. J. W. Verway and E. L. Heilmann and F. C. Romuijin; J. Chem. Phys. 15(4), (1947) 181-187.

2.25 L. G. VanUitert; J. Chem. Phys. 24(2), (1956).

2.26 Smit and W. J. P. Wijn; Ferrites, Philips Technical Libery C Wiley, New York, 1959.

2.27 A. A. Samokhvalov and A. G. Rustamov; SOV Phys. Solid State, 6, (1964) 744.

2.28 A. J. Bosmann and C. C. Creve; Phys. Rev. 144 (1966) 763.

2.29 B. Viswanathan, V. R. K. Muthy; "Ferrite Materials Science and Technology", Spring Vertay, Noarosa Publishing House, New Delhi, (1990).

2.30 G. H. Jonker; J. Phys. Chem. Solids, 9, (1959), 165 – 175.

2.31 J. H. Van Santan and G. H. Jonker; Physica, 19, 120 (1953).

2.32 R. V. Bhise, V. C. Mahjan, M. G. Petit, S. D. Lo,lke and S. A, Patil, S. D. Lolke and S. A. Patil; Indian J. Physics 33, (1995), 454-462.

2.33 B. V. Bhise, A. K. Ghatage, B. M. Kulkarni, S. D.Lotke and S. A. Patil; Bull Mater. Sci., 19(3), (1996)

2.34 M. G. Patil, V. C. Mahajan, B. V. Bhise, S. M. Chendke and S. A. Patil; Phys. State sol (a) 144, (1994), 415.

Chapter – III

3.1 L. B. Kong, Z. W. Li, G. Q. Lin and Y. B. Gan; "Magneto-dielectric properties of Mg-Cu-Co ferrite ceramics: II Electric, dielectric and magnetic properties", J. An. Ceram. SOC 90(7) (2007) 2104.

3.2 S. K. Sharma, Ravi Kumar, Shalendra Kumar, M. Knobel, C. T. Meneses, V. V. Siva Kumar, V. R. Reddy, M. Shingh and C. G. Lee; "Role of inter particle interactions on the magnetic behavior of $Mg_{0.95}Mn_{0.05}Fe_2O_4$ ferrite nano particle"; J. Phys. Condens. Matter 20(2008) 235214.

3.3 Soilah Zahi, Mansor Hashim and A. R. Daud; "Synthesis, Magnetic and microstructure of Ni-Zn ferrite by Sol-gel technique"; J. Magn. Magn. Mater. 308(2007) 177.

3.4 M. A. Hakim, D. K. Saha and A. K. M. Fazle Kibria; "Synthesis and temperature dependent structural study of nanocrystalline Mg-ferrite materials"; Bang. J. Phys. 3(2007) 57.

3.5 A. Bhaskar, B. Rajini Kanth and S. R. Murthy; "Electrical properties of Mn added Mg-Cu-Zn ferrites prepared by microwave sintering method"; J. Magn. Magn. Mater. 283(2004) 109.

3.6 ZhenXing Yue, Ji Zhou, Longtu Li and Zhilun Gui; "Effects of MnO_2 on the electromagnetic properties of Ni-Cu-Zn ferrites prepared by Sol gel auto-combustion"; J. Magn. Magn. Mater. 233(2001) 224.

3.7 C. W. Chen; Magnetism and Matallurgy, Soft Mag. Mat., North-Holland Pub. Com. XV(1977) 288.

3.8 C. Kittel; "Introduction to Solid State Physics"; 7th edition, John Wiley and sons, Inc., Singapore(1996).

3.9 J. B. Nelson, D. P. Riley; "an experimental investigation of extrapolation methods in the derivation of accurate unit-cell dimensions of crystals"; Proc. Phys. SOC London 57(1945) 160.

3.10 Tahir Abbas, M. U. Islam and M. Ashraf Ch; Mod. Phy. Letts. B 9(22), (1995) 1419.

3.11 J. Smit and H. P. Wijin; Ferrites, Wiely New York, (1959) 250.

3.12 Simon Forner; "Versatile and Sensitive Vibrating Sample Magnetometer"; Rev. Sci. Instr. 30(1959) 548.

Chapter – IV

4.1 J. B. Nelson, D. P. Riley; "An experimental investigation of extrapolation methods in the derivation of accurate unit-cell dimension of crystals"; Proc. Phys. SOC London 57 (1945) 160.

4.2 L. Vagards; "Die constitution der mischkristalle und die raumfullung der atome"; Z. Phys. 5 (1921) 17.

4.3 J. Smit, H. P. J. Wijn; Ferrites Wiley New York, (1959) p.143.4.4

4.4 L. John Berchamans, R. Kalali Selvan, P. N. Selva Kumar and C. O. Augustin; "structural and electrical properties of $Ni_{1-x}Mg_xFe_2O_4$ synrhesized by citrate gel process', j. Magn. Magn. Mater. 279 (2004) 10.

4.5 K. O. Low, F. R. Sale; J. Magn. Magn. Mater. 256 (2003) 221.

4.6 C. R. Foschini, L. Perazolli, J. A. Varela; J. Mat. Sci. 39(20040 5825.

4.7 A. Goldman; "Hand book of Modern Ferromagnetic Materials" Kulwer Academic Publishers, Boston, USA, 1999.

4.8 G. C. Jains, B. K. Das, R. S. Khandyja and S. C. Gupta; "Effect of itergranular porosity of initial permeability and coercive force in a manganese zinc ferrite"; J. Mater. Sci. II (1976) 1335.

4.9 S. Chikazumi; "Physics of Magnetism"; John Wiley and son, Inc. New York 1966.

4.10 B. Jeyadevan, C. N. Chinnasamy, K. Shinoda, K. Tohji; "Mn-Zn ferrite with higher magnetization for temperature sensitive magnetic fluid"; J. Appl. Phys., Vol.93 (2003) pp.8450.

4.11 A. Verma, R. Chatterjee; "Effect of zinc concentration on the structural, electrical and magnetic properties of mixed Mn-Zn and Ni-Zn ferrites synthesized by the citrate precursor technique"; J. Magn. Magn. Mater. 306(2006) 313-320.

4.12 J. L. Snoek; "Dispersion and absorption in magnetic ferrites at frequencies above on MC/S"; Physica, 14(4) (1948) 207.

4.13 J. J. Shrotri, S. D. Kulkarni, C. E. Deshpande, S. K. Date; "Effect of Cu substitution on the magnetic and electrical properties of Ni-Zn ferrite synthesized by soft chemical method"; Mater. Chem. Phys. 59 (1999) 1.

4.14 K. Overshott; "The causes of the anomalous cross in amorphous ribbon materials"; IEEE Trans. Magn. 17 (1981) 2698.

4.15 F. G. Brockman, P. H. Dowling and W. G. Steneck; "Dimensional effects resulting from a high dielectric constant found in a ferromagnetic ferrite"; Phys. Rev. 77 (1950) 85.

4.16 I. Neel; Ann. Phys. 3(1948) 137.

4.17 E. A. Schwabe and D. A. Campell; J. Appl. Phys. 34, 1251 (1963).

4.18 Igarashi H. and Dkazaki; K. J. Am. Cer. SOC 60[1-2], 51, (1977).

4.19 Ž. Cvejić, S. Rakić, S. Jankov, S. Shuban, A. Kapor; Processing and Application of Ceramics; 2(1) (2008) 53.

4.20 Nutan Gupta, S. C. Kashyap and D. C. Dube; "Dielectric and Magnetic properties of Citrate route processed Li-Co Spinel ferrites"; Phys. Stat. Solidi(a) 204(7) (2007).

4.21 C. B. Kolekar, P. N. Kamble, S. G. Kulkarni and A. S. Vaingankar; "Effect of Gd^{3+} substitution on dielectric behavior and copper-cadmium ferrites"; J. Matter. Sci. 30(1995) 5784.

4.22 Zhenxing Yue, Zhou Ji, Zhilun Gui and Longtu Li; "Magnetic and electrical properties of low temperature sintered Mn-doped Ni-Cu-Zn ferrites"; J. Magn. Magn. Mater. 264(2003) 258.

4.23 S. S. Bellad and B. K. Chougula; "Composition and frequency dependent dielectric properties of Li-Mg-Ti ferrites"; Mater. S. Chem. Phys. 66(2000) 58.

4.24 A Bhaskar, B. Rajini Kanth, S. R. Murthy; "Electrical properties of Mn added Mg-Cu-Zn ferrites prepared by microwave sintering method"; J. Magn. Magn. Mater. 283(2004) 109.

4.25 Zhenxing Yue, Zhou Ji, Longtu Li, Xiaolui Wang and Zhilun Gui; "Effect of copper on the electromagnetic properties of Mg-Zn-Cu ferrites prepared by Sol-gel auto-combustion method"; Mater. Sci. Eng.B 86(2001) 64.

4.26 Maxwell J.; 1873, Electricity and Magnetism; Vol.1 Oxford University Press. London Wanger K 1913 Ann. Phys. 40 817.

4.27 p. venugopal Reddy, T. Seshagiri Rao; "Dielectric behavior of mixed Li-Ni ferrites at low frequencies"; J. Less. Common Met. 86 (1982) 255.

4.28 B. Kumar Kunar, G. Srivastava; "Dispersion observed in electrical properties of titanium substituted lithium ferrites"; J. Appl. Phys. 75 (1994) 6115.

Publication

"Magnetic and Electrical Properties of High Temperature Sintered Ni-Cu-Zn Ferrites", **S. Bahadur**, S. S. Sikder, Shireen Akhter, Z. H. Khan and D. K. Saha; National Conference on Physics for Technology Development, 27-28 December 2012.